12-14-2016

# Micro-Mixing in Turbulent Premixed Flames

Michael Joseph Kuron
*University of Connecticut*, mike.kuron@gmail.com

Micro-Mixing in Turbulent Premixed Flames

Michael Joseph Kuron, PhD

University of Connecticut, 2016

The transported probability density function (TPDF) methods provide an elegant solution to the challenge of closing the mean chemical source term in turbulent combustion modelling as it appears in closed form in the TPDF equations and thus the turbulence-chemistry interaction can be solved for without aggressive assumptions. Despite some reported success in the literature, challenges remain when applying the TPDF method to turbulent premixed flames as the molecular mixing or micro-mixing term is unclosed, the modeling of which is considered to be a primary challenge. The objective of this dissertation is to evaluate the application of existing mixing models to turbulent premixed flames and to create high-fidelity scalar dissipation rate models to predict turbulent premixed combustion.

In the first step, DNS of a temporally evolving premixed flame is used as a numerical test bed to evaluate commonly used mixing models in the context of turbulent premixed flames. This study demonstrates that the Euclidean Minimum Spanning Tree (EMST) model is capable of predicting the behavior of a turbulent premixed flame assuming that an accurate model for the scalar mixing rate, and thus the scalar dissipation rate, can be provided. In the next stage of the dissertation, chemical explosive mode analysis (CEMA) and DNS data with realistic chemistry are used to identify physiochemical processes that govern the conditional scalar dissipation rate behavior in a turbulent premixed flame and evaluate mixing timescales.

A model for the Favre-averaged scalar dissipation rate is subsequently developed based on the insight gleaned from the DNS analysis, accounting for the scalar mixing rate behavior in both the turbulent mixing limit and the flamelet limit. Comparisons to the DNS are performed, with the new hybrid model performing exceptionally well. Finally, in the last stage of the dissertation, a transport equation for the conditional scalar dissipation rate of a reactive scalar is derived. Models for the unclosed terms in the leading order equation identified by an order of magnitude analysis are developed

and evaluated with DNS data. The resulting modelled equation is then compared to the DNS data, and excellent agreement between the new model and the DNS is observed.

# Micro-Mixing in Turbulent Premixed Flames

Michael Joseph Kuron

B.S., Villanova University, 2007

M.S., University of California, Los Angeles, 2008

A Dissertation

Submitted in Partial Fulfillment of the

Requirements for the Degree of

Doctor of Philosophy

at the

University of Connecticut

2016

# APPROVAL PAGE

Doctor of Philosophy Dissertation

Micro-Mixing in Turbulent Premixed Flames

Presented by

Michael Joseph Kuron, B.S.M.E, M.S.M.E.

Major Advisor_____

Dr. Tianfeng Lu

Associate Advisor_____

Dr. Zhuyin Ren

Associate Advisor_____

Dr. Xinyu Zhao

Associate Advisor_____

Dr. Jacqueline H. Chen

University of Connecticut

2016

## ACKNOWLEDGEMENT

Over the course of the roughly six years that it took to complete the coursework and research that manifest themselves in this dissertation, I have been immensely fortunate to have had the support, guidance, and encouragement of a great many people. I am deeply indebted to all of those who have helped me reach this point, and for bearing with me through the ups and downs of the Ph.D. process.

I would especially like to Dr. Tianfeng Lu and Dr. Zhuyin Ren for their guidance and patience as my advisors. I am lucky to have found mentors in you both that have been generous with your time and knowledge. You've helped me grow as an engineer and person, for which I'm forever grateful. I would also like to thank the members of my thesis committee, Dr. Xinyu Zhao and Dr. Jacqueline H. Chen, for their helpful feedback and the opportunity to learn from them. In particular, I would like to thank Jackie for hosting me at Sandia for four months in the summer of 2015, during which a substantial portion of this dissertation was completed.

I can safely say that none of this would have been possible without the assistance of my colleagues at CAE Associates who have supported my Ph.D. endeavor both financially and emotionally. I'd like to thank Peter Barrett for helping to make me a part of the CAEA family, his mentorship, and for always having my back. I'd also like to thank Dr. Michael Bak who encouraged me to follow in his footsteps and pursue my Ph.D at the University of Connecticut. It hasn't been quite as easy as you advertised, but I'm grateful for your encouragement and guidance. I can only hope to be as great of an engineer and person as you both.

Throughout my time at UCONN I have been lucky to have met and worked with a number of new friends and colleagues. A big thank you to Chao Xu, Yang Gao, Bifen Wu, Ji-woon Park, and Yuncaho Wu. I'm also very grateful to have had the opportunity to have visited Sandia for four months and met some incredibly smart and generous researchers. I'm especially grateful to Dr. Hemanth Kolla and Dr. Yuki Minamoto for their combustion expertise, help with S3D, and love of coffee.

I have been blessed with incredible friends and family, who have given me more love and support than I could ever return. I'd like to thank Dr. Joseph and Jessica Ingrassia for their support through the highs and the lows, and the more-than-occasional hot meal. I'm grateful to my brother Steve and his wife Jackie for keeping life interesting, and reminding me to stop and smell the roses every now and again. I'm thankful to my grandparents, Michael and Helen Grella, and Joseph and Rita Kuron, who have paved the way with sacrifice and hard work to make life easier for me. I hope that

I’ve made you proud. Finally, I owe the greatest debt of gratitude to my parents, Greg and Lorraine Kuron, without whom none of this would be possible. You’ve never wavered in your love and support for me, and have done everything short of learning calculus to help me succeed.

# TABLE OF FIGURES

# LIST OF TABLES

## TABLE OF CONTENTS

# Chapter 1: Introduction

## 1.1. Motivation

The ability to harness energy from the combustion of fossil fuels has had an immensely positive effect on modern society, enabling wide access to electricity, faster and more efficient modes of transportation, and effective heating for both home and industrial processes. While advances have been made in extracting energy from renewable sources such as wind and solar power, it is estimated that as much as 80% of today's global energy demands are met by the combustion of fossil fuels [1]. Furthermore, the combustion of fossil fuels is expected to remain the dominant global energy source for decades to come. Despite the obvious benefits of combustion as an energy source, there are drawbacks as well; namely the emission of air pollutants that potentially lead to climate change and harm human health. To mitigate the negative effects of combustion, world governments have imposed increasingly stringent regulations on the emissions output and efficiency of new power plant and engine designs [2].

The mode of combustion occurring in a power generating device such as an engine can be broadly classified into two different categories: non-premixed and premixed. In a non-premixed flame, the fuel and the oxidizer remain separated until they meet in the reaction zone. In this mode, fuel and oxidizer diffuse towards one another and combust along the stoichiometric surface, where the fuel and oxidizer are balanced. Non-premixed flames in practical systems typically operate at high temperatures, which lead to elevated concentrations of pollutants such as unburned fuel, nitrogen oxides, and soot. In a premixed flame, the fuel and oxidizer are fully mixed before entering the combustion zone. In this mode of combustion, the stoichiometry of the unburned mixture can be controlled to operate in fuel-lean conditions, avoiding unburned fuel in the combustion products and increasing thermal efficiency. Additionally, by operating at fuel lean conditions, in which the unburnt reactants contain an excess of

oxidizer, the peak flame temperature remains relatively low compared to stoichiometric or rich mixtures, thus avoiding NOx formation. The prospect of limited pollution and high thermal efficiency makes lean premixed combustion attractive from a design perspective [3].

While lean premixed combustion shows promise for its ability to increase efficiency and limit pollutants, there remain many challenges associated with its safe implementation in next generation engine designs. In particular, premixed flames exhibit a strong coupling between molecular diffusion and chemical reaction and are inherently unstable, with many of the physiochemical processes that lead to these instabilities not fully understood [4]. Designing safe and stable engines operating in lean turbulent premixed conditions will require investigations based in both experimental methods, for their realism and lack of assumptions, as well as numerical simulations, for the level of detailed information that can be obtained. Simulation methods have a distinct advantage over experimental studies in their ability to reduce design cycle time and expense, but are limited in their accuracy due to an imperfect understanding of the physical processes that must be modeled.

Numerical simulation of turbulent flows, with or without combustion, is a challenging problem due to the wide range of length and time scales that are present. Approaches to the simulation of turbulent reacting flows can be broadly classified into three techniques. The first and most accurate approach is called direct numerical simulation (DNS), in which all length and time scales of the flow field and flame fronts are resolved. By examining the turbulence Reynolds number, $Re_T = u"\Lambda/\nu$, where $u"$, $\Lambda$, and $\nu$ are characteristic values of the turbulence velocity fluctuations, turbulence integral length scale, and kinematic velocity, respectively, it can be shown that the range of length scales of a turbulent flow field scales as $Re_T{}^{3/4}$ and the range of time scales as $Re_T{}^{1/2}$ [5]. For practical flows where the Reynolds number is of the order of $10^6$, the consequence of the large range of scales is that the computational expense required to resolve such flow fields limits the range of applicability of DNS

to domain sizes of only a few cubic centimeters [6]. In spite of the computational limitations of this approach, DNS plays a valuable role as a research tool for its ability to supply insight into the basic physical processes of turbulent combustion and act as a means of validation for modeling hypotheses.

A second approach, which lies at the opposite end of the spectrum from DNS in terms of flow resolution, is the Reynolds-Averaged Navier-Stokes (RANS) methodology. In this approach, the non-linear governing equations are averaged either in time, ensemble, or phase, and a solution is sought for the mean quantities whose minimum length and time scales are much larger than the minimum scales of turbulence. This averaging technique leads to unclosed terms in the RANS governing equations which must be modeled, an issue which is exacerbated in the presence of nonlinear chemical reactions. In particular, the modelling of terms that arise due to turbulence-chemistry interaction are regarded as the most challenging aspect of the RANS approach to turbulent combustion simulation [7].

In the third approach of Large Eddy Simulation (LES), the governing equations are spatially filtered and the energy containing large scale motions of the turbulent flow field are resolved. As in RANS, the filtering procedure used in LES leads to unclosed terms representing the small scale, subgrid motions that require modeling. LES is attractive in its ability to accurately characterize large-scale fluctuations, which are more strongly influenced by the flow configuration and boundary conditions than the small-scale fluctuations. However, the chemical scales found in reacting flows of practical devices typically occur at or near the smallest scales of turbulence, and thus modeling of subgrid physical phenomena is of paramount importance in LES.

The primary modeling difficulty in both RANS and LES of reacting flows is the prediction of the mean or filtered nonlinear chemical source term, and the coupling of reaction and mixing. Most current modeling approaches can be grouped into two distinct categories based on their underlying assumptions: flamelet-like and probability density function (PDF)-like [8]. The flamelet-like models

imply that the species composition space, which is an N-dimensional space where N is the number of species, is confined to a low-dimensional manifold [8]. In practice this is accomplished for premixed flames by mapping the composition field to a single scalar like the progress variable, or assuming that the solution of a laminar flamelet can be used in some manner to close the mean reaction rate. In the context of premixed combustion, flamelet-like models include the Bray-Moss-Libby model [9-11], Presumed PDF and Flamelet-Generated Manifolds [12-15], Flame Surface Density [16-20], G-Equation [21,22], and Conditional Moment Closure [23-25] approaches. While these models are successful within the limits of their assumptions, their applicability is inherently limited by the flamelet assumption.

In the PDF-like models, no assumption is made that confines the species to a low-dimensional manifold. Instead, a statistical approach is taken to describe the inherently random, turbulent reacting flow field. The distribution of species is represented by an ensemble of samples for which the chemical reactions are treated without assumption, and no single mode of combustion must be assumed. PDF-like methods include the Linear Eddy Model [26,27], One-Dimensional Turbulence [28,29], Multiple Mapping Condition [30,31], and the Transported PDF (TPDF) methods [32-37]. The exact treatment of the chemical source term is the primary advantage of the PDF-like methods [34,37], as it allows for a more accurate description of the turbulence-chemistry interaction. However, because no assumption is made as to the coupling of molecular diffusion and reaction in the PDF-like methods, mixing must be modeled and is considered to be the primary challenge [38-40]. This is particularly acute for the simulation of turbulent premixed flames in which a close coupling between mixing and reaction exists.

This dissertation is aimed at improving the applicability of the TPDF methods to turbulent premixed flames. In particular, the mixing model has been identified as a weak component. This dissertation seeks to explore the mixing modeling in detail and provide development in the mixing model treatment for premixed flames.

## 1.2. Background

In practical engineering applications, the simulation of turbulent reacting flows is accomplished using either the RANS or LES framework. As noted above, the averaging or filtering procedures used in the derivation of these two approaches leads to unclosed terms in the governing equations that must be modeled. In general, the modeling methodologies used in LES are often adaptations or extensions of RANS modelling ideas [13], and so it is useful to review the density weighted equations for the mean flow field. The Favre average of a quantity $q$ can be defined as $\tilde{q} = \overline{\rho q}/\bar{\rho}$ where the overbar denotes the Reynolds averaging operator, and the Favre fluctuation of that quantity about its mean is denoted by the double prime, $q'' = q - \tilde{q}$. The equations for the mean density, mean velocity, mean mass fractions, and mean enthalpy (ignoring thermal radiation effects) can be written as [37]:

$$\frac{\partial \bar{\rho}}{\partial t} + \frac{\partial \bar{\rho}\tilde{u}_i}{\partial x_i} = 0 \tag{1.1}$$

$$\frac{\partial \bar{\rho}\tilde{u}_i}{\partial t} + \frac{\partial \bar{\rho}\tilde{u}_i\tilde{u}_j}{\partial x_j} = -\frac{\partial \bar{p}}{\partial x_i} + \frac{\partial}{\partial x_j}\left(\bar{\tau}_{ij} - \bar{\rho}\widetilde{u_i''u_j''}\right) \tag{1.2}$$

$$\frac{\partial \bar{\rho}\tilde{Y}_\alpha}{\partial t} + \frac{\partial \bar{\rho}\tilde{u}_j\tilde{Y}_\alpha}{\partial x_j} = \frac{\partial}{\partial x_j}\left(\bar{J}_j{}^{\alpha} - \bar{\rho}\widetilde{u_j''Y_\alpha''}\right) + \overline{\dot{\omega}_\alpha} \tag{1.3}$$

$$\frac{\partial \bar{\rho}\tilde{h}}{\partial t} + \frac{\partial \bar{\rho}\tilde{u}_j\tilde{h}}{\partial x_j} = -\frac{\partial \bar{\rho}\widetilde{u_j''h}}{\partial x_j} - \frac{\partial}{\partial x_j}\overline{\left(\rho\Gamma\frac{\partial h}{\partial x_j}\right)} + \frac{D\bar{p}}{Dt} + \overline{\tau_{ij}\frac{\partial u_j}{\partial x_i}} \tag{1.4}$$

In the equations above, the turbulent fluxes of momentum, species, and enthalpy appear unclosed and are typically modeled by solving additional equations for the mean turbulence scales. The molecular diffusion fluxes are also unclosed, but are typically small compared to the turbulent fluxes and, in practical flows of interest (i.e. large Reynolds number), are commonly ignored. The primary modeling challenge, and the major focus of turbulent combustion modeling, is in the closure of the mean chemical reaction rate, $\overline{\dot{\omega}_\alpha}$. Due to the influence of turbulence-chemistry interaction and the nonlinear nature of the chemical source term, the mean reaction rate cannot be reliably computed as a function of the mean composition field, i.e. $\overline{\dot{\omega}_\alpha}(\phi) \neq \dot{\omega}_\alpha(\tilde{\phi})$ [7].

The transported PDF methods provide an elegant closure to the challenge of modeling the mean chemical reaction source term. By introducing the one-point, one-time Eulerian composition PDF, $f_\phi(\psi;\boldsymbol{x},t)$, any mean function of the composition field can be computed by integrating over the PDF in sample space. So, for an arbitrarily complex reaction mechanism, the mean chemical source term can be closed in terms of the composition PDF:

$$\overline{\dot{\omega}_\alpha} = \int \dot{\omega}_\alpha(\psi) f_\phi(\psi;\boldsymbol{x},t)\, d\psi. \qquad (1.5)$$

Thus, if the composition PDF can be predicted, then the problem of closing the chemical source term has been resolved.

A transport equation for the composition PDF can be derived from the instantaneous governing equations for a reacting flow field following the approach of Pope [34]. The resulting N+1 dimensional transport equation is shown in Equation 1.6, where N is the number of chemical species, and the pressure transient and dissipation terms in the enthalpy equation have been neglected.

$$\frac{\partial \rho f_\phi}{\partial t} + \frac{\partial \rho \tilde{u}_j f_\phi}{\partial x_j} + \frac{\partial \dot{\omega}_\alpha f_\phi}{\partial \psi_\alpha} = -\frac{\partial}{\partial x_j}\left[\langle u_j^{"} | \psi \rangle \rho f_\phi\right] + \frac{\partial}{\partial \psi_\alpha}\left[\left\langle \frac{\partial J_j^\alpha}{\partial x_j} \middle| \psi \right\rangle f_\phi\right] \qquad (1.6)$$

The terms on the left-hand side, appearing in closed form, are the temporal evolution of the PDF, the transport in physical space by the mean velocity, and, most notably, the transport in composition space by chemical reaction. On the right-hand side are the transport in physical space by turbulent velocity fluctuations and transport in composition space due to molecular diffusion, both of which require modeling. In particular, the molecular mixing term is considered to be the primary modeling challenge in the PDF methods [37,40,41]. It is noted here that the composition PDF can be extended to include additional variables, such as the velocity and turbulence frequency, to provide a more complete description of the influence of turbulence fluctuations on the scalar field and PDF evolution [42-45]. In principle, the PDF can also be extended to include the scalar gradients to close the molecular mixing

term [46], however this introduces additional unclosed terms and substantially increases the dimensionality of the governing equations and thus has not been widely pursued.

Due to the high dimensionality of the composition space, and therefore of the PDF transport equation, the coupled set of RANS momentum and turbulence equations, and the composition PDF equations are typically solved using a hybrid Lagrangian particle, Eulerian mesh methodology [37]. In this method, the high dimensional composition PDF transport equation is recast in its Lagrangian form as a set of stochastic differential equations:

$$dx_i^* = \tilde{u}_i^* dt + dx_{i,turb}^* \quad (i = 1,2,3) \tag{1.7}$$

$$d\phi_\alpha^* = \dot{\omega}_\alpha(\phi^*)dt - \left\langle \frac{\partial J_j^\alpha}{\partial x_j} \middle| \psi \right\rangle dt \tag{1.8}$$

where the superscript * refers to a particle quantity and $dx_{i,turb}^*$ is the effect of turbulent velocity fluctuations on the particle position and $\left\langle \frac{\partial J_j^\alpha}{\partial x_j} \middle| \psi \right\rangle$ is the molecular mixing term, which must be modeled. The stochastic differential equations, Eqns. 1.7 and 1.8, can be solved with a Monte Carlo particle based method [32,34,37], while the Eulerian RANS momentum and turbulence equations are solved using standard finite-volume or finite-difference based methods. The Eulerian field provides the mean quantities required by the particle solver (i.e. mean velocity, turbulence scales, etc.) while the Lagrangian particles provide the mean density back to the Eulerian solver. Most significantly, the particle equations provide a means to estimate the statistics, including mass-weighted averages, of any quantity that can be computed from the composition variables, including the chemical source term.

The model for the molecular mixing term in Equation 1.8 is of paramount importance in the TPDF methods, and has been identified as the primary weakness of this approach [38,41,47-50]. Subramaniam and Pope identified a set of performance criteria and guiding principles that mixing models should follow [51]. These criteria include:

i) Conservation of means, as implied by mean scalar transport equation

ii) Decay of variances, as implied by the scalar covariance equation

iii) Boundedness of scalars

iv) Linearity and independence

v) Relaxation of the Scalar PDF to Gaussian for conserved scalars in homogeneous isotropic turbulence

vi) Localness of mixing in composition space

Many approaches to the closure of the molecular mixing term have been developed in the literature that satisfy these criteria to varying degrees. A simple micro-mixing model alternatively called the interaction by exchange with the mean (IEM) [52] or linear mean-square estimation (LMSE) [53] model can be constructed by assuming that the scalar field is statistically homogeneous and Gaussian. Under these conditions, it can be shown [5] that the conditional diffusion can be expressed as:

$$\left\langle \frac{\partial J_j^{\alpha}}{\partial x_j} \middle| \psi \right\rangle = \langle \Gamma \nabla^2 \phi | \psi \rangle = -\frac{1}{2} \Omega_{\phi} \left( \psi - \tilde{\phi} \right) \tag{1.9}$$

where $\Omega_{\phi} = \widetilde{\chi_{\phi}} / \widetilde{\phi''^2}$ is the scalar mixing frequency, $\widetilde{\chi_{\phi}} = 2\Gamma \widetilde{\nabla \phi'' \nabla \phi''}$ is the Favre-averaged scalar dissipation rate, $\widetilde{\phi''^2}$ is the Favre-averaged scalar variance [2], and Γ is the scalar's diffusivity. The IEM model is deterministic, and satisfies criteria i-iv above. However, this model maintains the PDF shape, does not enforce mixing that is local in composition space, and its applicability to general flows is suspect due to the strong assumptions made in its development. Regardless, the IEM model is widely adopted due to its simplicity and realizability.

The stochastic particle interaction model called the modified Curl (MC) [54-56] model has been developed based on an extension of a model for the mixing of liquid droplets. This model is similar to a Poisson process [34], and is most easily interpreted in terms of its corresponding particle equations. For an ensemble of N particles, the MC model selects $N\Omega_{\phi} dt$ particle pairs at random for pairwise-exchange mixing according to:

$$\phi^{p,t+\Delta t} = \phi^{p,t} + \frac{1}{2}a(\phi^{q,t} - \phi^{p,t}) \quad (1.10)$$

$$\phi^{q,t+\Delta t} = \phi^{q,t} + \frac{1}{2}a(\phi^{p,t} - \phi^{q,t}) \quad (1.11)$$

where $a$ is a random number uniformly distributed in (0,1) and the superscripts $p$ and $q$ refer to the pair of particles being mixed. The MC model satisfies criteria i-iv, but does not naturally allow the scalar PDF to relax to Gaussian, nor does it enforce localness. In particular, this pairwise exchange model allows for particles to mix across a strongly burning flame front due to its non-localness, and thus is found to perform poorly at high Damköhler number, where molecular transport and chemical reaction are tightly coupled [57]. Similar to the IEM model, the MC model is also widely adopted due to its simplicity and realizability.

The Euclidean minimum spanning tree (EMST) [51,57] is a complex particle-interaction model developed specifically to enforce criteria vi, mixing that is local in composition space. In this model, an EMST is constructed for an ensemble of particles based on their composition to determine the proximity of the particles to each other in composition space. Once the EMST is constructed, mixing pairs are selected based on their proximity in composition space, and the compositions evolve according to

$$\phi_\alpha^{t+\Delta t} = \phi_\alpha^t + bB_n\left(\phi_\beta^t - \phi_\alpha^t\right) \quad (1.12)$$

$$\phi_\beta^{t+\Delta t} = \phi_\beta^t + bB_n\left(\phi_\alpha^t - \phi_\beta^t\right) \quad (1.13)$$

where the subscripts $\alpha$ and $\beta$ denote two particles in a mixing pair, $b$ is determined by the scalar mixing frequency, and $B_n$ is a factor related to the proximity of the mixing pair to the center of the EMST in composition space. The EMST mixing model satisfies the conservation of means, decay of variances, boundedness, and most notably, the localness model principles. The compromise in model development to achieve localness is that the EMST model does not satisfy the principles of linearity and independence. The ability to enforce local mixing has shown promising improvements to the TPDF

method in the context of non-premixed flames with extinction and reignition [41,57]. While the EMST model is much more complex than the IEM or MC models, the routines used to implement the model have been made readily available [58], and thus it has become widely used in TPDF studies.

While the IEM, MC, and EMST models are widely implemented in the TPDF methods due to the simplicity of their implementation and realizability, many other creative attempts to close the micro-mixing term have also been constructed. Approaches such as the binomial Langevin model [59] and the mapping closure mixing model [60,61] have demonstrated excellent performance in simple test cases, however suffer from an implementation dependence on the species ordering as noted in [62]. Other stochastic mixing model approaches include the Fokker-Planck closure models of [49], which require the specification of the joint conditional scalar dissipation rate, a challenging task in its own right. More recently, the shadow position mixing model (SPMM) was proposed that is approximately local in composition space while maintaining the principles of linearity and independence [63]. Initial tests of this model for non-premixed flames have shown promising results, but difficulties in conditioning variables on the shadow position and the model sensitivity to input parameters have been identified [63-65].

The ability of the TPDF method and existing mixing models to capture complex phenomena such as extinction and re-ignition has been well demonstrated for non-premixed flames for a variety of experimental and computational configurations [37,41]. In contrast, fewer studies have been performed using the TPDF method in the context of premixed flames. Due to the complex coupling of molecular mixing and reaction in premixed flames, the accuracy of the molecular mixing models is critical for the overall performance of TPDF method. Pope and Anand [66] were among the first to study premixed flames with the TPDF method. They studied idealized premixed flames with one-step chemistry in both the flamelet and distributed reaction regimes, and suggested closing the molecular mixing term in the former by mapping the solution to a 1D, freely propagating premixed laminar flame. The results for the test cases studied showed distinctly different behavior of the TPDF solution between the

flamelet and distributed modes of combustion, but no comparison to experiments or DNS was made. Mura et al. [67] extended the model of Pope and Anand to account for the disruption of the preheat and post-flame zones by turbulence. The authors used their extended model to simulate the Bunsen burner in Ref. [68] and report qualitative agreement with the experimental results. It is unclear whether the discrepancy between this modeling method and the measurements is due to the micro-mixing modeling approach itself, or other aspects of the simulation such as the simplified chemistry or choice of turbulence model. Regardless, while promising developments have been demonstrated in this approach to closing the mixing term, the assumption of embedded laminar flamelets limits the generality of the TPDF method, making this type of closure unattractive from the broader perspective.

Several studies of simplified premixed combustion have been performed with more general mixing model closures. Correa [69] compared the performance of the IEM and MC mixing models in a partially stirred reactor (PaSR) with detailed chemistry. The mixing models demonstrated significantly different results even in a simplified flow environment, and a high degree of sensitivity to the input scalar mixing frequency. Bisseti et al. [70] applied the TPDF method to the homogeneous charge compression ignition (HCCI) DNS database in Ref. [71]. The IEM, MC, and EMST mixing models were compared and showed good agreement with the DNS in this simple geometric configuration. However, the authors similarly report a strong sensitivity to the specification of the scalar mixing frequency.

In a study of propagating turbulent flames, Hulek and Lindstedt [72] compared the binomial Langevin closure of the micro-mixing term coupled with simplified chemistry. Favorable agreement of the computed turbulent burning velocity with experimental measurements was found for low turbulence intensities, with much poorer agreement found at higher intensities. The poor agreement in this study is speculated to be due to the mixing model closure and the simplified chemistry. Similarly, Cannon et al. [73] performed a TPDF simulation of a lean bluff body stabilized premixed flame with

the IEM mixing model and found qualitative agreement with experimental data, pointing to the mixing model and mixing rate as the likely sources of modeling error.

Lindstedt and Vaos [74,75] found that the mixing models have a crucial impact on the computed turbulent burning velocities and that some mixing models suffer from significant shortcomings. In a study of piloted premixed flames, the authors found that the MC mixing model provided reasonable results and that modeling of the scalar mixing frequency was of high importance. Algebraic closures of the scalar dissipation rate [76] and simplified chemistry were found to produce good agreement with the prediction of major species profiles. Conversely, Stöllinger et al. [77] studied a piloted premixed burner and found that existing algebraic closures to the scalar dissipation rate, including that of Kuan et al. [76], were not capable of reproducing the experimental measurements. The authors speculate that the mixing frequency model is the major shortcoming in their study and suggest further study of this topic is merited.

Finally, Rowinski and Pope recently studied a series of piloted premixed jet flames [78] with strong finite-rate chemistry effects using the joint velocity-turbulence frequency-composition PDF method [39,40]. They found that the reaction progress is over-predicted to varying degrees depending on the jet velocity and that the mixing model behavior in this combustion regime is the likely cause for the observed discrepancy in reaction progress. As in previous PDF calculations of the premixed flames, the primary aspect of the simulations called into question is the mixing model format and specification of the mechanical-to-scalar timescale ratio, which is assumed to be constant, regardless of the combustion regime.

Thus, the impetus for further development of the TPDF methodology for turbulent premixed flames is focused on exploration of the mixing model format, as well as the model for the scalar mixing frequency. The scalar mixing frequency in TPDF simulations of both premixed and non-premixed

flames is commonly assumed to be linearly proportional to the turbulence mixing frequency, as in Equation 1.14 [37], where $C_\phi$ is a model constant termed the mechanical-to-scalar timescale ratio.

$$\Omega_\phi = C_\phi \Omega_{turb} \quad (1.14)$$

However, as described in [79], reactive scalar mixing rates in turbulent premixed flames depend on the local state of both the flow turbulence and the chemical reactions, which can be characterized by the Damköhler number, $Da = \tau_{turb}/\tau_{chem}$, where $\tau_{turb}$ and $\tau_{chem}$ are characteristic turbulence and chemical timescales, respectively. In the limit of large global Damköhler number, reactions occur in propagating thin structures that resemble laminar flames and thus scalar mixing rates can be expected to strongly affected by the chemical timescales. Conversely, for low global Damköhler number, the scalar mixing rate can be expected to be controlled by the small scale turbulent motions, which in turn are driven by large-scale motions, as is found to be a reasonable approximation in studies of passive scalar mixing [34].

The importance of reactive scalar dissipation rate modeling has been recognized since the development of the BML modeling approach [9-11], which posits that the mean reaction rate of the progress variable can be expressed as

$$\bar{\dot{\omega}} = \frac{\bar{\rho}\tilde{\chi}_c}{2C_m - 1} \quad (1.15)$$

where $C_m$ is a model parameter computed from the solution of a 1D, freely propagating premixed flame. Mantel, Borghi, and coworkers [80-82] derived a transport equation for the scalar dissipation rate of a reactive scalar in constant density flow. Algebraic models for the scalar dissipation rate were proposed based on an order of magnitude analysis in the limit of large Reynolds and Damköhler numbers. However, these approaches ignored the effects of dilatation, which can be significant in turbulent premixed flames.

Swaminathan and Bray [83] extended the work of Borghi et al. to variable density flows, and derived an exact equation for the scalar dissipation rate of a reaction progress variable. The individual

terms in the governing transport equation have been studied by a number of researchers [81,84-91], and models have been proposed for the leading order terms through scaling analyses. Kolla et al. demonstrated by an order of magnitude analysis that for finite values of the Damköhler number, the exact transport equation for the Favre-averaged scalar dissipation rate of the progress variable, $\widetilde{\chi_c}$, can be approximated to leading order by the effects of dilatation, turbulence-scalar interaction, chemical reaction, and molecular dissipation as in Equation 1.16 [90].

$$\overline{2\rho\chi_c \frac{\partial u_l}{\partial x_l}} - 2\overline{\rho\Gamma_c}\left(\frac{\partial c''}{\partial x_j}\widetilde{\frac{\partial u''_j}{\partial x_k}}\frac{\partial c''}{\partial x_k}\right) + 2\left(\overline{\frac{\partial c''}{\partial x_k}\frac{\partial \dot{\omega}''}{\partial x_k}}\right) - \overline{2\rho\left(\Gamma_c \frac{\partial^2 c''}{\partial x_j \partial x_k}\right)^2} \approx 0 \qquad (1.16)$$

The terms in Equation 1.16 require closure, and the model proposed by Kolla et al. to account for the dominant physics of reactive scalar mixing can be written as:

$$\widetilde{\chi_c} = \frac{C_3}{\beta'}\frac{\tilde{\varepsilon}}{\tilde{k}}\widetilde{c''^2} + \frac{1}{\beta'}\left(2K_c^* \frac{S_L^0}{\delta_L^0} - \tau C_4 Da_L\right)\widetilde{c''^2} \qquad (1.17)$$

where $C_3$, $C_4$, and $\beta'$ are model constants; $K_c^*$ is a constant computed based on the laminar flame structure; $\tau = (T_{ad} - T_u)/T_u$ is the heat release parameter with $T_{ad}$ and $T_u$ defined as the adiabatic flame temperature and the unburnt mixture temperature, respectively; and $Da_L = \frac{S_L^0/\delta_L^0}{\tilde{\varepsilon}/\tilde{k}}$ with $S_L^0$ and $\delta_L^0$ representing the unstrained laminar flame speed and thermal thickness, respectively.

The first term in Equation 1.17 accounts for the influence of turbulence on the scalar mixing, while the second term is intended to account for the influence of the flame structure, including reaction and dilatation. Other models have been proposed in similar format with variation in treatment of the leading order terms [75,76,82]. However, as noted by Bray et al. [79], existing models of this kind do not properly recover the correct mixing limit in the flamelet limit, and further development in this area is merited.

## 1.3. Objectives and Organization of the Dissertation

The objective of this dissertation is to rigorously examine existing TPDF mixing models in the context of turbulent premixed flames and to propose a new model for the scalar mixing frequency. In Chapter 2, DNS of a premixed hydrogen-air slot jet is used as a numerical test bed to validate commonly used mixing model formats. It is found that the EMST mixing model performs significantly better than the IEM and MC mixing models if an accurate model for the scalar mixing frequency can be provided. Further, it is reported that the commonly used constant mechanical-to-scalar timescale ratio approach to modeling the scalar mixing frequency is not a viable approach for turbulent premixed flames. In Chapter 3, chemical explosive mode analysis (CEMA) and DNS data with realistic chemistry is used to identify physiochemical processes that govern the conditional scalar dissipation rate behavior and evaluate mixing timescales. A local Damköhler number is defined based on the CEMA results and four flame zones are identified. Two mechanisms have been identified that account for the large degree of scalar dissipation rate scatter: flame-flame interactions and flame-assisted ignition.

A model for the Favre-averaged scalar dissipation rate is developed in Chapter 4 based on the insight gleaned from the CEMA study. The hybrid model accounts for mixing rates in both the turbulence-dominated and flamelet-like combustion regimes. The new model is validated using an *a priori* DNS study and an *a posteriori* TPDF simulation. In Chapter 5, the transport equation for the conditional scalar dissipation rate of a reactive scalar is derived and an order of magnitude analysis performed to evaluate the importance of each term in the governing equation. The order of magnitude analysis is verified with the DNS data of turbulent premixed flames and an equation of the leading order terms is identified. Models for the unclosed terms in the leading order equation are developed and evaluated with DNS data, leading to a new model for the conditional scalar dissipation rate. Finally, in Chapter 6, a summary of the dissertation is presented and recommendations for future work are made.

1.4. List of Peer-Reviewed Publications

- **Kuron, M.**, Hawkes, E.R., Ren, Z., Tang, J.C.K., Zhou, H., Chen, J.H., Lu, T., "Performance of Transported PDF Mixing Models in a Turbulent Premixed Flame", *Proceedings of the Combustion Institute*, 2016, In Press
- **Kuron, M.**, Ren, Z., Hawkes, E.R., Zhou, H., Kolla, H., Chen, J.H., Lu, T., "A Mixing Timescale Model for TPDF Simulations of Turbulent Premixed Flames", *Combustion and Flame*, Accepted.
- **Kuron, M.**, Ren, Z., Swaminathan, N., Kolla, H., Chen, J.H., Lu, T., "Analysis and Modeling of the Conditional Scalar Dissipation Rate Transport Equation for a Turbulent Premixed Flame", *Combustion and Flame*, In preparation
- Ren, Z., **Kuron, M.**, Zhao, X., Lu, T., Chen, J.H., "Micro-mixing Models for PDF Simulations of Turbulent Premixed Flames", *Combustion Science and Technology*, Submitted.

# Chapter 2: Mixing Model Performance in a Turbulent Premixed Flame

## 2.1. Introduction

As mentioned in Chapter 1, the ability of the TPDF method to capture complex phenomena such as extinction and re-ignition has been well demonstrated for non-premixed flames for a variety of experimental and computational configurations [37,41]. In contrast, fewer studies have been performed using the TPDF method in the context of premixed flames. Due to the complex coupling of molecular mixing and reaction in premixed flames, the accuracy of molecular mixing models is critical for the overall performance of TPDF and it is necessary to systematically assess the performance of these mixing models for simulating premixed combustion. Several studies have been performed [77,92,93] for this purpose using widely adopted mixing models such as the Interaction by Exchange with the Mean (IEM) [52], Modified Curl (MC) [54,55], and Euclidean Minimum Spanning Tree (EMST) [51]. While it has been posited that the mixing model is the primary source of error [39], it is not clear whether the error is due to the mixing model formulation or other modelled features, such as the scalar mixing rate.

In the present study, DNS of a temporally evolving premixed Hydrogen-Air slot jet [94] is used as a numerical test bed to evaluate the IEM, MC and EMST mixing models in the context of turbulent premixed flames. The DNS database is used to supply the initial conditions and all time varying inputs to the governing equations in the composition TPDF method, including the mean velocity, turbulent diffusion coefficient, and mixing rate. The same thermodynamic properties and chemical reaction mechanism used in the DNS are used in the TPDF simulations to limit the potential sources of modeling error to the mixing model. The aim of this study is to rigorously benchmark the performance of the three mixing models using DNS data to assess their suitability for turbulent premixed flames. The effects of different progress variable definitions on the model performance, as well as the conditional diffusion and turbulent flame speed implied by each mixing model, are explored. Furthermore, in

practical implementations of the TPDF methods, the mixing rate is often modelled as being linearly proportional to the turbulent time scale with a constant coefficient $C_\phi$, which must be chosen *a priori* and is an approach founded on the basis of passive scalar mixing. The viability of using a constant $C_\phi$ for reactive scalar mixing is also evaluated in the present study.

## 2.2. Analysis Methodology

### *2.2.1. DNS Configuration*

The 3-D DNS dataset of a lean $H_2$-air turbulent premixed flame with detailed chemistry in [94] is used as the basis for the TPDF simulations. The configuration is described in detail in [94] and is only summarized here. In the simulation, two initially planar flames propagate into a slab of fresh reactants in the domain center, with strong turbulence sustained by the mean shear. The flames begin to interact with the shear layer after the $11^{th}$ jet time and the sheared turbulence is fully developed after 14 jet times, with the maximum flame wrinkling occurring near the $17^{th}$ jet time. The temperature of the unburned reactants is 700 K, the background pressure is atmospheric, and the equivalence ratio is $\phi$ = 0.7.

The physical domain is 16H x 20H x 12H in the x, y, and z directions, respectively, where H is the initial fuel jet thickness. The size was selected to provide adequate statistical convergence and avoid scale-saturation over the simulation period. The grid number of ~7 billion is selected to resolve the flame thickness with at least 14 grid points while the ratio of the Kolmogorov scale to grid size was 0.5, following standard practice [5]. The boundaries in the streamwise (x) and spanwise (z) directions are periodic while the boundaries in the transverse direction (y) are treated as non-reflecting outflows. The simulation was performed using the Sandia DNS code, S3D [95]. A detailed chemical kinetic model of hydrogen oxidation with 9 species and 21 reversible chemical reactions was employed [96], along with mixture-averaged molecular transport. The DNS configuration allows for RANS averaging in the streamwise and spanwise directions, as well as the use of symmetry across the domain centerline

in the transverse direction. After averaging, the simulation is reduced to statistical dependence on the transverse direction and time. Three cases are simulated in [94] by fixing the jet Reynolds number at $Re_{jet} = UH/\nu_0 = 10{,}000$ and varying the jet Damköhler number, where U is the jet velocity and $\nu_0$ is the unburnt mixture viscosity. Each case is separated by a factor of approximately two in jet Damköhler number. From the three cases simulated, the two cases "$Da^-$" and "$Da^+$" are selected for the present study, which differ by a factor of four in Damköhler number. Relevant simulation parameters for each case are summarized in Table 2-1.

Table 2-1: Hydrogen-Air Slot Jet DNS Parameters

| | Case $Da^-$ | Case $Da^+$ |
|---|---|---|
| $Da_{jet}$ | 0.13 | 0.54 |
| H (mm) | 2.7 | 5.4 |
| U (m/s) | 312.6 | 156.3 |
| $\Delta x$ (μm) | 18 | 36 |
| $\Delta t$ (ns) | 2.5 | 5 |
| $t_j = H/U$ (s) | 8.64e-6 | 3.45e-5 |
| $S_L$ | 7.9 m/s | |
| $\delta_L$ | 0.503 mm | |

Figure 2-1b shows the trajectories on a regime diagram of the point in the domain that has the maximum turbulent Reynolds number, $Re_t = u"l_t/\tilde{\nu}$, at a given time where $u"$ is the RMS velocity fluctuation and $l_t$ is the integral length scale of the initial turbulence field, while $\tilde{\nu}$ is the mean viscosity. The trajectories are colored by the simulation time normalized by the characteristic jet time. The peak $Re_t$ for each case is approximately 1,000 and the Karlovitz number at the point of peak Reynolds number is 92 in Case $Da^-$ and 22 in Case $Da^+$. The regime diagram shows that Case $Da^-$ has Da smaller than unity throughout the simulation, while Case $Da^+$ always has Da greater than unity. Based on the non-dimensional flame parameters, both cases are in what is usually characterized as the thin reaction zones regime.

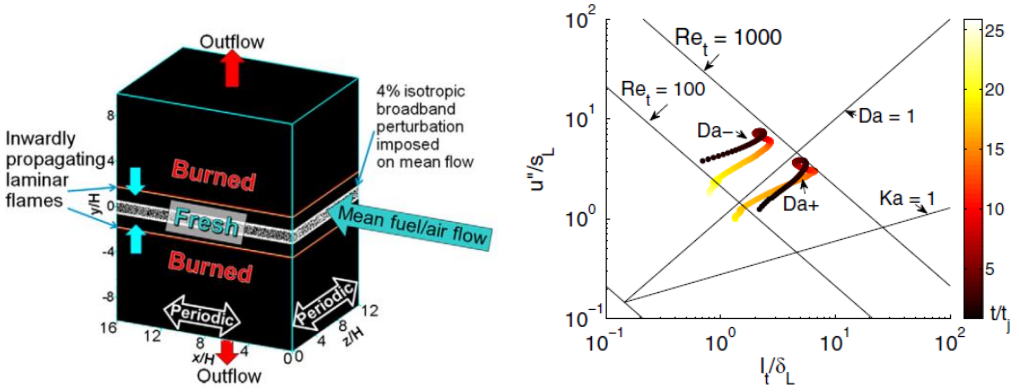


Figure 2-1: DNS configuration diagram (left) and regime diagram, reproduced from Hawkes et. al. [13]

### *2.2.2. TPDF Solution Methodology*

The TPDF solver has been implemented using a hybrid particle-mesh methodology in the RANS context as in a previous study of mixing models in non-premixed flames by Krisman et. al. [9]. A 1-D Eulerian mesh is created with the extents in the transverse direction of half of the DNS domain on account of the symmetry about the centerline. The Eulerian mesh is populated with notional Lagrangian particles which obey the set of governing stochastic differential equations, Equations 2.1 and 2.2 [2,9], which solve for transport in physical and composition space:

$$\mathrm{dx}^*(\mathrm{t}) = \left[\tilde{\nabla} + \frac{\nabla \widetilde{\Gamma}_t \overline{\rho}}{\overline{\rho}}\right]\mathrm{dt} + \left(2\widetilde{\Gamma}_t\right)^{1/2}\mathrm{dW} \qquad (2.1)$$

$$\mathrm{d}\phi^*(\mathrm{t}) = [\mathrm{m}]\mathrm{dt} + \dot{\omega}(\phi^*)\mathrm{dt} \qquad (2.2)$$

where $x^*$ and $\boldsymbol{\phi}^*$ are the spatial location and composition, respectively, of a particle, $\tilde{V}$is the mean transverse velocity, $\tilde{\Gamma}_t$ is the turbulent diffusion coefficient, $dW$ is the increment of a Wiener process, $\dot{\omega}(\boldsymbol{\phi}^*)$ is the chemical source term, and $[m]$ is the rate of change in composition due to mixing. Note that mean drift due to molecular diffusion is ignored in Eq. 2.1 as it is found that the turbulent diffusion coefficient is larger than the molecular diffusion coefficient by at least an order of magnitude throughout the flame brush.

The mean transverse velocity and turbulent diffusivity are both extracted directly from the DNS results at each time step and fed to the TPDF solver. The turbulent diffusion coefficient is computed as $\tilde{\Gamma}_t = \frac{|\widetilde{\rho v c} - \bar{\rho}\tilde{v}\tilde{c}|}{\bar{\rho}|\nabla\tilde{c}|}$ where $v$ is the velocity, $\rho$ is the density, and c is the progress variable [2]. Additionally, each mixing model requires as an input a mixing rate, which is defined as $\Omega = \widetilde{\chi_c}/\widetilde{c''^2}$ where $\widetilde{\chi_c}$ is the Favre-averaged scalar dissipation rate of the progress variable and $\widetilde{c''^2}$ is the Favre-averaged variance of the progress variable [2]. The scalar dissipation rate is computed as $\widetilde{\chi_c} = 2D_c\widetilde{\nabla c''\nabla c''}$, where $D_c$ is the diffusivity of the progress variable. As with the velocity and turbulent diffusion coefficient, the mixing rate is extracted from the DNS results at each time step and supplied to the TPDF solver.

For turbulent premixed flames with strong differential molecular diffusion effects, the scalar dissipation rate is sensitive to the choice of progress variable and therefore its potential impact on flame propagation and structure are also investigated in this study, the results of which are shown in the next section. The progress variable defined by a reactant species is computed as $c = (Y_R - Y_{R,u})/(Y_{R,b} - Y_{R,u})$, while the progress variable defined by a product species is computed as $c = Y_P/Y_{P,b}$ , where the subscripts u and b refer to the unburnt and equilibrium states, respectively.

All input data required by the TPDF solver has been computed by Favre-averaging the DNS data in the statistically homogeneous x and z directions at each time step. The variation of representative input data for Case Da$^-$ in space and time is shown for different progress variable definitions in Figure 2-2 and Figure 2-3. The simulations are initialized from the DNS data at the 11$^{th}$ jet time, which is when the flame begins to interact with the shear layer.

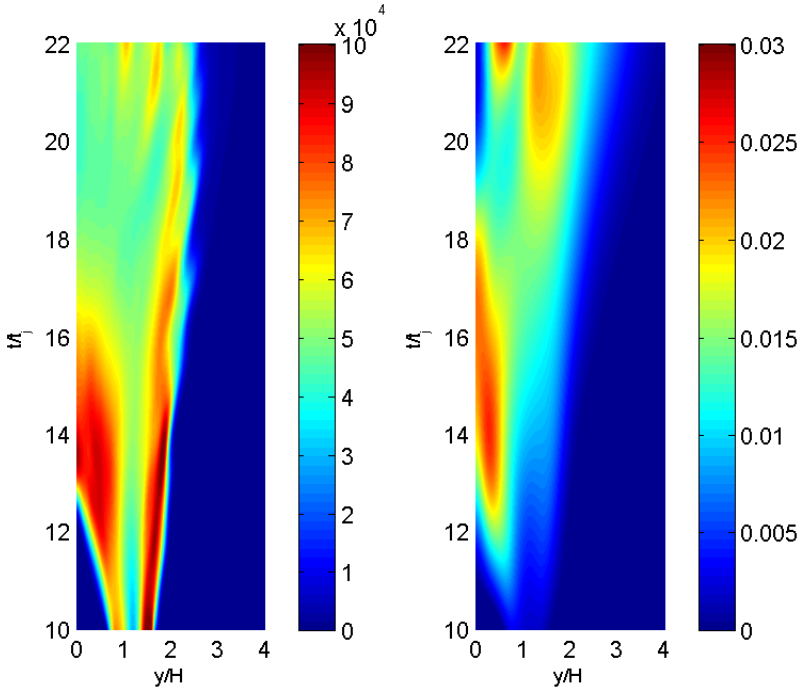


Figure 2-2: Input quantities for Case Da- with progress variable defined by the mass fraction of $H_2$. Left: Scalar mixing rate, (1/s). Right: turbulent diffusion coefficient, ($m^2$/s).

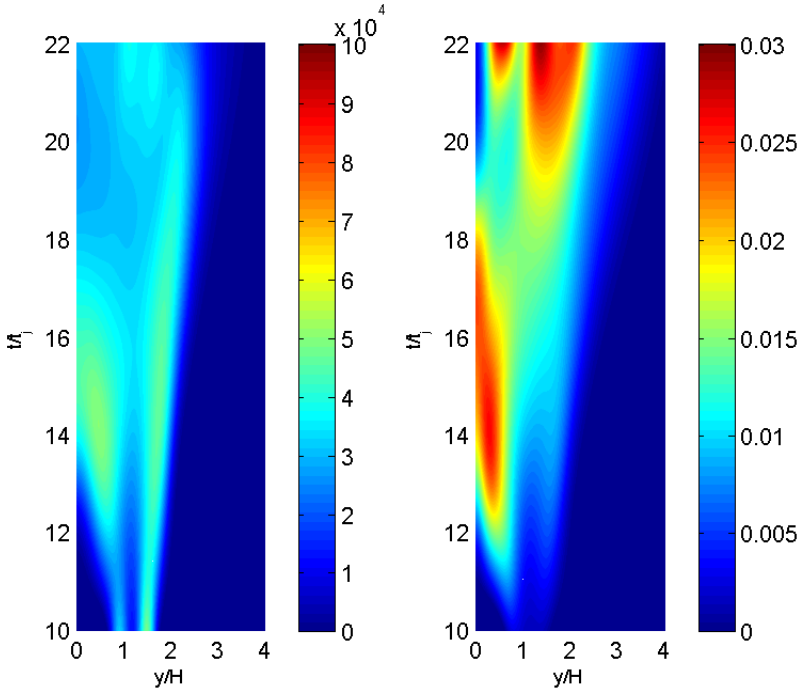


Figure 2-3: Input quantities for Case Da- with progress variable defined by the mass fraction of $O_2$. Left: Scalar mixing rate, (1/s). Right: turbulent diffusion coefficient, ($m^2$/s).

### *2.2.3. Micro-Mixing Models*

The features and limitations of the three mixing models compared in this study have been previously discussed in Chapter 1, and are only briefly reviewed here. The IEM model is deterministic and forces the particle compositions to linearly relax to the local mean. The MC model is a stochastic model which randomly pairs particles within a cell whose compositions instantaneously change to an intermediate state. The EMST model is a stochastic model that organizes the particles within a cell into a minimum spanning tree such that pairwise mixing only occurs between particles that are nearest neighbors in composition space. The IEM and MC models are both simplistic in nature. For instance, the IEM model is only strictly valid for passive scalars in a statistically homogenous Gaussian field [5]. The MC model places no restrictions on which particles in a cell can mix, so in practice a particle can be mixed across a strongly burning flame front [57]. The EMST model seeks to rectify these shortcomings by enforcing that mixing is local in composition space. This property ensures that only particles of similar states can be mixed, which is expected to be beneficial for premixed flames where strong coupling between mixing and reaction are present [97]. Note that in a study of these three mixing models for non-premixed flames [9], it was suggested that the simpler IEM and MC models should suffice for flames without significant local extinction, while the EMST model should be used in more challenging conditions.

In addition to the mixing format, the mixing rate plays a central role in all three mixing models. The mixing rate is often modelled as being linearly proportional to the turbulent time scale with a constant $C_\phi$, which is called into question in turbulent premixed flames where micro-mixing of reactive scalars is governed by both turbulence and chemical reactions [3,10].

## 2.3. Results and Discussion

### *2.3.1. Convergence Study*

To minimize the influence of numerical errors, a convergence study is performed to determine a suitable level of spatial and temporal resolution. The key numerical parameters are the number of Eulerian cells, $N_{cell}$; number of particles per cell, $N_{pc}$; and the time step used to integrate the TPDF equations, $t_{step}$. The convergence study has been performed using Case $Da^-$ and the IEM mixing model with the progress variable defined based on the mass fraction of $H_2$.

The sensitivity of the mean and RMS temperature profiles to the key numerical parameters are shown in Figure 2-5 and Figure 2-4, respectively. The mean values converge much more quickly than the RMS values, as expected. Thus, the numerical parameters are chosen based on the convergence of the RMS quantities. In the top row of Figure 2-4 the sensitivity to the number of Eulerian cells is shown to converge quickly as the number of cells increases. The solutions for variable number of cells are generated using 4,000 particles per cell and an integration time step of 2.5 ns. The sensitivity of the solution to the number of particles per cell, shown in the bottom row of Figure 2-5, is generated using 300 cells and an integration time step of 2.5 ns. The results demonstrate that the smoothness of the solution profiles is most sensitive to the number of particles per cell and that the solutions reach a sufficient level of smoothness at 4,000 particles per cell.

Based on the behavior observed in this convergence study, all results in this study for Case $Da^-$ are generated using 300 cells, 4,000 particles per cell, and a time step of 5 ns. A similar study has been performed for Case $Da^+$, resulting in the numerical parameters of 600 cells, 4,000 particles per cell, and a time step of 10 ns. It is noted that the TPDF solver used in this study does not perform any smoothing, and thus the convergence rate is slow and requires significantly more particles. If smoothing were to be applied, the convergence rate would be much faster, and a particle level of 20-100 particles per cell, as found elsewhere in the literature, could be expected to achieve a converged solution [98].

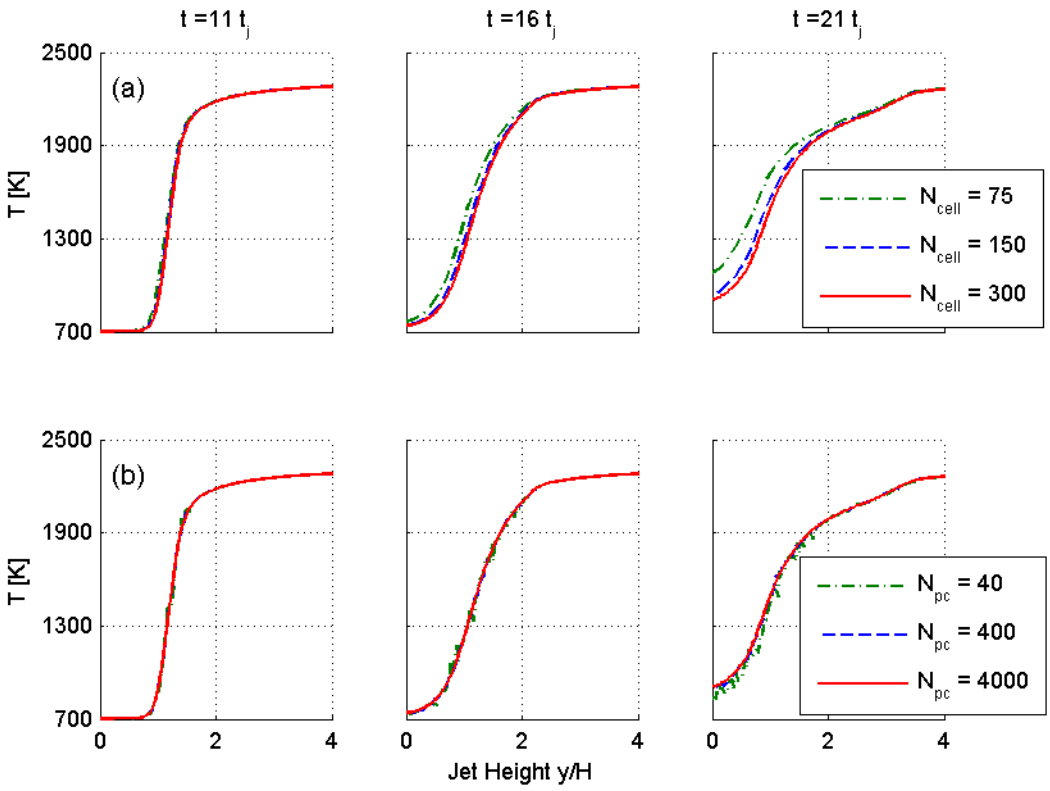


Figure 2-4: Mean Temperature convergence behavior with varying numerical parameters, Case Da-. Row (a): variable number of cells. Row (b): variable number of particles per cell.

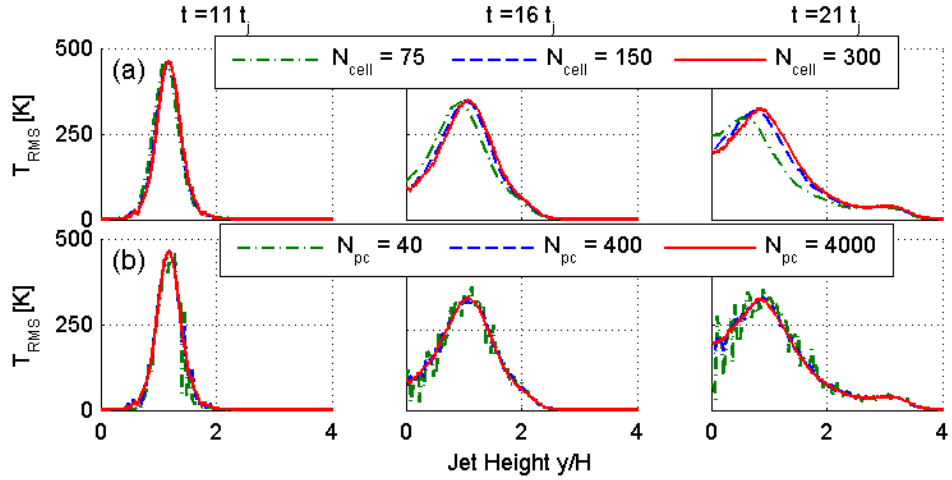


Figure 2-5: RMS Temperature convergence behavior with varying numerical parameters, Case Da-. Row (a): variable number of cells. Row (b): variable number of particles per cell.

### *2.3.2. Effects of Mixing Models on Flame Propagation and Flame Structure*

Due to the strong coupling between molecular mixing and reaction in premixed flames, the mixing model performance can have significant effects on TPDF solutions. The mixing model directly affects

the evolution of the RMS scalar values, which in turn can affect the mean scalar values through the reaction term. The temporal evolution of the mean and RMS temperature, computed using a progress variable defined on the mass fraction of $H_2$ for both DNS cases, are shown in Figure 2-6.

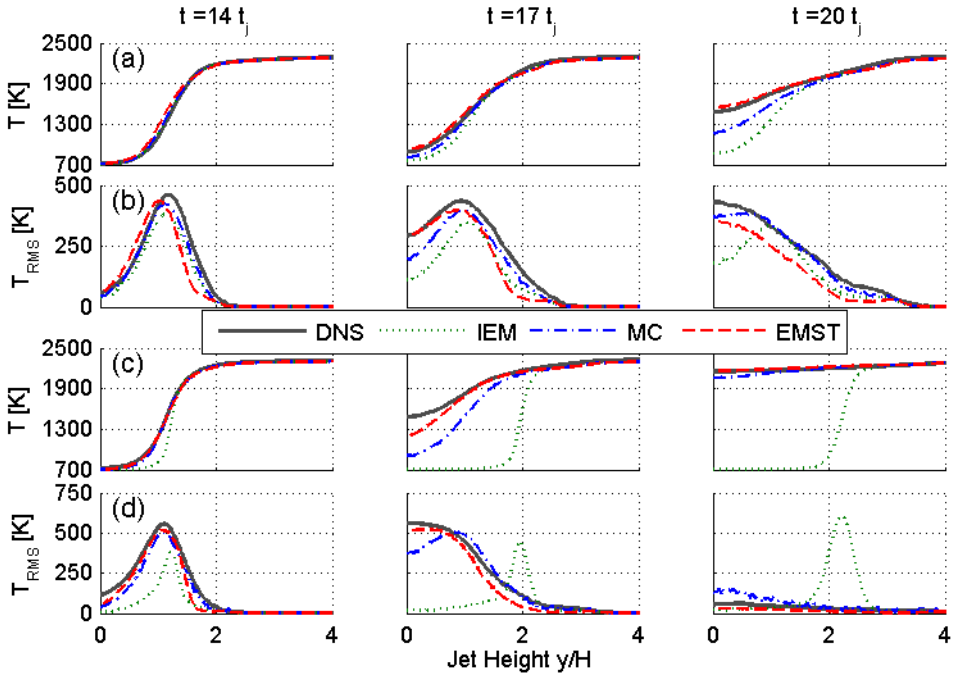


Figure 2-6: Comparison of mixing model performance at different times using the progress variable defined on $H_2$ mass fraction. Rows (a) and (b): Case $Da^-$. Rows (c) and (d): Case $Da^+$.

In both cases, the IEM model under-predicts the propagation of the mean flame profile and provides a qualitatively incorrect prediction of the spatial RMS profiles. The MC model provides better predictions of the mean flame structure than the IEM model, but still tends to under-predict the mean flame propagation speed. Similar to the IEM model, the MC model is non-local in composition space, resulting in difficulty in maintaining the correct scalar profiles. In contrast, the EMST mixing model demonstrates the best performance among the three models. It is seen that the mean DNS spatial temperature profiles are closely tracked by the EMST model, and the RMS temperature profiles are captured reasonably well for both cases. The superior performance of the EMST model can be attributed to its ability to enforce mixing that is local in composition space. This feature allows the

EMST model to reasonably approximate the flame structure while the IEM and MC models fail. The complete flame structure is plotted in Figure 2-7 through Figure 2-12 to further demonstrate the performance of each mixing model.

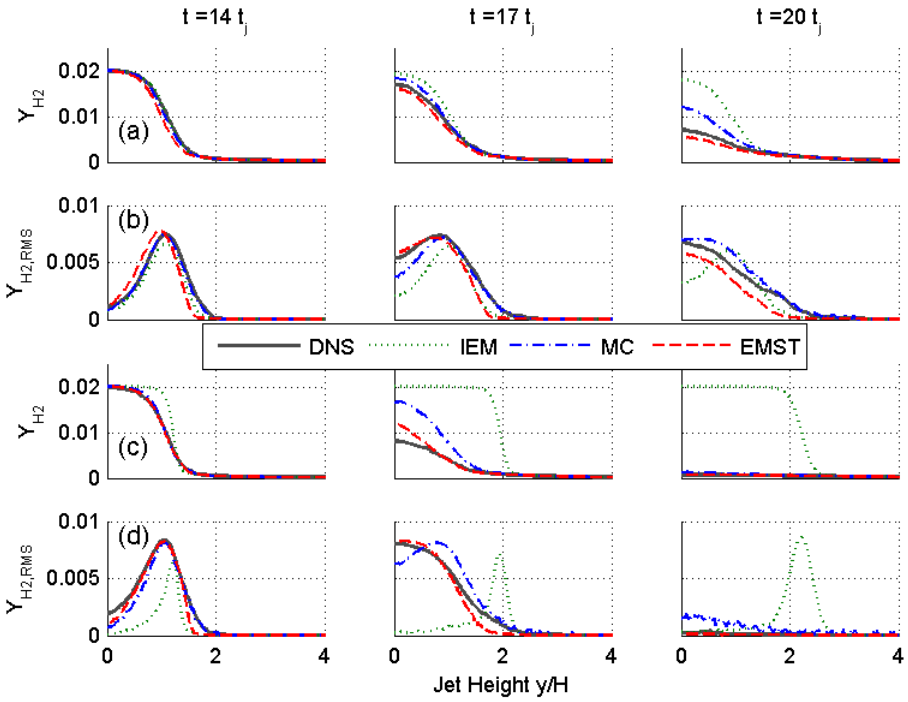


Figure 2-7: Comparison of $H_2$ mass fraction predictions over time using $H_2$ mass fraction to define the progress variable. Rows (a) and (b): Case $Da^-$. Rows (c) and (d): Case $Da^+$.

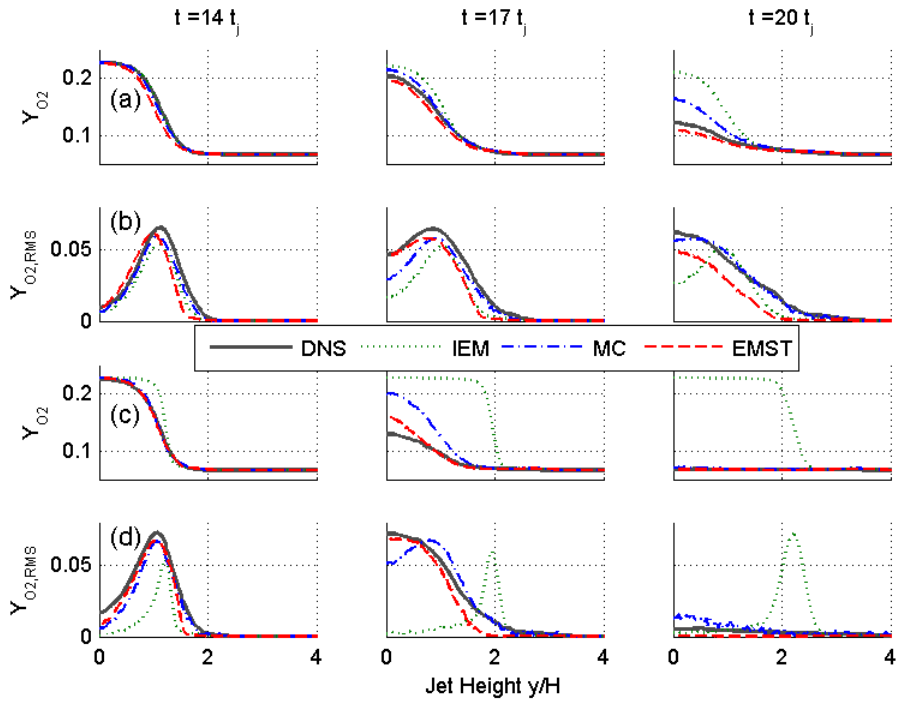


Figure 2-8: Comparison of $O_2$ mass fraction predictions over time using $H_2$ mass fraction to define the progress variable. Rows (a) and (b): Case $Da^-$. Rows (c) and (d): Case $Da^+$.

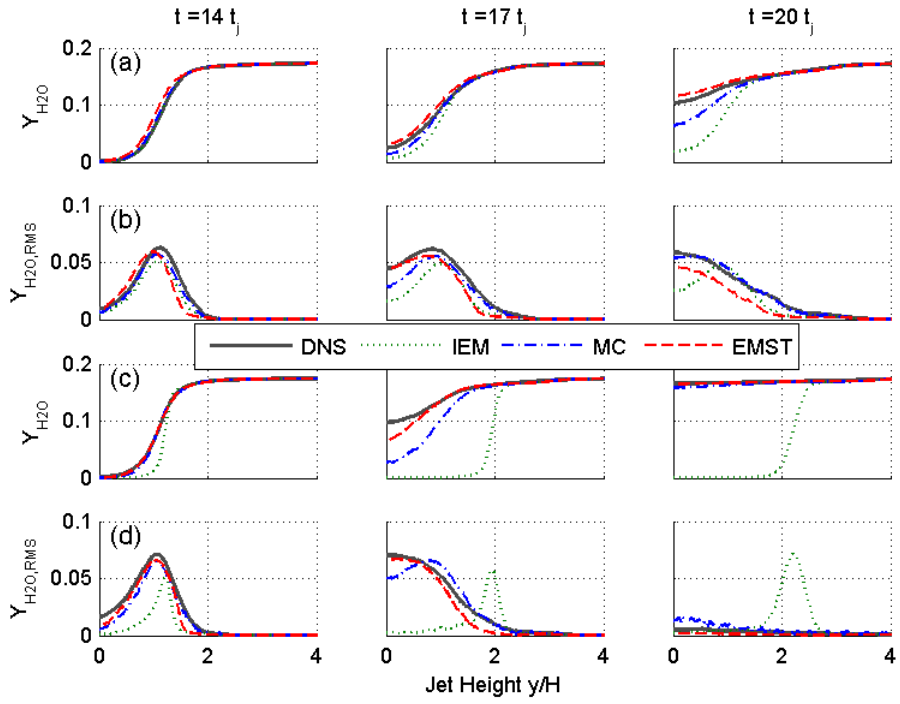


Figure 2-9: Comparison of $H_2O$ mass fraction predictions over time using $H_2$ mass fraction to define the progress variable. Rows (a) and (b): Case $Da^-$. Rows (c) and (d): Case $Da^+$.

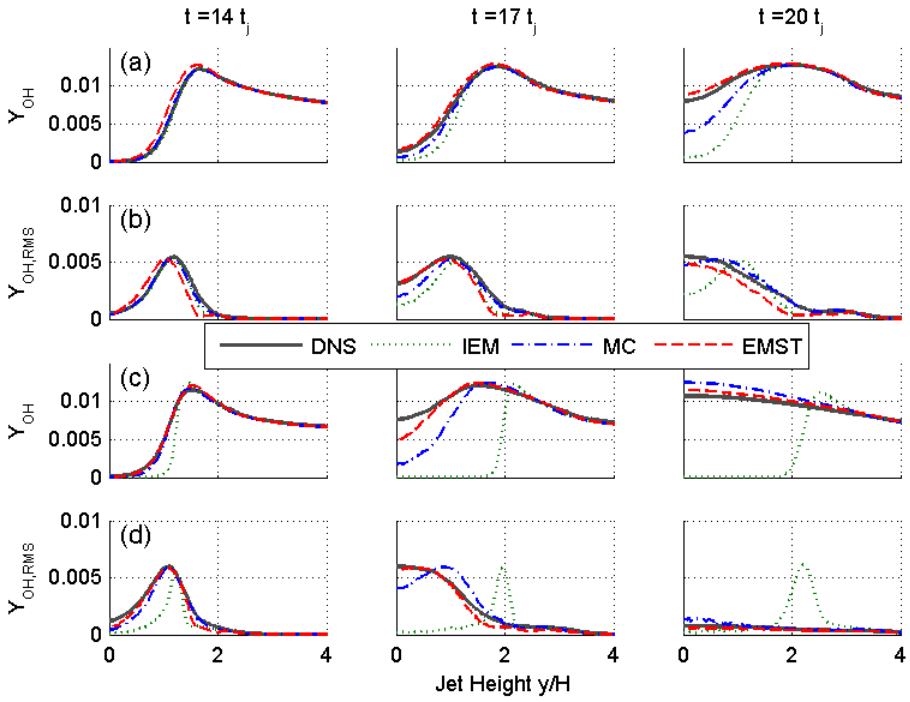


Figure 2-10: Comparison of OH mass fraction predictions over time using $H_2$ mass fraction to define the progress variable. Rows (a) and (b): Case $Da^-$. Rows (c) and (d): Case $Da^+$.

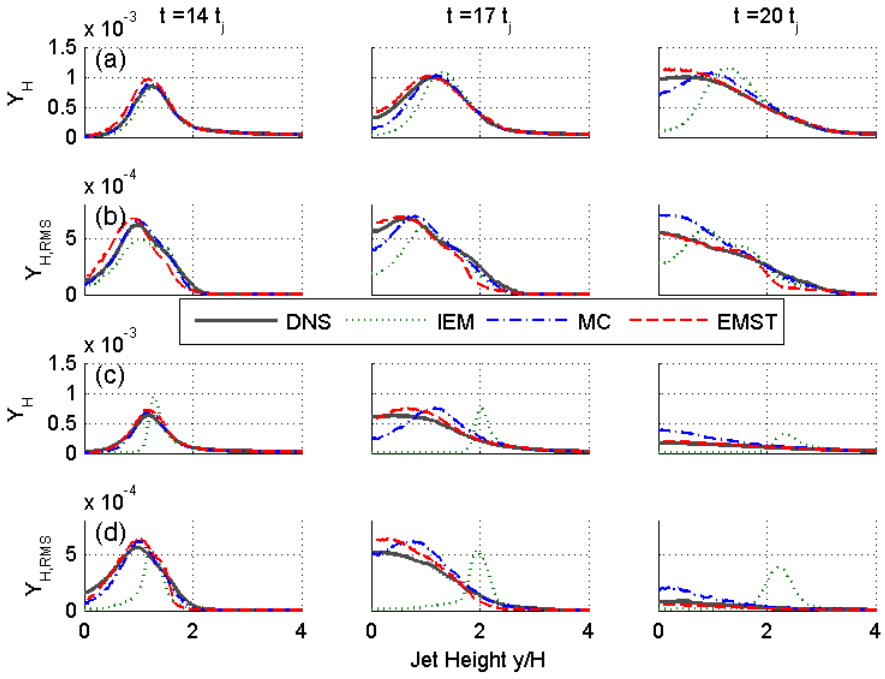


Figure 2-11: Comparison of H mass fraction predictions over time using $H_2$ mass fraction to define the progress variable. Rows (a) and (b): Case $Da^-$. Rows (c) and (d): Case $Da^+$.

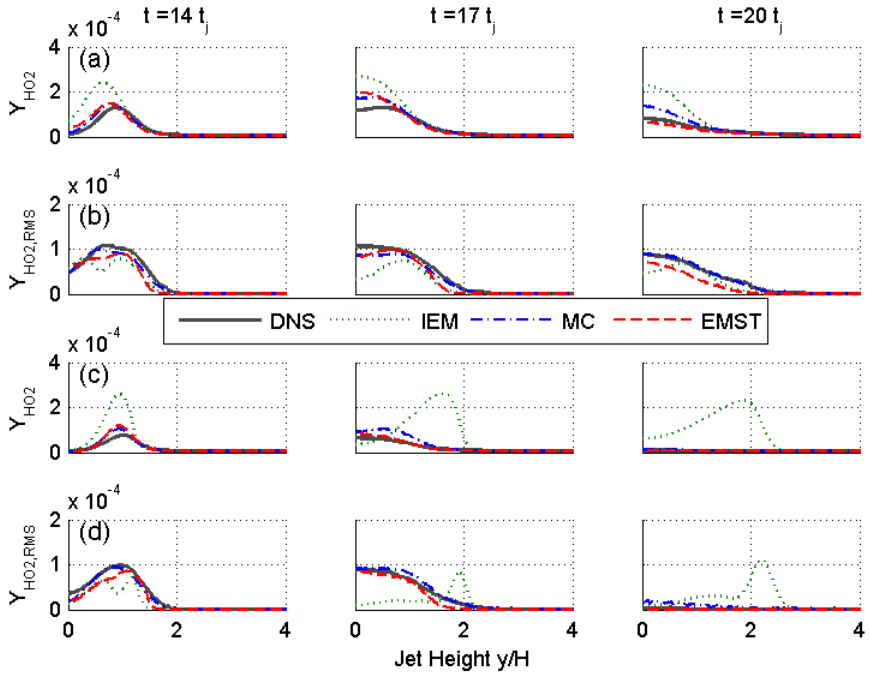


Figure 2-12: Comparison of $HO_2$ mass fraction predictions over time using $H_2$ mass fraction to define the progress variable. Rows (a) and (b): Case $Da^-$. Rows (c) and (d): Case $Da^+$.

To further quantify the effect of the mixing models on flame propagation, the turbulent flame speed, $S_T$, defined based on the global consumption rate (for comparison with the DNS data) is constructed as:

$$S_T = \frac{1}{\rho_u}\int_0^{ymax} \overline{\dot{\omega}_c}(y)\, dy \qquad (2.3)$$

where $\overline{\dot{\omega}_c}$ is the mean mass production rate of the progress variable defined based on $H_2$, and $\rho_u$ is the density in the unburnt reactants. As shown in Figure 2-13, the EMST model provides the best prediction of the flame speed variation for both cases. The MC model is reasonably accurate for Case $Da^-$, but is less accurate in the more flamelet-like Case $Da^+$, while the IEM model fails for both cases. In case $Da^-$, the flame speed for the EMST model deviates from the DNS early in the simulation. The deviation can be attributed to the EMST mixing model over-predicting the mass fractions of the radical species during the early stages of the simulation, making the mixture in the EMST results more

reactive, on average. Thus, the flame tends to propagate more quickly initially, before becoming more closely aligned with the DNS data for this case.

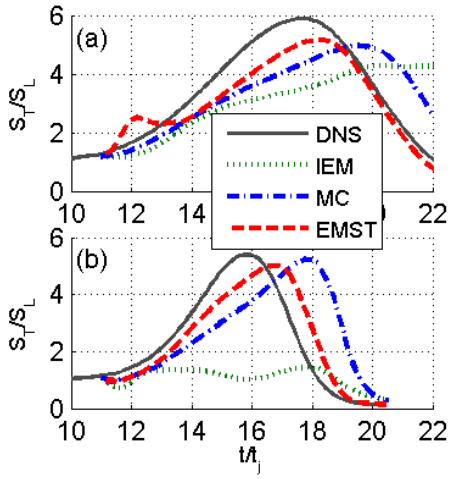


Figure 2-13: Turbulent flame speed vs. time. (a) Case $Da^-$. (b) Case $Da^+$

### *2.3.3. Differential Diffusion Effects*

For the hydrogen flame considered here, the scalar dissipation rate, and thus the mixing rate, is sensitive to the choice of progress variable due to strong differential diffusion effects. Tests on progress variables defined based on temperature and mass fractions of $H_2$, $O_2$, $H_2O$ and OH show that the mixing rates computed from $H_2$ and $O_2$ bound the solution space for this flame. As demonstrated in Figure 2-14, the TPDF solution from the EMST model is sensitive to the progress variable definition, particularly in the more flamelet-like Case $Da^+$. Similar sensitivity is observed for the IEM and MC models as well. The progress variable definition can therefore affect the TPDF solution through the mixing rate magnitude and spatial profile, as shown in Figure 2-2 and Figure 2-3. It is seen that mixing rate based on the deficient reactant, $H_2$, most closely tracks the results from the DNS, whereas the mixing rate based on $O_2$ results is the least accurate.

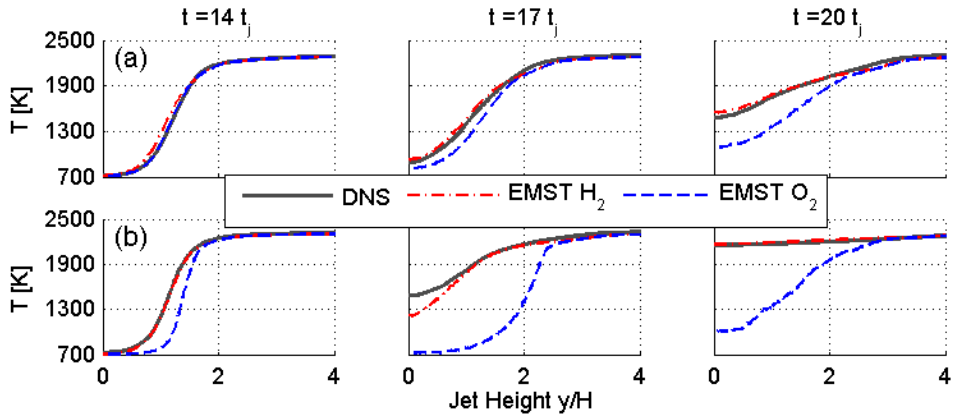


Figure 2-14: Evolution of mean temperature from the TPDF solutions with EMST for different progress variable definitions. Row (a): Case $Da^-$. Row (b): Case $Da^+$

The significant difference in the mixing rate can be partially attributed to the difference in molecular weight, indicating the important role that differential diffusion plays in this flame. Note that in the present test, all scalars are assumed to mix over the same timescale in the mixing models which renders the results sensitive to the definition of the progress variable. This effect is expected to be weaker for hydrocarbon flames where differential diffusion effects are less important.

### *2.3.4. Mixing Model Characteristics*

The qualitative behavior of each model can be evaluated by inspecting the behavior of a minor species, such as H radical, which plays in important role in the fuel oxidation process. In Figure 2-15 and Figure 2-16, scatter plots of H radical mass fraction against temperature are shown for the DNS and each mixing model at $14t_j$. The figures show qualitatively different behavior from each model; IEM pulls compositions to the center of temperature space, drawn away from the DNS conditional mean. The scatter plot for the MC mixing model demonstrates the nonlocal nature of the mixing format as notional particles with H radical mass fraction values that are an order of magnitude smaller than the conditional mean exist within the reaction zone, unlike the DNS. The EMST compositions stay near to the conditional mean, which closely tracks the DNS values, however the conditional fluctuations appear to be underestimated. The ability of each model to reproduce the conditional mean mass fraction at $14t_j$ is directly compared in Figure 2-17. Only the EMST mixing model is able to

accurately capture the conditional mean H radical mass fraction in the preheat zone, while the IEM and MC models under-predict the conditional mean by as much as an order of magnitude.

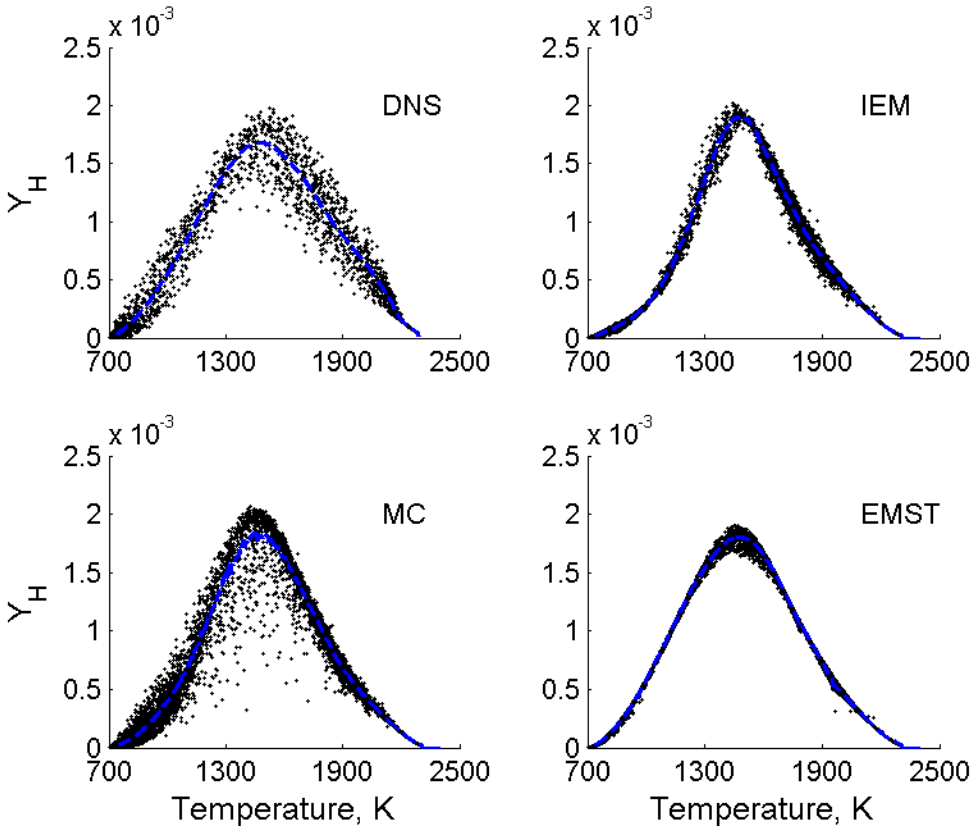


Figure 2-15: Scatter plots of H radical mass fraction, $Y_H$, against Temperature, T, from Case $Da^-$ at $14t_j$. Lines represent the mean mass fraction, $Y_H$, conditioned on Temperature.

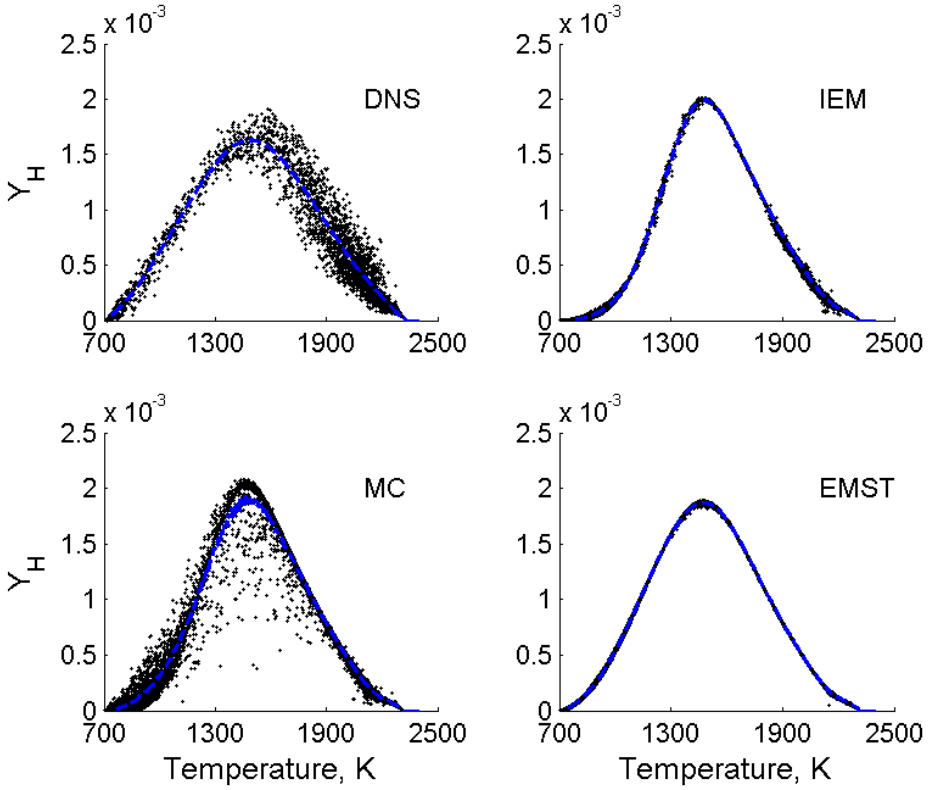


Figure 2-16: Scatter plots of H radical mass fraction, $Y_H$, against Temperature, T, from Case $Da^+$ at $14t_j$. Lines represent the mean mass fraction, $Y_H$, conditioned on Temperature.

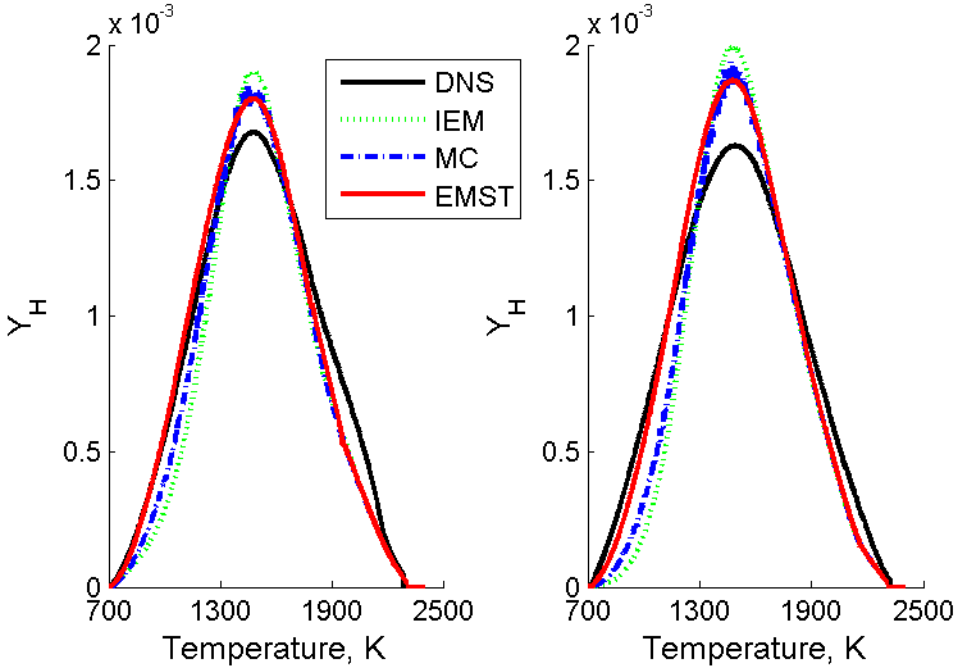


Figure 2-17: Mean $Y_H$ conditioned on Temperature at $14t_j$. Left: Case $Da^-$. Right: Case $Da^+$.

The influence of the mixing models on the evolution of the progress variable PDF's for each model is shown in Figure 2-18 and Figure 2-19. In both cases, the PDF from the DNS evolves with time, changing both shape and magnitude. In Case $Da^-$, the IEM model maintains the same PDF shape as required by the model assumptions, a clear shortcoming of this approach. The PDF implied by the MC model in Case $Da^-$ changes shape, but does not evolve to the correct profile. Finally, the PDF predicted by the EMST mixing model in Case $Da^-$ closely follows the DNS in both shape and magnitude over time. Similar behavior is seen in Case $Da^+$, with only the EMST mixing model adequately approximating the PDF at $20t_j$, where little unburnt mixture still exists in the DNS.

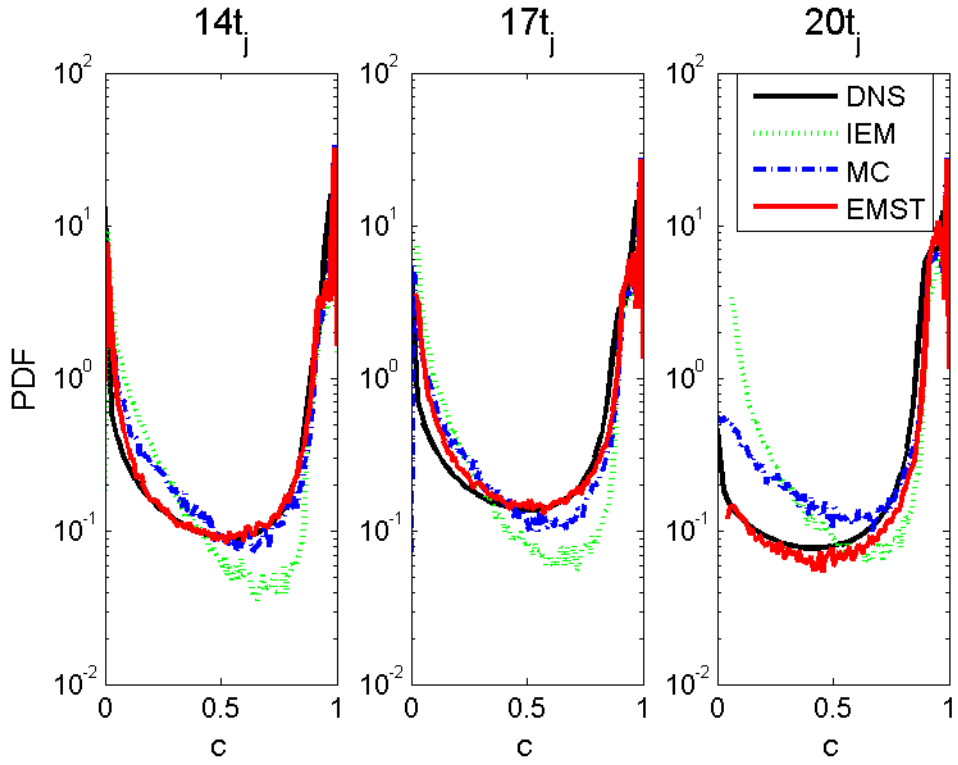


Figure 2-18: Evolution of the PDF of the progress variable for Case $Da^-$.

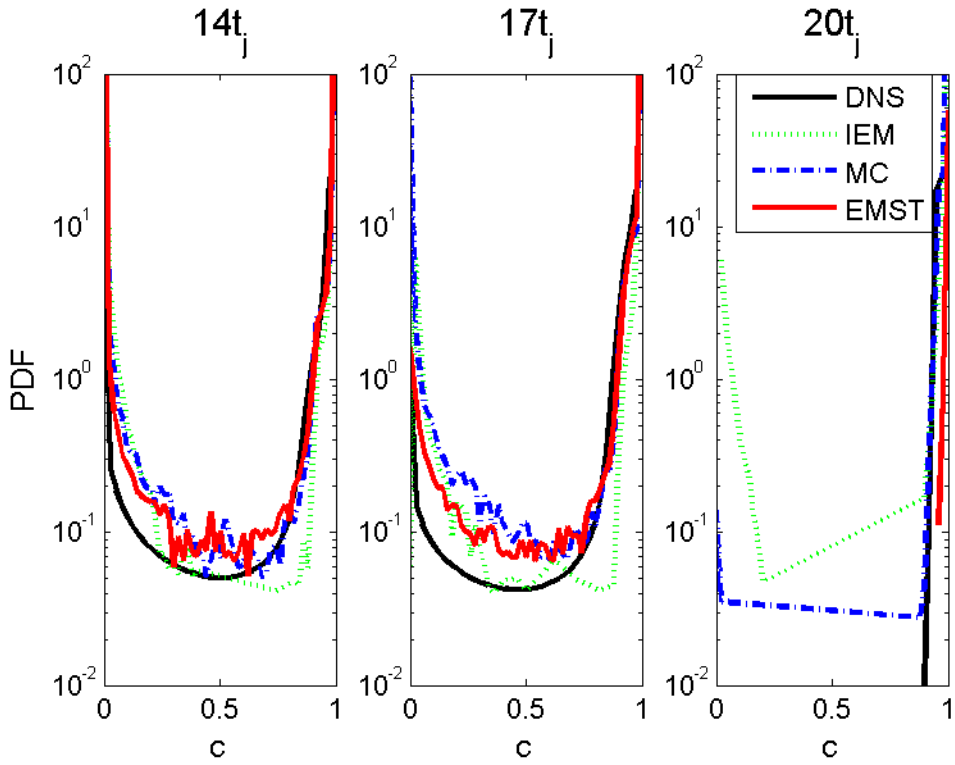


Figure 2-19: Evolution of the PDF of the progress variable for Case $Da^{+}$.

### *2.3.5. Conditional Diffusion*

The aim of each mixing model is to accurately mimic the conditional diffusion using the methods described in section 2.2.3. To evaluate the ability of each mixing model to mimic the conditional diffusion rate, we have extracted the diffusion rates conditionally averaged on the progress variable that are implied by each mixing model in the TPDF simulations for comparison to the DNS. The conditional mean diffusion rates are extracted from the DNS data by first computing the diffusion rate of each species at each grid point in the DNS domain at each time point using mixture-averaged transport properties. Then, the conditional mean diffusion rates for a given time point are computed by conditionally averaging the diffusion rate of each species on the progress variable. The conditional mean diffusion rate implied by each mixing model is computed in the TPDF solution by storing the incremental change in the composition vector due only to mixing over a given time step for each

particle. The incremental change in composition due to mixing is divided by the time step size to compute the implied diffusion rate for each species in each particle, and the particle diffusion rates are then conditionally averaged on the progress variable to compute the conditional mean diffusion rate for each mixing model at each time point.

The conditional mean diffusion rates of $H_2$ implied by each mixing model for the TPDF simulations, based on the progress variable defined on $H_2$, are shown in Figure 2-20 for both cases at time $14t_j$. It is seen that the IEM model fails to capture the correct conditional mean diffusion rate entirely, while the MC model qualitatively captures the conditional mean diffusion rate behavior but over-predicts the diffusion rate on the burned side of the flame. This inaccuracy in the diffusion rate can be attributed to the non-locality and inherent randomness of the model, which in principle allows for particles to be mixed across strongly burning flame fronts. The EMST model most accurately captures the conditional diffusion rate, implying that EMST has the correct mixing format in composition space for a turbulent premixed flame.

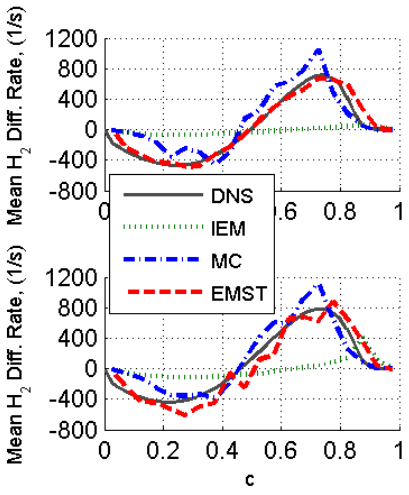


Figure 2-20: Conditional mean diffusion rates for Case $Da^-$ (top) and Case $Da^+$ (bottom) at $14t_j$.

### *2.3.6. The Mixing Rate Model*

In practical TPDF calculations the scalar mixing rate is not known *a priori* and must be modeled. In many applications, the mixing rate is assumed to be inversely proportional to the turbulent timescale, $\Omega = C_\phi \, \Omega_t = C_\phi \, \tilde{\varepsilon}/\tilde{k}$, where $\Omega_t$ is the turbulence mixing rate and can be reconstructed based on the turbulence dissipation rate, $\tilde{\varepsilon}$, and the turbulence kinetic energy, $\tilde{k}$, in the RANS context. The constant $C_\phi$ is typically assumed to be 2.0 for passive scalar mixing, although several DNS studies have shown that the optimal choice even for non-premixed flames is unclear [2]. For premixed flames, where the scalar mixing timescale is also influenced by reaction, it is questionable whether a constant mechanical-to-scalar timescale ratio is applicable. To address this question, the turbulent mixing rate is extracted from the DNS in the same manner as the scalar mixing rate and a parametric study is performed on the timescale ratio.

Figure 2-21 shows the effect of the mechanical-to-scalar timescale ratio on the TPDF solution at 17tj for both cases, after the sheared turbulence has developed from the initial conditions. For Case $Da^-$ the results indicate that the optimal value for $C_\phi$ is between 2 and 4, while for Case $Da^+$ the optimal value for $C_\phi$ is between 4 and 6. The spatial and temporal distribution of $C_\phi$ is extracted from the DNS using the mixing rate based on $H_2$ and plotted in Figure 2-22. The local value of the timescale constant varies by up to an order of magnitude. It is therefore clear that there is no single value of the mechanical-to-scalar timescale ratio that is optimal for all cases, and variation in the optimal choice of the $C_\phi$ parameter between these two cases by a factor of 2 makes the turbulent timescale a poor choice for the mixing rate. Additionally, the RMS profiles are qualitatively incorrect in the middle of the flame brush for both cases, indicating that the spatial distribution of the turbulent mixing rate is inconsistent with the spatial distribution of the scalar mixing rate.

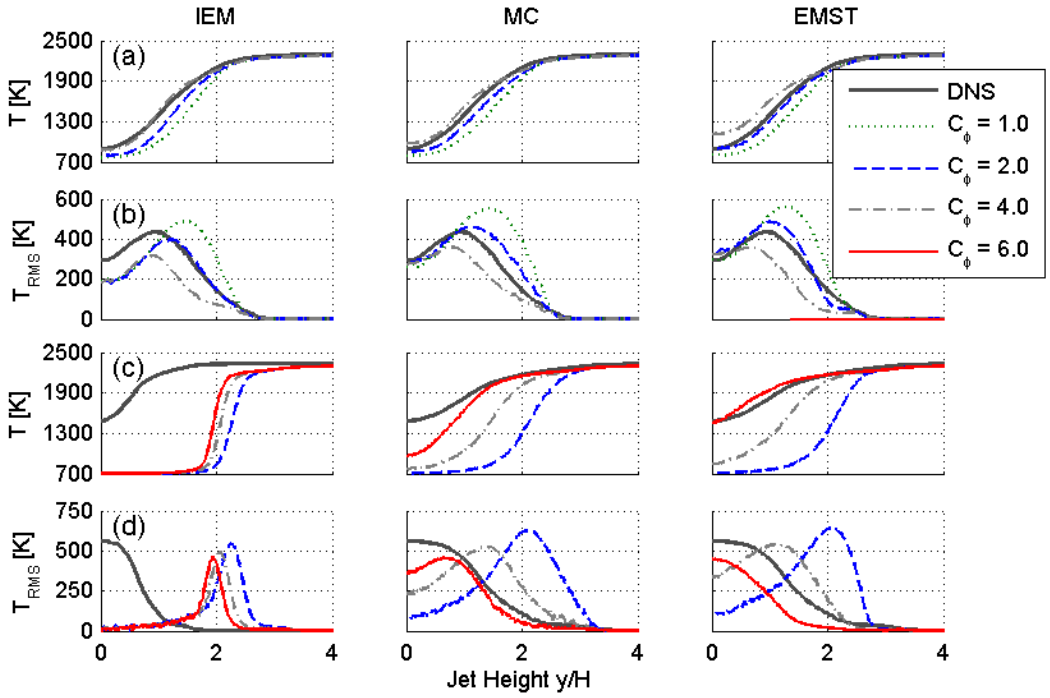


Figure 2-21: Influence of the mechanical-to-scalar timescale ratio on the TPDF solution at t = 17tj. Rows (a) and (b): Case Da$^-$. Rows (c) and (d): Case Da$^+$.

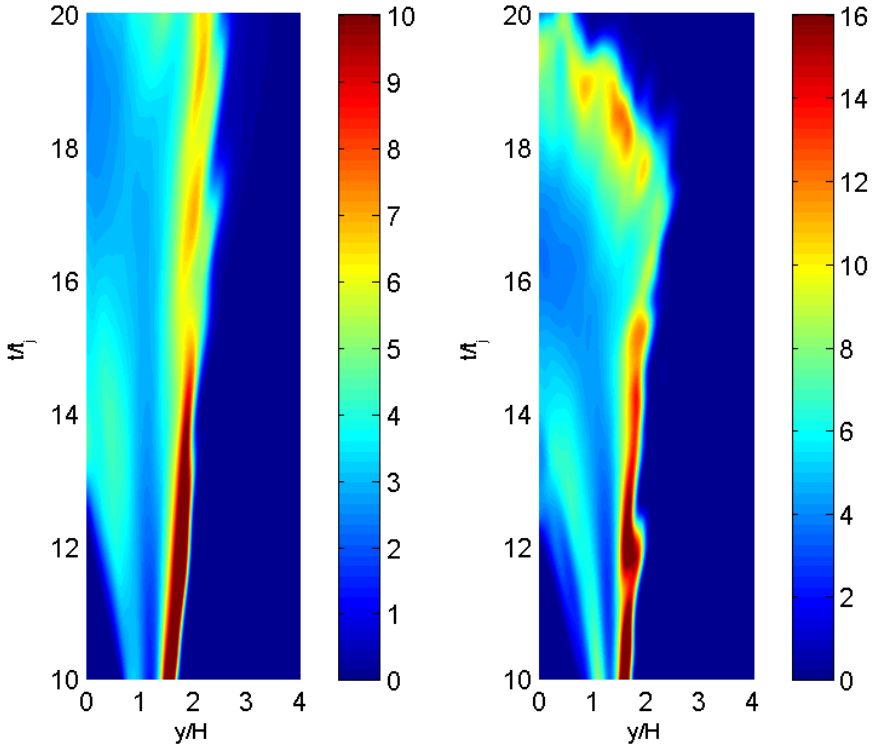


Figure 2-22: Mechanical-to-scalar timescale ratio $C_\phi = \Omega_{H2}/\Omega_t$. Left: Case Da$^-$. Right: Case Da$^+$.

## 2.4. Conclusions

Three widely adopted mixing models are evaluated in the present study in the context of the RANS composition TPDF method using DNS data of a turbulent premixed $H_2$-air flame. The methodology employed here allows for the quantification of the errors in mixing model formulations incurred in the TPDF solution. Direct comparison of the TPDF predictions of the mean and RMS values with those from the DNS reveals that the EMST mixing model provides the most accurate solutions for the present flame, and that the EMST model can accurately capture the conditional mean diffusion rates. The conditional diffusion implied by the IEM model is qualitatively incorrect for turbulent premixed flames. The MC model is able to qualitatively capture the mean conditional diffusion. The improved performance of EMST compared with IEM and MC can be attributed to the local mixing in composition space.

The commonly used method of specifying the mixing rate by assuming that it is inversely proportional to the turbulence timescale with a constant mechanical-to-scalar timescale ratio is examined. It is found that the TPDF solutions are sensitive to the mechanical-to-scalar timescale ratio, and that the optimal values for the two DNS cases differ by a factor of two. Given that such a wide variation in the optimal choice of the mechanical-to-scalar timescale ratio exists even for a flame in the same configuration, this commonly used approach does not appear to be viable for turbulent premixed flames. The development of accurate timescale models, and in particular models for the scalar dissipation rate for reactive scalar mixing merits further study, and is explored in the following chapters.

## Chapter 3: Scalar Dissipation Rate Behavior in a Turbulent Premixed Flame

### 3.1. Introduction

The mixing model study performed in Chapter 2 demonstrates the importance of accurately modeling the scalar mixing frequency in TPDF simulations. In particular, the component of the scalar mixing frequency that requires modeling is the scalar dissipation rate. This quantity has been the focus of many previous studies as the scalar dissipation rate is a quantity of fundamental importance in turbulent combustion modeling, appearing as a central parameter in many modeling approaches [7,99]. Underscoring the importance of the scalar dissipation rate is its direct link to the conditional diffusion, which appears in the governing PDF transport equation, Eqn. 1.6, by the following relation [5]

$$\frac{\partial}{\partial \psi}\left[\langle \Gamma \nabla^2 \phi | \psi \rangle f_\phi\right] = \frac{1}{2}\frac{\partial^2}{\partial \psi^2}\left[\left\langle \chi_\phi \middle| \psi \right\rangle f_\phi\right] - \Gamma \nabla^2 f_\phi. \quad (3.1)$$

In most closures of the conditional turbulent diffusion used in the transported PDF method, the conditional mean scalar dissipation rate is typically assumed to be linearly proportional to the local turbulent timescale with a constant model parameter. This assumption has proven to be useful for non-premixed combustion systems where turbulence is the rate limiting process. However, for premixed flames, it has been shown that this relationship is insufficient to accurately describe the mixing timescales and that scalar mixing may occur on scales smaller than the Kolmogorov scale due to fast chemical reactions [100].

Detailed studies of the scalar dissipation rate behavior in premixed turbulent flames have largely focused on its behavior in a Favre-averaged sense, which is suitable in RANS modelling approaches [84,87,88,101,102]. In a study of a 2-D turbulent premixed H2-air flame, Swaminathan and Bilger [103] noted the spatially intermittent nature of the scalar dissipation rate and the importance of its conditional fluctuations. The instantaneous scalar dissipation rate is defined here as

$$\chi = 2\,\Gamma\,\nabla c \cdot \nabla c \quad (3.2)$$

where $c$ is the reaction progress variable and $\Gamma$ is the relevant diffusivity. In the context of large eddy simulation (LES), the conditional scalar dissipation rate is dependent on the local flame structure and typical global modelling approaches and quasi-steady assumptions may not be appropriate. Thus, a detailed investigation of the conditional scalar dissipation rate of reactive scalars is warranted.

In the present work, computational flame diagnostics are applied with direct numerical simulation (DNS) data to study the conditional scalar dissipation rate and its fluctuation in a turbulent premixed flame of hydrogen-air subjected to intense sheared turbulence.

## 3.2. Analysis Methodology

### *3.2.1. Flame Features and Data Analysis Procedure*

The 3-D DNS dataset of a lean $H_2$-air turbulent premixed flame with detailed chemistry [94], identical to the one used in Chapter 2, is employed for analysis of the scalar dissipation rate. Data from both cases are analyzed at $11t_j$, $13t_j$, and $15t_j$, after the transition to fully developed sheared turbulence has occurred. Data for this analysis is collected from a 2H x 4H x 1.7H sub-volume of the full computational domain. The subdomain studied here extends from the centerline (y = 0) outward into one of the inwardly propagating flames, and contains approximately 55 million grid points.

2D slices of temperature isocontours of the sub-volume for the two cases at the different time instances are shown in Figure 3-1. Note that the flame becomes increasingly wrinkled in time, and eventually pockets of hot products appear near the centerline as the two opposing flames approach the domain center. The Karlovitz number (Ka) is larger than unity for both cases, and the disturbance of the preheat zone can be clearly seen. Case $Da^+$ has Ka = 22 at the instance of peak $Re_t$, while Case $Da^-$ has Ka = 92 at its corresponding instance of peak $Re_t$. Both cases are in the thin reaction zones regime.

In the present analysis, the progress variable is defined using the hydrogen mass fraction,

$$c = \left(Y_{H2} - Y_{H2,u}\right)/\left(Y_{H2,b} - Y_{H2,u}\right) \quad (3.3)$$

where $Y_{H2,u}$ and $Y_{H2,b}$ are the hydrogen mass fractions in the unburned and burned gases, respectively. The Favre conditional average of the scalar dissipation rate conditioned on the progress variable is defined as

$$\langle \chi | c \rangle_\rho = \langle \rho \chi | c \rangle / \langle \rho | c \rangle. \qquad (3.4)$$

Conditional averages are comprised of ensemble-averaged bins in progress variable space, with each bin containing approximately 50,000 sample points.

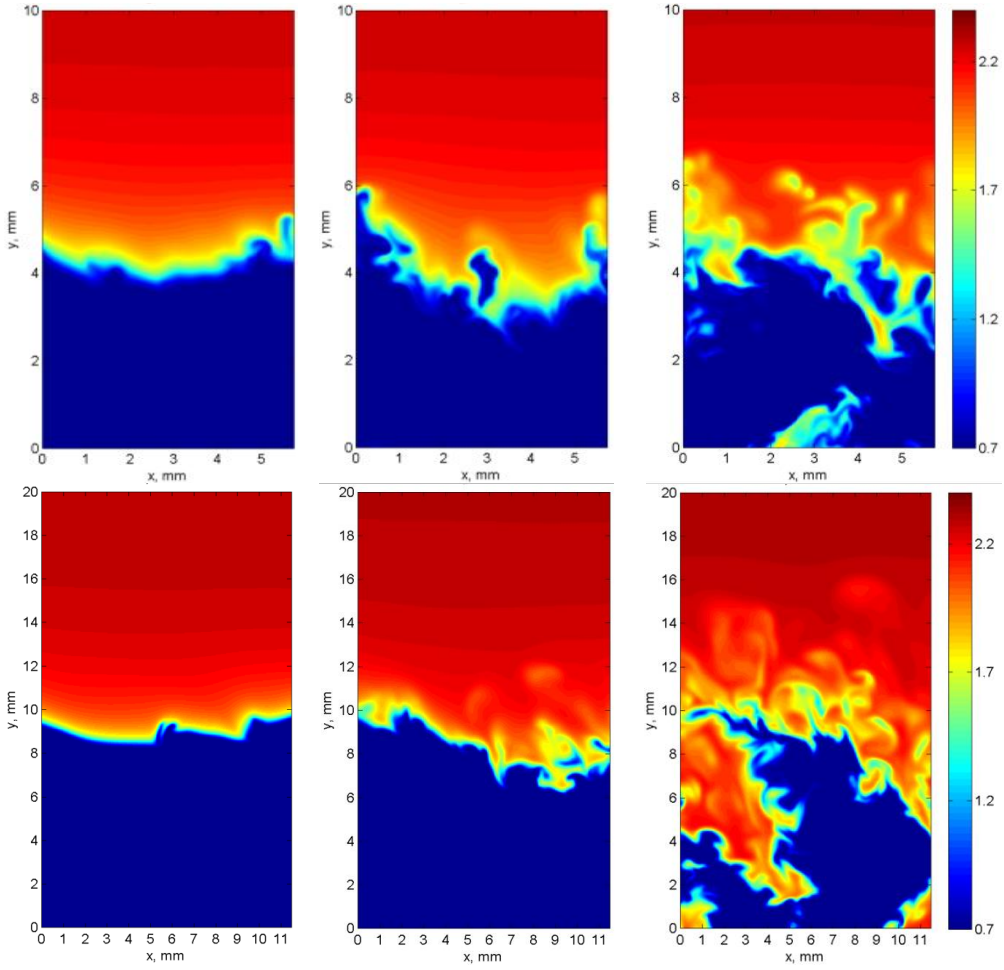


Figure 3-1: Isocontours of temperature/1,000 K of the selected sub-volume in the DNS data for $t/t_j$ = 11, 13, and 15 (left to right), and for Cases $Da^-$ (top) and $Da^+$ (bottom), respectively.

*3.2.2. CEMA for premixed flames*

To examine the flame structure and for insight into the physiochemical processes that lead to fluctuations of the scalar dissipation rate, chemical explosive mode analysis (CEMA) [104,105] is employed to identify different flame zones in the DNS data. CEMA is based on eigen-analysis of the chemical source term, $\boldsymbol{\omega}(\boldsymbol{y})$ in the governing equations of a reacting flow:

$$\frac{D\boldsymbol{y}}{Dt} = \boldsymbol{g}(\boldsymbol{y}) = \boldsymbol{\omega}(\boldsymbol{y}) + \boldsymbol{s}(\boldsymbol{y}) \quad (3.5)$$

where *D/Dt* is the material derivative and $\boldsymbol{y}$ is the vector of dependent variables (i.e. species concentrations and temperature), and $\boldsymbol{s(y)}$ is the non-chemical source term, e.g. diffusion. The local chemical properties of the mixture are encoded in the Jacobian matrix of the chemical source term:

$$\boldsymbol{J_\omega} = \partial\boldsymbol{\omega} / \partial\boldsymbol{y} \quad (3.6)$$

An eigenmode of $\boldsymbol{J_\omega}$ is a chemical mode associated with an eigenvalue as well as a pair of (left and right) eigenvectors. The non-conservative chemical mode with the largest eigenvalue is denoted the chemical explosive mode (CEM) and its eigenvalue is denoted $\lambda_e$. Mixtures with a positive real part of $\lambda_e$ , $\mathrm{Re}(\lambda_e)$, are explosive and can show igniting behavior if isolated, while $\mathrm{Re}(\lambda_e)$ is negative in post-ignition mixtures. As such the CEM can be used to distinguish between burnt and unburnt mixtures in complex flow fields. In a premixed flame, $\mathrm{Re}(\lambda_e)$ peaks in the preheat zone and becomes negative in the post-flame zone where the characteristic time scale represents the rate at which the mixture relaxes toward equilibrium. To quantify the competition between the chemistry and mixing, a local Damköhler number is defined as in Equation 3.7.

$$Da_e = \lambda_e / \chi \quad (3.7)$$

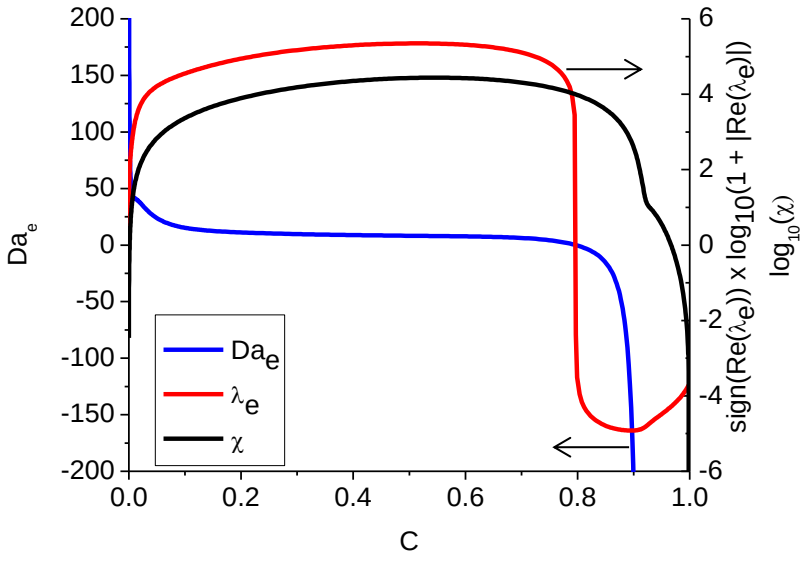


Figure 3-2: $Da_e$, $\lambda_e$, and $\chi$ as a function of progress variable, c, in a 1-D steady premixed flame at $T_0$ = 700K, $p$ = 1 atm, and $\phi$= 0.7.

The variation of $Da_e$, $\lambda_e$ and $\chi$ in a 1-D laminar freely propagating $H_2$-air flame is shown in Figure 3-2, with the inlet condition being the same as that in the DNS data. It is seen in this steady flame that $Da_e$ varies between ±100 over the majority of the flame as a function of progress variable. The value of $\lambda_e$ increases sharply in the preheat zone and remains positive through the bulk of the flame. The mixture ignites at c = 0.8 and the value of the value of $\lambda_e$ becomes negative in the post-flame zone. The value of the scalar dissipation rate peaks in the reaction zone, defined as the region $10 < Da_e < -10$, and $0.27 < c < 0.8$. In the following, CEMA is applied to the 3D DNS dataset to segment the flame into different zones and the zone-dependent behavior of the scalar dissipation rate is investigated.

## 3.3. Results and Discussion

The scatter of the instantaneous scalar dissipation rate at $t/t_j$ = 15 is shown in Figure 3-3. The solid black lines represent the conditional average of the instantaneous scalar dissipation rate, $\langle\chi|c\rangle$, and the dash-dotted black lines represent the scalar dissipation rate reconstructed from the steady 1-D premixed flame solution in Figure 3-2. Additionally, the dashed red lines represent the conditional root-mean-square of the scalar dissipation rate, which is defined as $\langle\chi|c\rangle_{RMS} = \sqrt{\langle\chi''^2|c\rangle}$ where $\chi'' = \chi - \langle\chi|c\rangle$.

Overall, the 1-D flame solution provides a reasonable approximation to the global conditional average from the DNS data. Case $Da^-$ shows more severe scatter of the scalar dissipation rate than in Case $Da^+$, because the flame in Case $Da^+$ is less disturbed, having a Damköhler number larger by a factor of approximately four.

The agreement between the 1-D steady laminar flame solution and the global conditional mean is good also at the earlier time points analyzed, not shown here for conciseness. The degree of scatter in the instantaneous scalar dissipation rate increases with time as the flame front interaction with the flow increases which is observed in the temperature field in Figure 3-2. The local deviation of the instantaneous scalar dissipation rate from the global mean is orders of magnitude, as illustrated by the magnitude of the conditional RMS in Figure 3-3, which is larger than the conditional mean for both cases. Hence, the global conditional mean statistics are a poor approximation of the local flame behavior, particularly in the preheat zone where mixing is dominant. Since accurate prediction of the mixing rate is crucial for capturing local flame propagation, accurately capturing the variance of the instantaneous scalar dissipation rate is an important modeling consideration for turbulent premixed flames.

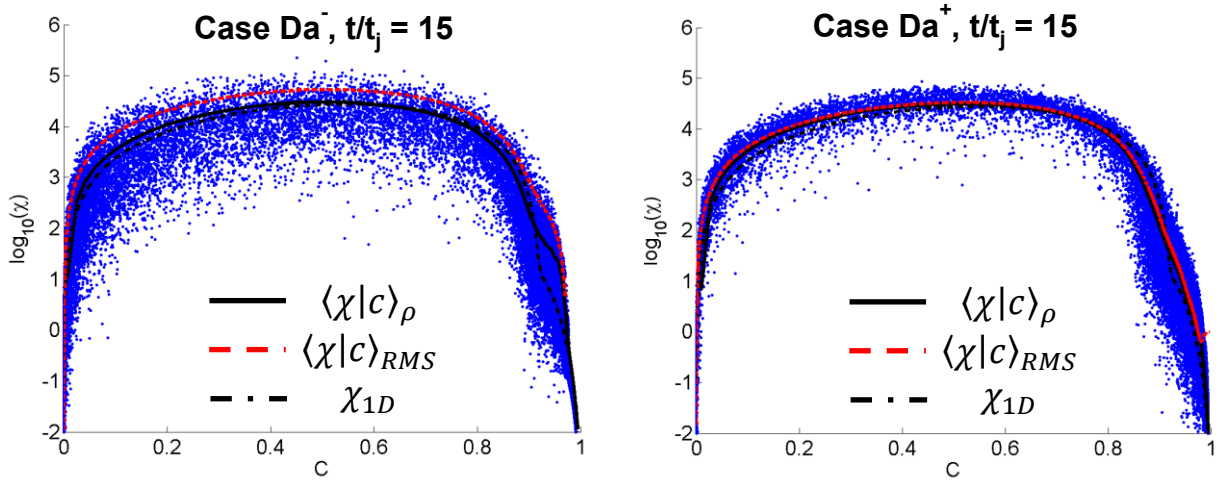


Figure 3-3: Instantaneous conditional scalar dissipation rate (blue dots). Solid black line: global conditional average SDR. Dashed red line: conditional root-mean-square SDR. Dash-dot black line: conditional SDR from the laminar 1-D premixed flame in Fig. 3.

Based on the behavior of $Da_e$ in the steady premixed flame in Figure 3-2, four distinct flame zones are identified by applying CEMA to the DNS data. The structure and locations of each flame zone from a representative 2-D slice at $t = 15t_j$ are shown in Figure 3-4. The fresh mixture zone, where $|\lambda_e| < 1\ s^{-1}$, corresponds to locations where reaction is too slow to be important such that the mixture can be approximated as non-reacting. The explosive zone consists of regions where $Da_e > 100$ and is found in distributed regions away from the flame front, as well as near regions where the flame front interacts with itself. The flame propagation zone, for which $Da_e$ ranges between $\pm 100$, exists in the vicinity of the flame front, defined by $\lambda_e = 0$. Finally, the post-flame zone, where $Da_e < -100$, represents the region where the burnt mixture relaxes toward equilibrium.

In Figure 3-5, the instantaneous fluctuations in scalar dissipation rate are colored using the flame zone coloring scheme from Figure 3-4. The scalar dissipation rate in the flame propagation zone ranges within an order of magnitude above or below the global condition mean for this case. However, the scalar dissipation rate in the explosive zone is smaller than the global conditional mean by an order of magnitude or more. The explosive zone largely exists as a subset of the preheat zone when compared with the 1-D flame solution, but exhibits much longer mixing timescales as compared to chemistry than in the idealized flame, leading to a question regarding what physical processes lead to the extreme fluctuations in the scalar dissipation rate in the explosive zone. Based on Figure 3-4, two prominent mechanisms for the extreme fluctuation in the scalar dissipation rate are conjectured. The first is flame-flame interaction, which occurs where the flame front becomes highly corrugated. The second may be attributed to flame assisted ignition, which occurs when an explosive zone develops far upstream of the flame front.

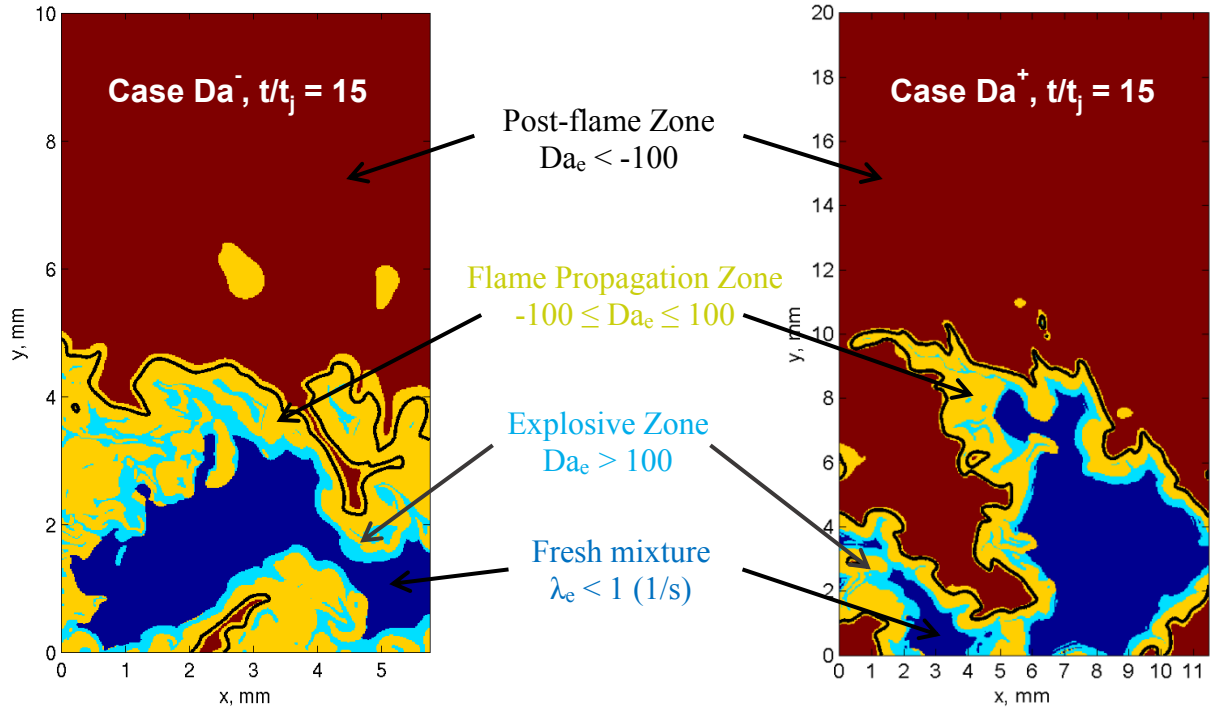


Figure 3-4: Flame zones segmented based on CEMA. The black isoline indicates $\lambda_e = 0$.

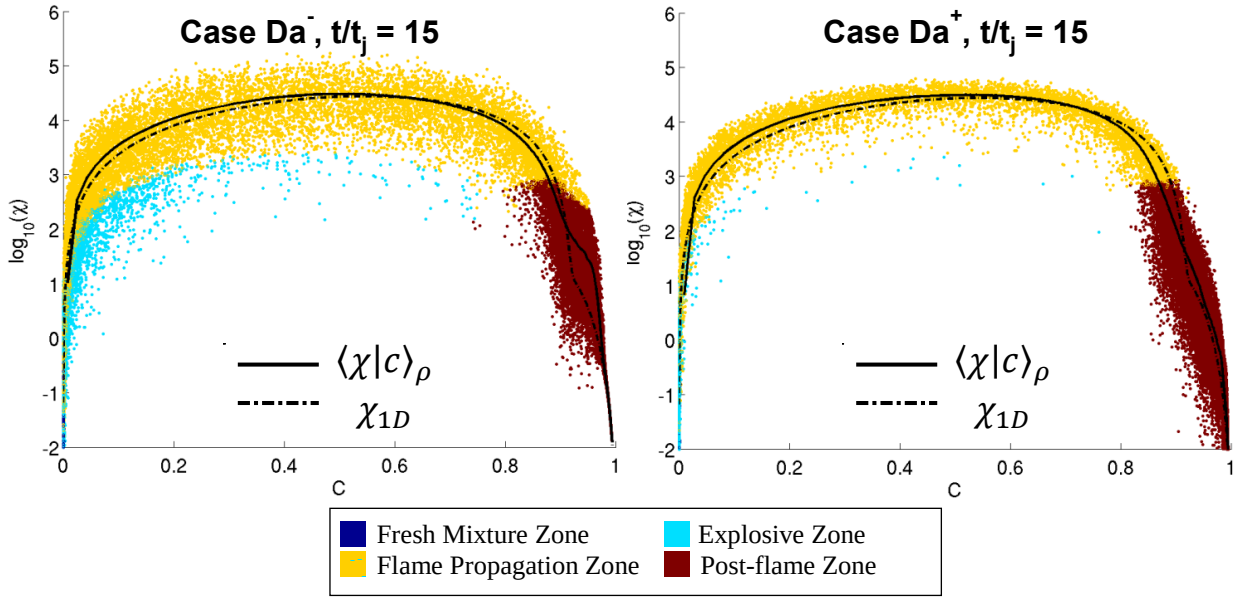


Figure 3-5: Instantaneous conditional scalar dissipation rate colored by flame zone. Conditional mean SDR (solid black line) and conditional laminar 1D flame (dash-dot black line) are overlaid.

To demonstrate the effect that these two mechanisms have on the transient behavior of the scalar dissipation rate, idealized transient 1-D flame simulations are performed using ANSYS Fluent.

The schematic of the configuration for each case is shown in Figure 3-6. In Case A, a freely propagating premixed flame impinges on a symmetry boundary, mimicking the transient upstream flame-flame interaction mechanism in the explosive zone. In Case B, an initially quiescent mixture with spatially varying temperature autoignites and transitions into a freely propagating premixed flame, which mimics the flame assisted ignition behavior found in the DNS dataset. In both cases the domain is 27 mm in length, which corresponds to one half of the full length of the DNS domain in the transverse direction for Case Da-. The chemical mechanism and transport properties used in the Fluent simulations are identical to those used in the DNS. Additionally, both cases use the same numerical settings and boundary conditions, differing only in the initial conditions described above.

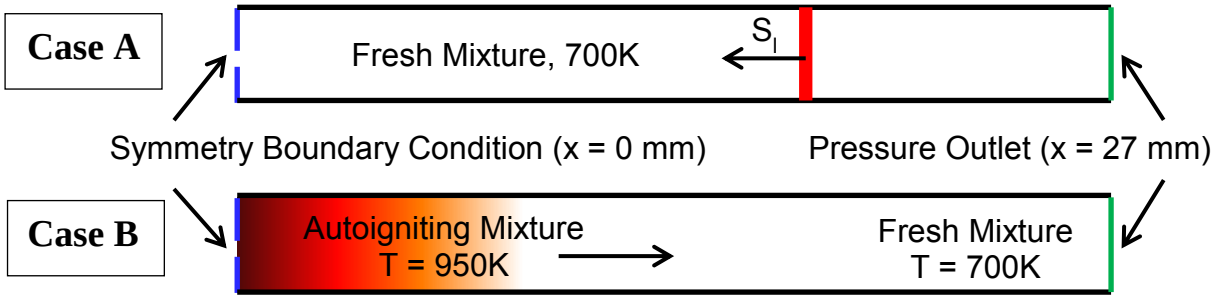


Figure 3-6: Unsteady 1-D Flame Configuration Diagrams

The ANSYS Fluent simulations are solved using the coupled, pressure based solver in a planar 2D configuration. The domain is discretized with a single cell across the domain height, and using a 1 μm cell size along the domain length. Symmetry boundary conditions are enforced at the top and bottom boundaries to reduce the problem to quasi-1D. The boundary at the left hand side of the domain is also treated as symmetric, while the boundary at the right hand side is a pressure outlet at 1 atm. The flow is laminar and mixture averaged transport properties are used along with the stiff chemistry solver. Spatial gradients are evaluated using the Green-Gauss node based method. The discretization schemes used for each set of equations is summarized in Table 3-1. A 2nd order implicit transient scheme is used to advance the solution in time, with a fixed time step size of 5e-8 seconds.

Table 3-1: Spatial Discretization Schemes in ANSYS Fluent Cases

| Equation | Discretization Scheme |
|---|---|
| Pressure | 2nd Order |
| Density | 3rd Order MUSCL |
| Momentum | 3rd Order MUSCL |
| Species | 3rd Order MUSCL |
| Energy | 3rd Order MUSCL |

In Figure 3-7, the behavior of the progress variable and the instantaneous conditional scalar dissipation rate are shown at distinct time instances as the flame impinges on the symmetry boundary in Case A. As the flame propagates toward the symmetric boundary, the spatial gradient of the progress variable vanishes near the symmetry boundary and this effect propagates upstream, where the spatial gradients of the progress variable, and consequently the scalar dissipation rate are significantly reduced as compared to a freely propagating flame. As the transient process proceeds, the progress variable continues to increase at the symmetry boundary. The significance of the flame self-interaction process for the scalar dissipation rate is that the conditional mean is no longer single valued for a given value of the progress variable during the transient event, as can be seen in Figure 3-7.

In Figure 3-8 the temporal evolution of the progress variable and scalar dissipation rate is shown for Case B. As the autoigniting mixture explodes, the progress variable distribution, which is initially uniform, develops into an increasingly steep flame front as it propagates upstream, and eventually transitions into a freely propagating premixed flame. Similar to Case A, the conditional scalar dissipation rate is no longer single valued for a given value of the progress variable as the flame front develops.

The transient scalar dissipation rate behavior found in Cases A and B, when manifested in the turbulent flame, contributes to the large degree of scatter observed in the scalar dissipation rate and poses a challenge in modeling of the conditionally averaged scalar dissipation rate. In the context of LES where local subgrid behavior must be accurately modelled, these two mechanisms demonstrate

that, when present, the local scalar dissipation rate may not be well represented by quasi-steady or equilibrium approaches. The evolution of the local flame topology and chemical reaction mode has a clear influence on the scalar dissipation rate and needs to be captured accurately in submodels. For large Karlovitz flames the transient flame zones likely need to be identified and modeled separately from quasi-steady flame zones.

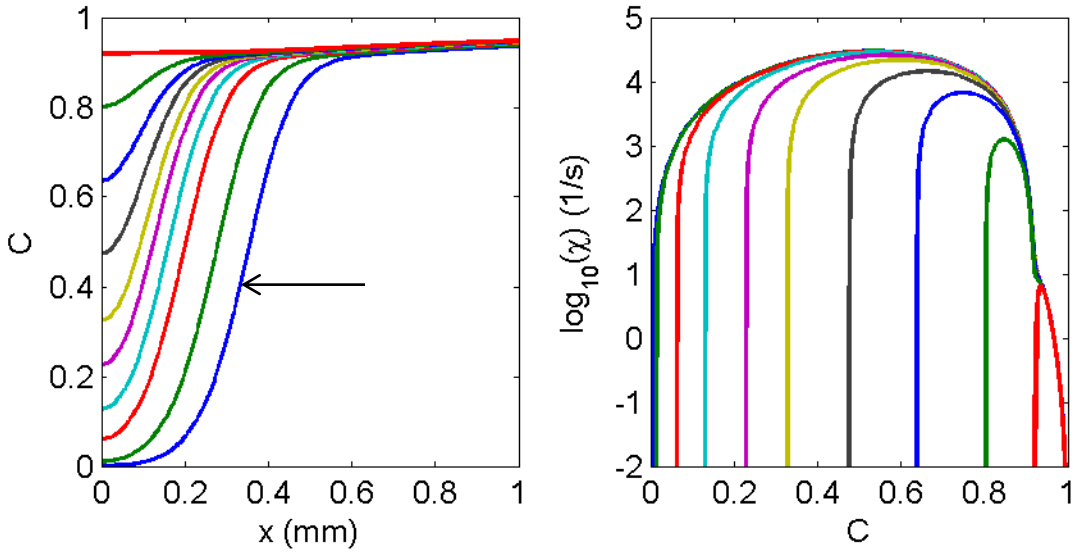


Figure 3-7: Case A. Left: Progress variable. Flame propagates from right to left, as indicated by the black arrow. Right: Conditional scalar dissipation rate

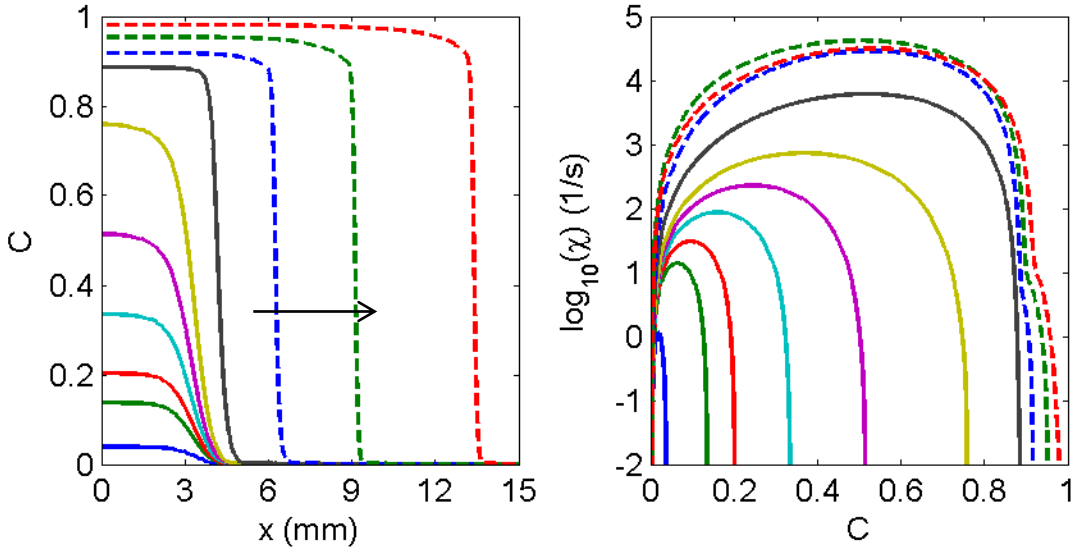


Figure 3-8: Case B. Left: Progress variable. Flame propagates from left to right, as indicated by the black arrow. Right: Conditional scalar dissipation rate

## 3.4. Conclusions

CEMA has been utilized to study the behavior of the conditional scalar dissipation rate of the progress variable in a lean $H_2$-air premixed turbulent flame with detailed chemistry in the thin reaction zones regime. A local Damköhler number is defined based on the CEMA results and four flame zones are identified. It is found that large fluctuations in the instantaneous scalar dissipation rate occur in the explosive zone, where the local Damköhler number is much larger than unity.

Two mechanisms are identified to account for the large degree of scatter in the explosive zone: flame-flame interactions and flame-assisted ignition. One-dimensional laminar flames are then simulated with ANSYS Fluent to mimic the behavior of the conditional scalar dissipation rate in these two scenarios. The results of the 1-D analyses demonstrate that the conditional scalar dissipation rate is not single valued for a given value of the progress variable where flame-flame interaction or autoignition occur. This behavior leads to the large variance of the scalar dissipation rate which cannot be explained by turbulent intermittency alone.

The consequence for the modelling of the conditional scalar dissipation rate in the context of LES is that the quasi-steady and equilibrium modelling approaches widely used in RANS applications may not be applicable in the presence of highly transient flame behavior. Further, the behavior of the scalar dissipation rate under the two conditions that have been identified in this flame invalidate the primary assumptions in many flamelet-based modeling approaches, namely that the mixing term is adequately described by the instantaneous scalar dissipation rate. The effects of such transient flame behavior on the variance of the scalar dissipation rate likely will need to be captured in modelling, which is a topic that merits further study.

# Chapter 4: An Algebraic Mixing Timescale Model for TPDF Simulations

## 4.1. Introduction

As was noted in Chapter 1, there have been many approaches to the closure of the molecular mixing term that have been developed in the literature. While these mixing models describe the manner in which mixing occurs, each requires the specification of a Favre-averaged mixing rate. In typical TPDF simulations [39,92], the scalar mixing rate is assumed to be linearly proportional to the turbulent mixing rate, with the constant of proportionality called the mechanical-to-scalar timescale ratio. In previous PDF calculations of the premixed flames [93,100], the primary aspect of the mixing models called into question is the specification of the mechanical-to-scalar timescale ratio, which is assumed to be constant, regardless of the combustion regime. This approach is founded on studies of passive scalar mixing, and does not adequately describe the mixing dynamics of reactive scalars in the limit of large Damköhler number [84].

It has been demonstrated in Chapter 2 that both mixing model formulation and the scalar mixing rate are crucial for turbulent premixed combustion, and that the EMST mixing model is capable of accurately modeling the micro-mixing in a turbulent premixed flame provided that an accurate model of the mixing rate can be provided [106]. To this end, several algebraic models for the mixing rate of reactive scalars that account for the effects of small scale turbulent mixing as well as reaction and dilatation have been proposed [82,90,107]. However, these models do not properly recover the correct mixing behavior in the limit of thin flamelets [79]. Closures specific to flamelet-regime turbulent premixed flames, such as that of Pope and Anand [66], close the mixing and reaction term by mapping the mixture state to a 1D freely propagating premixed flame, have also been proposed. However, the intrinsic assumption of embedded laminar flamelets limits the applicability of such closures, as they are unable to capture the transition to more intense turbulent combustion regimes. Another issue is that

this fast-chemistry, premixed-flame specific approach throws away the significant advantages of PDF methods in treating problems involving relatively slow processes such as NOx or soot formation.

In this chapter, a new algebraic mixing rate model is proposed that aims to model the transition in scalar mixing rate behavior from the limit of turbulence-dominated mixing to thin flamelet mixing behavior. A variant of this hybrid timescale model has been proposed and preliminarily studied for PDF simulations of turbulent premixed flames [108], though systematic *a priori* and *a posteriori* testing is not reported. In the remainder of this paper, we first derive the mixing rate model in section 2 and then perform an *a priori* comparison of the new model with a previously reported series of DNS modelling temporally evolving premixed hydrogen-air slot jet flames [94]. Finally, an *a posteriori* TPDF evaluation of the new mixing rate model is undertaken by using DNS as a numerical test bed as was done in Chapter 2.

## 4.2. Model Development

As described in [79], reactive scalar mixing rates in turbulent premixed flames depend on the local state of both the flow turbulence and the chemical reactions, which can be characterized by the Damköhler number, $Da = \tau_{turb}/\tau_{chem}$, where $\tau_{turb}$ and $\tau_{chem}$ are characteristic turbulence and chemical timescales, respectively. In the limit of large global Damköhler number, reactions occur in propagating thin structures that resemble laminar flames and thus scalar mixing rates can be strongly affected by the chemical timescales. Conversely, for low global Damköhler number, the scalar mixing rate can be expected to be controlled by the small scale turbulent motions, which in turn are driven by large-scale motions, as is found to be a reasonable approximation in studies of passive scalar mixing [34]. Kolla et al. demonstrated by an order of magnitude analysis that for finite values of the Damköhler number, the exact transport equation for the Favre-averaged scalar dissipation rate of the progress variable, $\widetilde{\chi_c}$, can be approximated to leading order by the effects of dilatation, turbulence-scalar interaction, chemical reaction, and molecular dissipation as in Equation 4.1 [90].

$$\overline{2\rho\chi_c \frac{\partial u_l}{\partial x_l}} - 2\overline{\rho\Gamma_c}\left(\frac{\partial c''}{\partial x_j}\widetilde{\frac{\partial u''_j}{\partial x_k}}\frac{\partial c''}{\partial x_k}\right) + 2\left(\overline{\frac{\partial c''}{\partial x_k}\frac{\partial \dot{\omega}''}{\partial x_k}}\right) - \overline{2\rho\left(\Gamma_c \frac{\partial^2 c''}{\partial x_j \partial x_k}\right)^2} \approx 0 \quad (4.1)$$

The terms in Equation 4.1 require closure, and the model proposed by Kolla et al. to account for the dominant physics of reactive scalar mixing can be written as:

$$\widetilde{\chi_c} = \frac{C_3}{\beta'}\frac{\tilde{\varepsilon}}{\tilde{k}}\widetilde{c''^2} + \frac{1}{\beta'}\left(2K_c^* \frac{S_L^0}{\delta_L^0} - \tau C_4 Da_L\right)\widetilde{c''^2} \quad (4.2)$$

where $C_3$, $C_4$, and $\beta'$ are model constants; $K_c^*$ is a constant computed based on the laminar flame structure; $\tau = (T_{ad} - T_u)/T_u$ is the heat release parameter with $T_{ad}$ and $T_u$ defined as the adiabatic flame temperature and the unburnt mixture temperature, respectively; and $Da_L = \frac{S_L^0/\delta_L^0}{\tilde{\varepsilon}/\tilde{k}}$ with $S_L^0$ and $\delta_L^0$ representing the unstrained laminar flame speed and thermal thickness, respectively. The first term in this equation accounts for the influence of turbulence on the scalar mixing, while the second term is to account for the influence of the flame structure. However, as noted by Bray et al. [79], this model and others of its kind do not properly recover the correct mixing rate in the flamelet limit, which merits further investigation with DNS data.

A new mixing timescale model is hereby proposed to account for both flamelet-controlled and turbulence-controlled mixing to more accurately model local mixing rates. In the limit of passive scalar mixing, Mantel and Borghi [81] showed by an order of magnitude analysis of the Favre-averaged scalar dissipation rate transport equation that the turbulence-scalar interaction and molecular dissipation terms in Equation 1 are balanced in the leading order. They proposed a model for the mixing rate that is proportional to the turbulence timescale according to the classical expression in Equation 4.3.

$$\Omega_t = \widetilde{\chi_\phi}/\widetilde{\phi''^2} = C_\phi\, {\tau_{turb}}^{-1} \quad (4.3)$$

The constant of proportionality $C_\phi$ is the mechanical-to-scalar timescale ratio and is typically taken to be 2.0 based on studies of passive scalar mixing in shear flows [109], which in order of magnitude is also supported by DNS of reactive non-premixed jet flames [110]. In the RANS context, the turbulence

timescale is defined as the ratio of the turbulent kinetic energy, $\tilde{k}$, to the turbulent kinetic energy dissipation rate, $\tilde{\varepsilon}$.

Conversely, in the limit of laminar flamelets embedded in a turbulent flow field, the mixing rate is expected to be dependent on the laminar flame structure. Assuming that the premixed flamelets can be adequately described by a single reaction progress variable, c, the Favre-averaged mixing rate can be expressed in terms of the conditional scalar dissipation rate, $\langle \chi_c | c \rangle$, as

$$\Omega_f = \widetilde{\chi_c} / \widetilde{c''^2} = \int_0^1 \langle \chi_c | \zeta \rangle \widetilde{P}_c(\zeta) d\zeta \, / \widetilde{c''^2} \qquad (4.4)$$

where $\widetilde{P}_c(\zeta)$ is the Favre-averaged probability density function of the progress variable and $\zeta$ is the sample space variable. This expression is advantageous in that the PDF of the progress variable is computed naturally as a part of the TPDF solution, and thus only a model for the conditional scalar dissipation rate in the flamelet limit is required. As a first attempt, we close the model by reconstructing the conditional scalar dissipation rate from a 1D freely propagating premixed flame. The model format implies that the large variation in the mixing rate can be primarily attributed to the strong local variation in the progress variable PDF and that the local flamelets are reasonably approximated by the conditional scalar dissipation rate of the freely propagating flame at a known unburnt condition. Note that the model can in principle account for the strain/stretch effect on the flame structure by reconstructing the conditional scalar dissipation rate from a stretched premixed flame.

In practice, local mixing conditions in a turbulent premixed flame may vary such that neither of these limiting assumptions are valid for the entire flow field, and thus some intermediate local state between the two limits must be sought. To accomplish this, we define the segregation factor, $\eta = \widetilde{c''^2} / [\tilde{c}(1-\tilde{c})]$, [79,103] to act as the blending variable between the two limiting states. As the local Damköhler number tends to infinity and the progress variable PDF becomes bimodal, the variance reaches its maximum possible value of $\tilde{c}(1-\tilde{c})$. Conversely, in the limit of infinitely strong

turbulence, the variance disappears due to perfect mixing. Accordingly, the blended, hybrid timescale model can be constructed as

$$\Omega_{hybrid} = (1-\eta)C_{\phi}{\tau_{turb}}^{-1} + \eta \int_0^1 \langle \chi_c|\zeta\rangle \widetilde{P}_c(\zeta)d\zeta \,/\widetilde{c''^2} \qquad (4.5)$$

The new timescale model, which is referred to as the hybrid model for the remainder of this chapter, is constructed to take advantage of the statistical data naturally available in a TPDF simulation and to properly describe the mixing rate in the flamelet limit. In the following section an *a priori* assessment of the accuracy of the new model is performed by comparison with DNS results.

## 4.3. *A priori* evaluation using DNS

The 3-D DNS dataset of a lean H2-air turbulent premixed flame with detailed chemistry [94], identical to the one used in Chapter 2, is employed for the a priori evaluation of the timescale model. The same DNS have been previously used in studies fractal flame characteristics [111] and in modeling in studies of different TPDF mixing models [106], one-dimensional turbulence models [112], and strained flamelet models [113].

The DNS configuration allows for Favre-averaging in the streamwise and spanwise directions, as well as the use of symmetry across the domain centerline in the transverse direction. After averaging, the simulation is reduced to statistical dependence on the transverse direction and time. A reaction progress variable can be constructed based on the mass fraction of $H_2$ as $c = (Y_{H2} - Y_{H2,u})/(Y_{H2,b} - Y_{H2,u})$, where the subscripts u and b refer to the unburnt and equilibrium states, respectively. The study in Chapter 2 on the performance of TPDF mixing models in this flame showed that differential diffusion can have a significant effect, and that using a progress variable definition based on the mass fraction of $H_2$ provides accurate TPDF solutions [106]. Therefore, the progress variable definition based on $H_2$ is used throughout the remainder of this work.

After Favre-averaging the progress variable field in the DNS, the mixing rate is computed as $\Omega = \widetilde{\chi_c}/\widetilde{c''^2}$ where the scalar dissipation rate is defined as $\widetilde{\chi_c} = 2\,\Gamma_c \widetilde{\nabla c'' \nabla c''}$. The diffusivity of the progress

variable, $\Gamma_c$, is defined as the molecular diffusivity of $H_2$ [106]. The turbulent mixing rate is extracted from the DNS by computing the turbulent kinetic energy and its dissipation rate. The flamelet component of the hybrid timescale model is extracted by first computing the Favre-averaged PDF of the progress variable at each transverse location in space and at each time step. The conditional progress variable scalar dissipation rate is reconstructed from a freely propagating, 1D laminar flame calculated using PREMIX under the same unburnt conditions as the DNS. The product of the Favre PDF and the 1D conditional scalar dissipation rate are then integrated at each location in space and time to form the flamelet mixing rate in Equation 4.4. Finally, the hybrid timescale model, which blends together the turbulent and flamelet mixing rates using the segregation factor, is reconstructed by computing the segregation factor at each location in space and time, and combing the turbulent mixing rate with the flamelet mixing rate according to Equation 4.5.

## 4.4. *A priori* results and discussion

The instantaneous temperature field for Case $Da^-$ is shown on a representative cross-section of the DNS domain at four important flame times in Figure 4-1. The two flames propagate inwards, and the $11^{th}$ jet time is approximately when the flame first begins to interact with the shear layer. At the $14^{th}$ jet time, the turbulence is considered to be fully developed, and the maximum flame wrinkling occurs near the $17^{th}$ jet time [94]. By the $20^{th}$ jet time, the flame is in its final stage and is burning the remainder of the fresh reactants at the domain center.

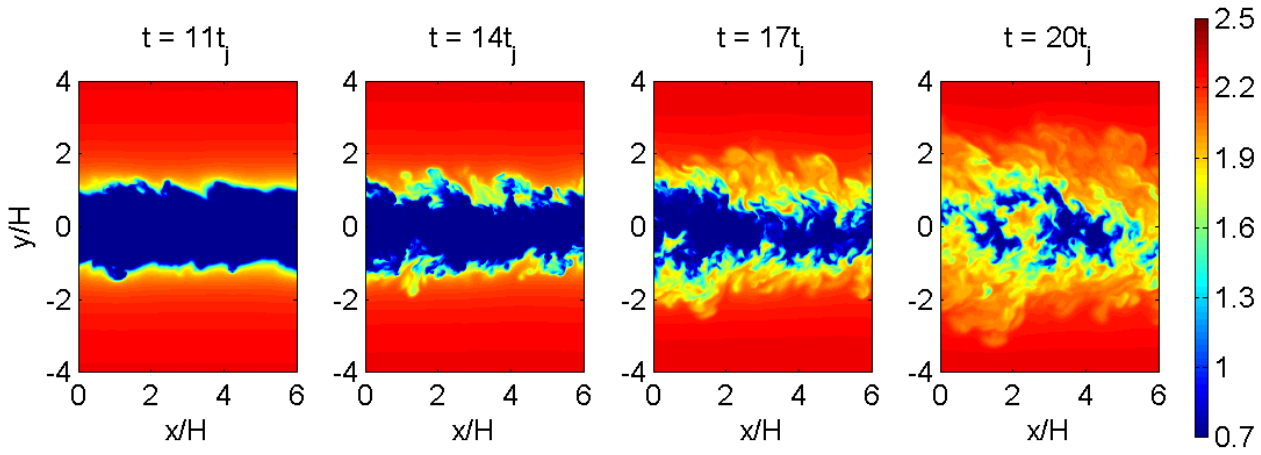


Figure 4-1: Instantaneous temperature (T/1000 K) field on a representative section of the central spanwise plane at several time instances from the DNS for Case Da$^-$

In the hybrid mixing rate model, the scalar dissipation requires closure while the scalar variance can be computed directly from the TPDF simulation. Therefore, we compare here the spatial and temporal variation of the progress variable scalar dissipation rate extracted from the DNS as well as the scalar dissipation rate implied by the new hybrid model, $\tilde{\chi}_{hybrid} = \Omega_{hybrid}\widetilde{c''^2}$, which are shown in the contour plots in Figure 4-2. The values for both the DNS and modeled scalar dissipation rates are normalized for each DNS case by the maximum value across space and time of the DNS scalar dissipation rate, which is computed as: $\max(\tilde{\chi}_{c,DNS}(y,t))$. The trajectory of the location in the flame brush with a mean progress variable of $\tilde{c} = 0.5$ is overlaid on each plot, along with the trajectory of the leading edge ($\tilde{c} = 0.01$) and the trailing edge ($\tilde{c} = 0.95$) of the flame brush. At the leading edge of the flame brush through the center of the flame, the hybrid timescale model accurately captures the spatial and temporal variation of the scalar dissipation rate. The peak magnitude of the scalar dissipation rate, which occurs in the center of the flame brush, is under-predicted by 18% for Case Da$^-$ and 10% for Case Da$^+$. Towards the trailing edge of the flame brush the hybrid timescale model tends to under-predict the magnitude of the scalar dissipation rate for both cases. However, at this location in the flame brush, the mixing rate is less critical for accurate flame prediction as the burnt mixture is relaxing to chemical equilibrium.

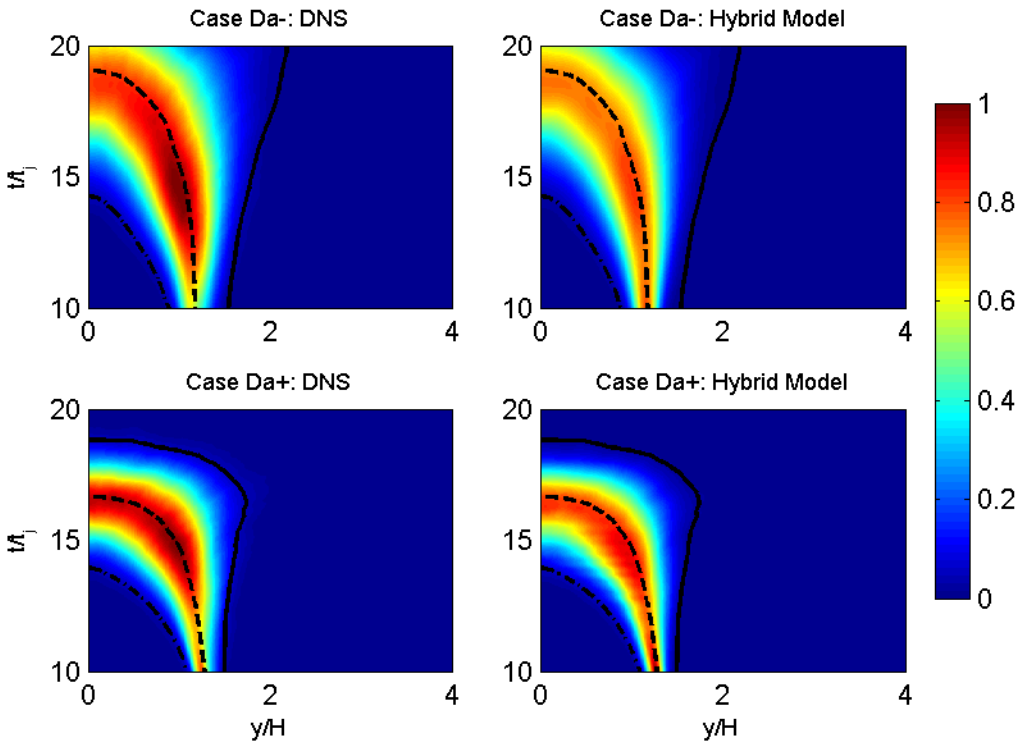


Figure 4-2: Scalar dissipation rate normalized by the maximum DNS value for Case Da$^-$ (top) and Case Da$^+$ (bottom). Left Column: DNS. Right Column: Hybrid model from Eqn. (5). Dash-dotted line: $\tilde{c} = 0.01$, dashed line: $\tilde{c} = 0.5$, solid line: $\tilde{c} = 0.95$.

The spatial and temporal distribution of the segregation factor, $\eta$, which blends together the contributions of the turbulent mixing and flamelet mixing components of the hybrid model is extracted from the DNS and shown in Figure 4-3. The segregation factor is larger in the more flamelet-like Case Da$^+$ than in Case Da$^-$ throughout space and time as expected. The variation of the segregation factor through the flame brush is shown in Figure 4-4. It can be seen that the segregation factor is small towards the leading edge of the flame in Case Da$^-$, indicating the disruption of the preheat zone by the turbulence and the strong mixing in this region. Conversely, the segregation factor peaks towards the leading edge of the flame in the more flamelet-like Case Da$^+$.

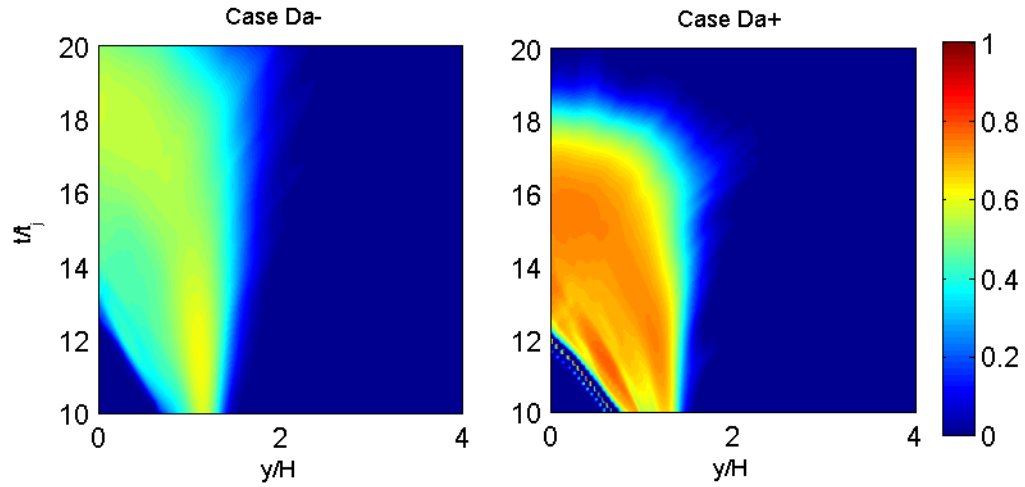


Figure 4-3: The segregation factor $\eta$ reconstructed from the DNS data.

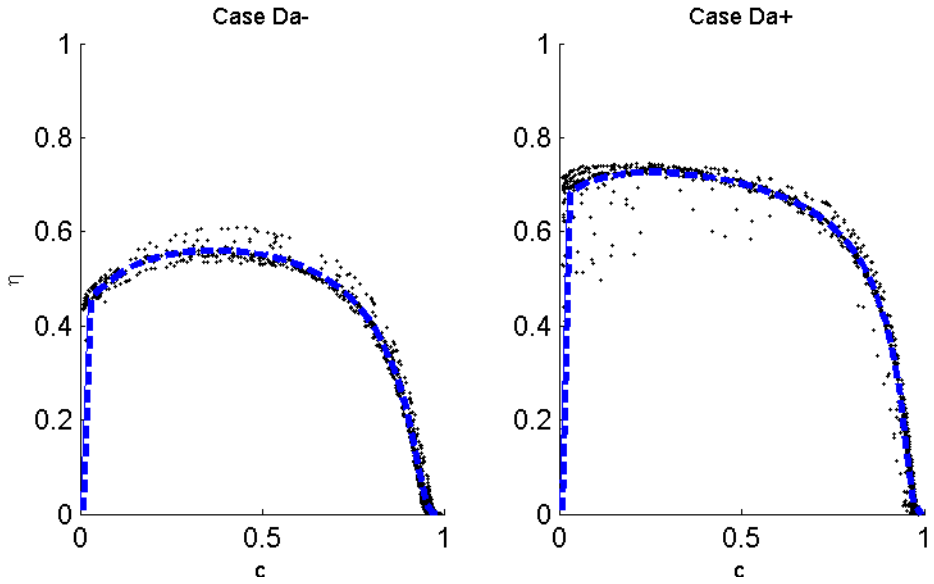


Figure 4-4: The segregation factor $\eta$ vs. mean progress variable. Dashed blue line represents the segregation factor conditionally averaged on the mean progress variable

The scatter plots in Figure 4-5 and Figure 4-6 show the normalized averaged scalar dissipation rate variation through the flame brush for the DNS and the hybrid timescale model, along with each of the limiting components that are combined to form the hybrid timescale model for a random sample of locations across the entire spatial domain and time. As in Figure 4-2, the values for both the DNS and modeled scalar dissipation rates are normalized for each DNS case by the maximum value across space and time of the DNS scalar dissipation rate. Overlaid on the plots is the conditional average of the

scalar dissipation rate, $\langle \widetilde{\chi_c} | \tilde{c} \rangle$, which is computed by conditionally averaging on the mean progress variable across the entire domain for all times. In both cases it can be seen that the passive scalar mixing rate approach of Equation 4.3 leads to a peak dissipation rate skewed more towards the burnt side of the flame brush, which is qualitatively different than the variation seen in the DNS data. For the standard mechanical-to-scalar timescale ratio value of 2.0, the turbulent mixing rate model under-predicts the mixing rate magnitude for both cases. Conversely, the flamelet model in Equation 4 tends to more accurately capture the variation through the flame brush of the dissipation rate, showing a peak on the unburnt side of the flame brush. However, the magnitude of the mixing rate tends to be over-predicted by the flamelet model, particularly for Case $Da^+$. It can be seen from the scatter plots that the scalar dissipation rate extracted from the DNS lies in between the limiting values of the turbulent mixing rate and flamelet mixing rate throughout the flame brush.

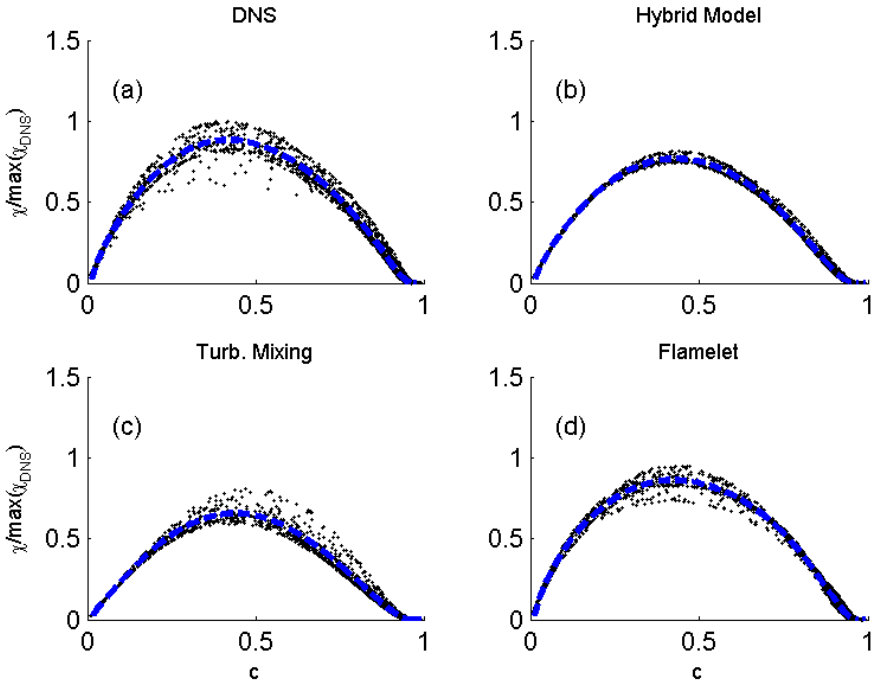


Figure 4-5: Scalar dissipation rate normalized by the maximum DNS value vs. mean progress variable for Case $Da^-$. (a) DNS. (b) Equation 5. (c) Equation 3. (d) Equation 4. Dashed black line represents the mean scalar dissipation rate conditionally averaged on the mean progress variable.

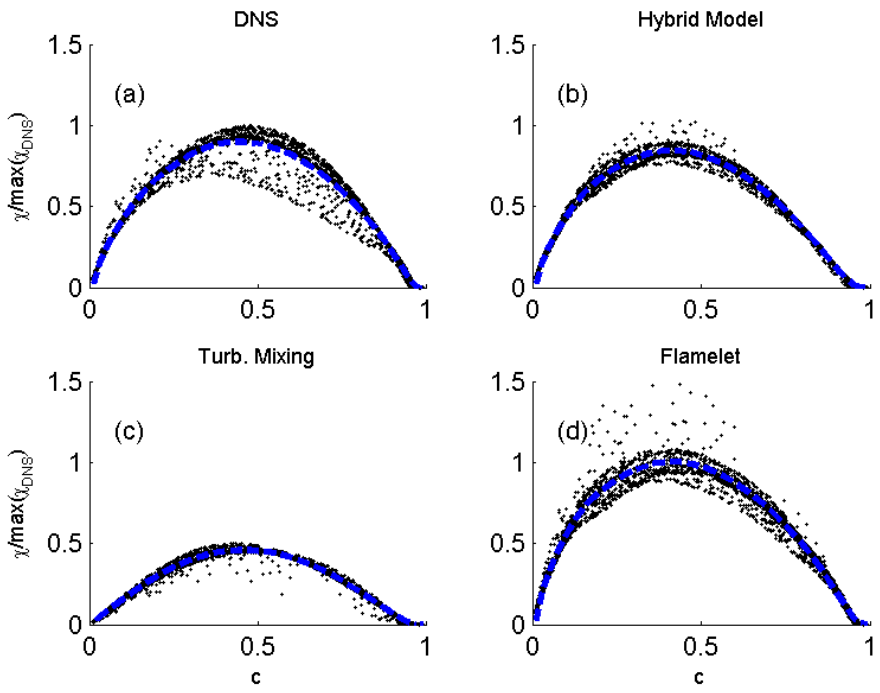


Figure 4-6: Scalar dissipation rate normalized by the maximum DNS value vs. mean progress variable for Case $Da^+$. (a) DNS. (b) Equation 5. (c) Equation 3. (d) Equation 4. Dashed black line represents the mean scalar dissipation rate conditionally averaged on the mean progress variable.

The hybrid timescale model, which combines the limiting behavior of the turbulent mixing and flamelet models, accurately predicts the scalar dissipation rate magnitude and variation throughout most of the flame brush for both DNS cases as shown in Figure 4-7. The peak conditionally averaged mean scalar dissipation rate is under-predicted by 13% in Case $Da^-$ and 6% in Case $Da^+$. It is notable that the hybrid timescale model tends to under-predict the dissipation rate in the post-flame zone. This is due to the value of the segregation factor in the post-flame zone, which skews the hybrid model more towards the passive scalar mixing behavior than the flamelet behavior in this location of the flame brush. However, as noted earlier, at this location in the flame brush most of the reaction has occurred and the mixture is relaxing to chemical equilibrium. Therefore, accurate prediction of the mixing rate in the post-flame zone may not be of critical importance.

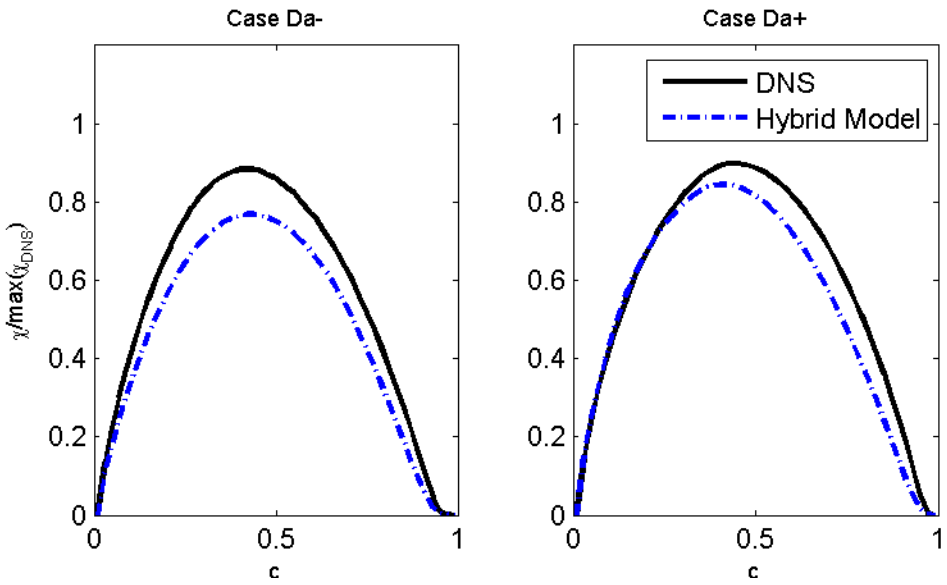


Figure 4-7: Normalized mean scalar dissipation rate conditionally averaged on the mean progress variable

4.5. *A postereori* evaluation of timescale model for TPDF simulations

We now perform an *a posteriori* TPDF evaluation of the new mixing rate model using the same DNS database from section 3 as a numerical test bed in a similar manner to the study performed in Chapter 2. The DNS database is used to supply the initial conditions and all time-varying inputs to the governing equations in the composition TPDF method, including the mean velocity, turbulent diffusion coefficient, and mixing rate model components. This approach, employed in previous studies [41,114], deliberately removes uncertainties of turbulence and scalar transport modeling in order to expose only the effect of the mixing model. The same thermodynamic properties and chemical reaction mechanism used in the DNS are used in the TPDF simulations to limit the potential sources of modeling error to the closure of the molecular mixing term. For comparison purposes, we investigate the new mixing rate model coupled with the EMST micro-mixing model and compare it to the more popular mechanical timescale model as well as the mixing term closure proposed by Pope and Anand [66]. The EMST model was chosen because our previous study [114], which took the mixing timescale input directly from the DNS, demonstrated EMST's superiority over IEM and MC models for premixed flames. It is emphasized that the purpose of the present study is to evaluate the mixing timescale model,

and not the mixing format, and thus it is possible that other untested mixing format models may produce similar results.

## 4.6. TPDF Methodology

The TPDF solver has been implemented in the RANS context using a hybrid particle-mesh methodology exactly as in Chapter 2, and as in several previous studies of mixing models [41,106]. For the given flame configuration, a 1D Eulerian mesh is generated covering half of the DNS domain in the transverse direction with a symmetric boundary condition accounting for the centerline. The Eulerian mesh is populated with notional Lagrangian particles, which obey the set of governing stochastic differential equations, Equations 4.6 and 4.7 [37,41], in physical and composition space:

$$\mathrm{dx}^*(\mathrm{t}) = \left[\widetilde{\mathrm{V}} + \frac{\nabla\tilde{\Gamma}_\mathrm{t}\bar{\rho}}{\bar{\rho}}\right]\mathrm{dt} + \left(2\tilde{\Gamma}_\mathrm{t}\right)^{1/2}\mathrm{dW}, \quad \text{and} \tag{4.6}$$

$$\mathrm{d}\phi^*(\mathrm{t}) = [\mathrm{m}]\mathrm{dt} + \dot{\omega}(\phi^*)\mathrm{dt} \tag{4.7}$$

where $x^*$ and $\boldsymbol{\phi}^*$ are the spatial location and composition, respectively, of a particle, $\tilde{V}$ is the mean transverse velocity, $\tilde{\Gamma}_t$ is the turbulent diffusion coefficient, $dW$ is the increment of a Wiener process, $\dot{\omega}(\boldsymbol{\phi}^*)$ is the chemical source term, and $[m]$ is the rate of change in composition due to mixing. Note that mean drift by molecular diffusion is ignored in Equation 4.7 as it is found that the turbulent diffusion coefficient is larger than the molecular diffusion coefficient by at least an order of magnitude throughout the flame brush.

The mean transverse velocity, turbulent diffusivity, and mixing rate are all extracted directly from the DNS results at each time step and fed to the TPDF solver. The turbulent diffusion coefficient is computed as $\tilde{\Gamma}_t = \frac{|\widetilde{\rho v}\tilde{c} - \bar{\rho}\tilde{v}\tilde{c}|}{\bar{\rho}|\nabla\tilde{c}|}$ where $v$ is the velocity, $\rho$ is the density, and c is the progress variable [2]. All input data required by the TPDF solver has been computed by Favre-averaging the DNS data in the statistically homogeneous x and z directions at each time step. The simulations are initialized from the DNS data at the 11$^{\text{th}}$ jet time, which is when the flame begins to interact with the shear layer.

In the current study, the stochastic governing equation for the composition vector, Equation 4.7, can evolve over time in two ways. In the first method, the EMST mixing model is used to close the molecular mixing term and is supplied with either the turbulent mixing rate or the new hybrid model mixing rate, which have been extracted from the DNS as described in section 4.3. The chemical source term is integrated using a 6-stage, 4th order Runge–Kutta numerical scheme [115].

In the second method, the laminar flamelet closure of Pope and Anand [66] is used to advance the particle composition. In this method, the mean progress variable is first computed for each cell. In cells near the leading ($\tilde{c} < 0.05$) and trailing ($\tilde{c} > 0.95$) edges of the flame brush where turbulent mixing is expected to be the dominant generator of scalar gradients, the particle composition is advanced in the same manner as in the first method using the turbulent mixing rate. For all other cells, the progress variable of each particle is calculated and the evolution of the composition vector is then computed according to Equation 4.8, where the diffusion and reaction contributions are interpolated from the 1D laminar flame solution for the given value of the particle progress variable.

$$d\phi^*(t) = [\nabla\Gamma\nabla\phi + \dot{\omega}(\phi)]_{c=c^*}dt \qquad (4.8)$$

In this approach, particles in the middle of the flame brush evolve as if they were embedded in a locally 1D laminar flamelet. This laminar flamelet closure method is referred to as Pope's method through the remainder of this work.

Based on the convergence study performed Chapter 2, all results in this paper for Case $Da^-$ are generated using 300 cells, 4,000 particles per cell, and a time step of 5 ns. All results for Case $Da^+$ are generated using 600 cells, 4,000 particles per cell, and a time step of 10 ns. It is noted that the TPDF solver used in this study does not perform any smoothing, and thus the convergence rate is slow and requires significantly more particles. If smoothing were to be applied, the convergence rate would be much faster, and a particle level of 20-100 particles per cell, as found elsewhere in the literature, could be expected to achieve a converged solution [98].

## 4.7. Results and Discussion

The predictions of the TPDF solution with the three closure methods described above are compared to the DNS data at three important time instances in the flame evolution. In the figures that follow, the results denoted by "Pope" refer to the solution computed using Pope and Anand's laminar flamelet closure; the results denoted by "Turb. Mixing" refer to the solution computed using the EMST mixing model and the turbulent mixing timescale in Equation 4.3; and the results denoted by "Hybrid" refer to the solution computed using the EMST mixing model and the hybrid mixing timescale in Equation 4.5. The TPDF mean and RMS temperature distribution are compared to the DNS data for both cases in Figure 4-8. All three methods provide reasonably accurate predictions of the mean spatial temperature profile in Case $Da^-$. Pope's method provides a poor approximation to the RMS temperature field as the decay of scalar variance because turbulence is not properly described in this closure in the present high Ka conditions. In Case $Da^+$, Pope's closure performs poorly for both the mean and RMS temperature fields, simply propagating the flame elements along as if it were laminar and not capturing the turbulent flame acceleration found in this configuration. The relative success of Pope's closure for Case $Da^-$ and failure for Case $Da^+$ can be attributed to the influence of the EMST mixing model, which is invoked at the leading edge of the flame brush. While the timescales implied by the right-hand side of Equation 4.6 and that of the hybrid mixing rate model are similar in magnitude, the use of the EMST model coupled with the turbulent mixing rate at the leading edge of the flame controls the flame propagation in Pope's model until the flame brush begins to interact with the symmetry boundary. The performance of Pope's model is dependent on the specification of the value of $\tilde{c}$ at which the transition between the use of the EMST mixing model and the laminar flamelet closure occurs. Note that this transition is needed as the laminar flamelet closure is ill-conditioned as the progress variable tends towards zero. For the flames considered here, better agreement may be obtained by tuning the $\tilde{c}$ value at which the transition occurs, however the optimal value for transition is case-dependent. The

turbulent mixing rate provides a reasonable solution in Case $Da^-$ and therefore so does Pope's closure, while both fail for Case $Da^+$.

The EMST mixing model coupled with the turbulent mixing rate model shows acceptable accuracy for the mean temperature behavior in Case $Da^-$, but provides increasingly inaccurate predictions of the RMS temperature as the flame progresses. For Case $Da^+$, the turbulent mixing rate under-predicts the flame propagation and is entirely inaccurate for both the mean and RMS profiles. While the mixing rate constant, $C_\phi$, can in principle be tuned to achieve closer agreement for the mean temperature field predictions, previous studies have shown that even for a flame in the same configuration, the optimal choice of $C_\phi$ can vary by a factor of two or more [106], which would be problematic for practical application where $C_\phi$ is not known *a priori*. It is clear from the results that the turbulent mixing rate alone does not have the appropriate spatial and temporal distribution to represent the scalar mixing in this premixed flame.

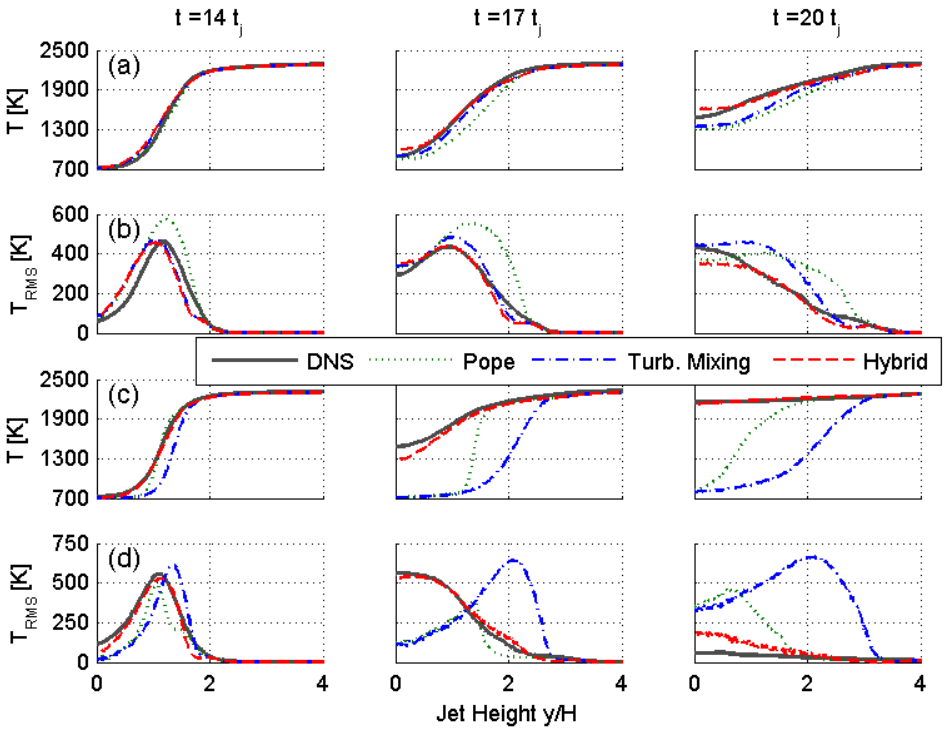


Figure 4-8: Predicted mean and RMS spatial temperature profiles from the DNS and TPDF solutions. Rows (a) and (b): Case $Da^-$. Rows (c) and (d): Case $Da^+$.

The TPDF solution using the hybrid mixing rate model shows excellent agreement with the DNS mean and RMS temperature fields for both cases. As shown in section 4.3, the hybrid mixing rate model is able to accurately capture the spatial and temporal distribution of the mixing rate, particularly in the preheat zone. This leads to close agreement of the TPDF solution with the DNS both in space and time without the need to arbitrarily choose the mixing rate constant $C_\phi$ to achieve an accurate prediction.

To evaluate the influence of the closure models on flame propagation, the turbulent flame speed, $S_T$, defined based on the global consumption rate as in Equation 2.3, is computed from the results. The turbulent flame speed normalized by the laminar flame speed is shown in Figure 4-9. The hybrid timescale model closure provides the best prediction of the temporal flame speed variation for both DNS cases. The turbulent mixing rate model provides a reasonable approximation for Case $Da^-$, but under-predicts the flame speed for Case $Da^+$. When evaluated by the global consumption speed, Pope's closure fails for both cases as the flame acceleration is not properly captured.

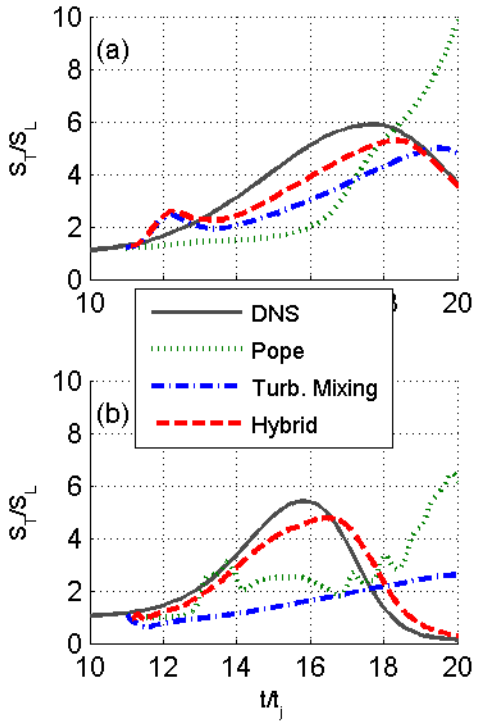


Figure 4-9: Turbulent flame speed vs. time. (a) Case $Da^-$. (b) Case $Da^+$

To more closely examine the behavior of all three closures, the major species spatial profile predictions are shown at the 17$^{th}$ jet time in Figure 4-10 and Figure 4-11. The major species profiles behave similarly to the temperature field, with all three models providing reasonable predictions of the mean fields for Case Da$^{-}$. However, only the hybrid mixing rate model is able to accurately capture the correct flame structure in Case Da$^{+}$.

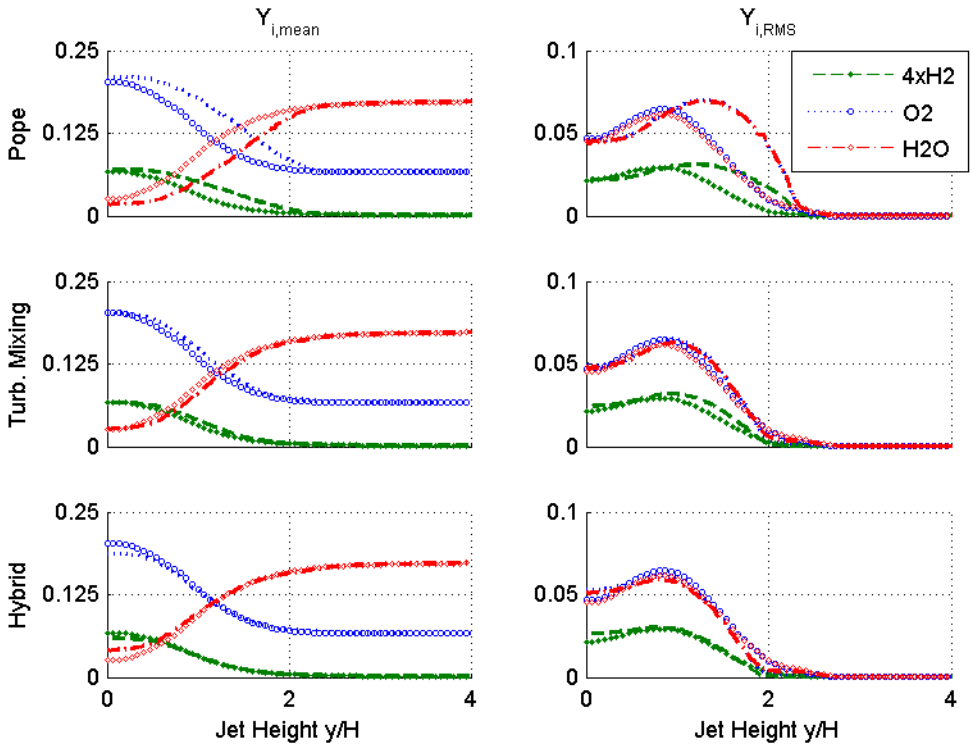


Figure 4-10: Major species mean and RMS profiles at 17$t_j$ for case Da$^{-}$. Markers: DNS. Lines: TPDF.

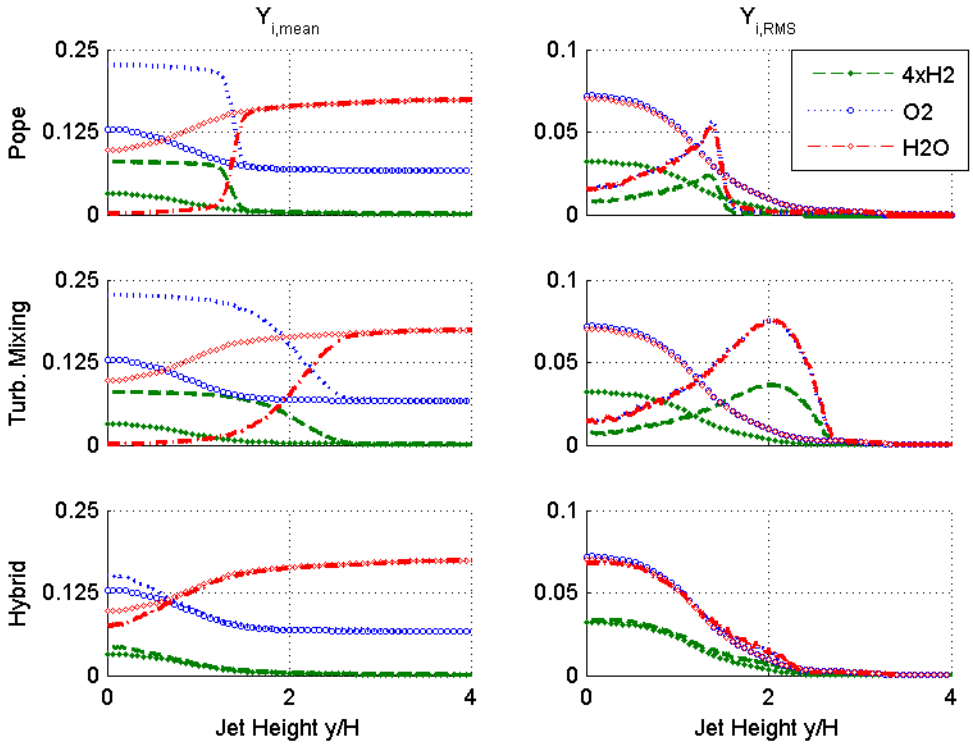


Figure 4-11: Major species mean and RMS profiles at $17t_j$ for case $Da^+$. Markers: DNS. Lines: TPDF.

Similarly, the minor species spatial profiles are shown at the 17th jet time in Figure 4-12 and Figure 4-13. It can be seen that the solution produced by Pope's closure is less accurate for the minor species profiles than for the major species in Case $Da^-$. This can be attributed to the fact that turbulence-chemistry interaction effects are not accurately accounted for in the middle of the flame brush in this approach. The turbulent mixing rate and hybrid mixing rate model show similar levels of accuracy for the minor species as for the major species in Case $Da^-$. As with the major species predictions in Case $Da^+$, only the hybrid mixing rate model is able to accurately capture the flame structure. The hybrid mixing rate model shows close agreement with the DNS data for all three minor species plotted.

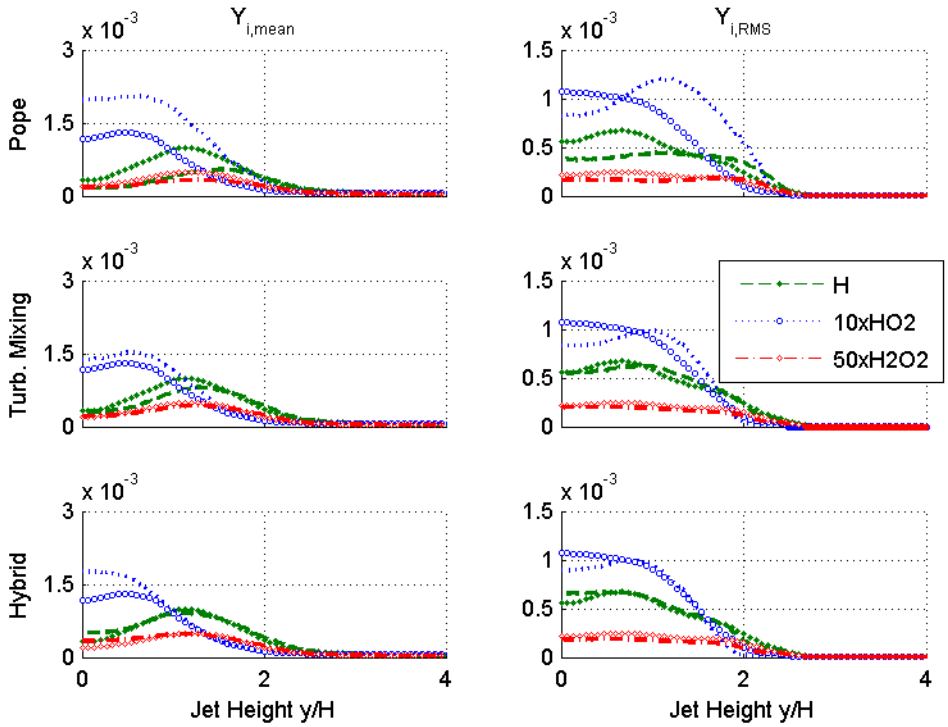


Figure 4-12: Selected minor species mean and RMS profiles at $17t_j$ for case Da$^-$. Markers: DNS. Lines: TPDF.

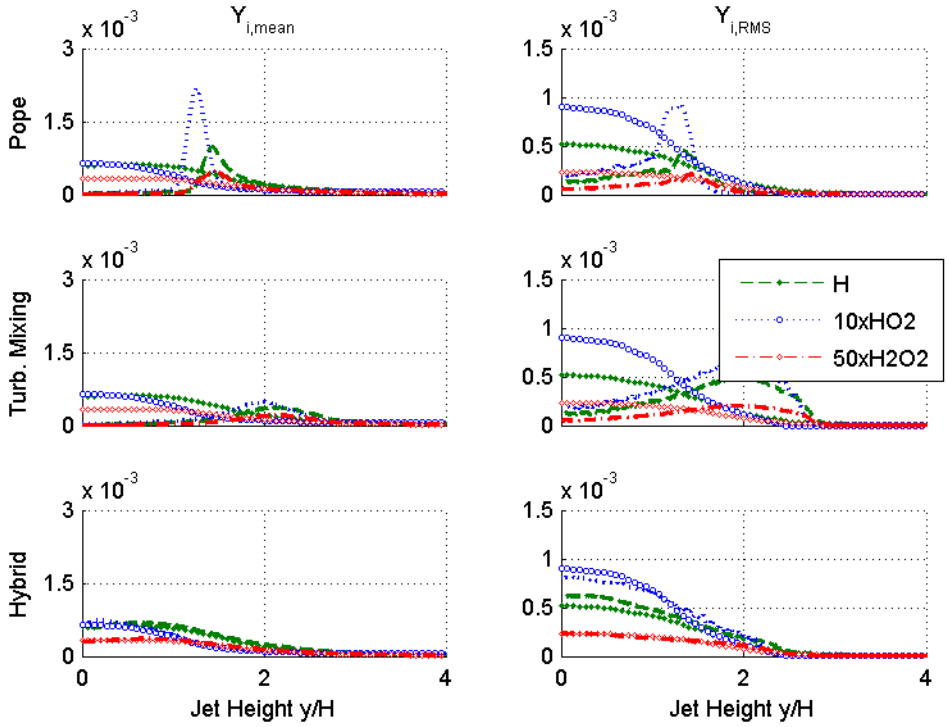


Figure 4-13: Selected minor species mean and RMS profiles at $17t_j$ for case Da$^-$. Markers: DNS. Lines: TPDF.

## 4.8. Conclusions

In this chapter, a new hybrid mixing rate model is developed which aims to account for the scalar mixing rate behavior in both the turbulent mixing limit and the flamelet limit. In the turbulent mixing limit, the model uses the classical expression assuming the rate of scalar mixing is inversely proportional to the turbulence timescale. In the flamelet limit, the new timescale model reconstructs the mixing rate by integrating the local PDF and the conditional scalar dissipation rate from a 1-D freely propagating premixed flame. The two mixing timescale model components are then blended together using the segregation factor to more accurately describe the local mixing behavior. The new hybrid timescale model is notable for its treatment of the flamelet mixing limit, an area where existing timescale models do not properly recover the correct mixing behavior [79].

Using DNS data of a temporally evolving premixed hydrogen-air slot jet flame, an *a priori* comparison of the new mixing rate model is performed. The *a priori* evaluation demonstrates that the commonly used turbulent mixing rate model does not have the correct spatial or temporal distribution for this flame. Additionally, the commonly chosen mechanical-to-scalar timescale ratio of 2.0 is found to largely under-predict the mixing rate magnitude throughout the flame brush. Conversely, the new hybrid timescale model more accurately captures the scalar mixing rate spatial profiles without the need for an arbitrarily chosen timescale constant.

Finally, an *a postereori* assessment using DNS as a numerical test bed for the TPDF solution is performed, comparing the new mixing rate model coupled with the EMST mixing model to the commonly used turbulent mixing rate model and the laminar flamelet closure of Pope and Anand [23]. The TPDF solution demonstrates that of the three closures tested in this work, the hybrid mixing rate model coupled with the EMST mixing model provides the best accuracy for this flame. The new model is able to accurately capture the flame structure in both cases tested, whereas the turbulent mixing rate model and the laminar flamelet closure under-predict the flame propagation.

# Chapter 5: The Conditional Scalar Dissipation Rate

## 5.1. Introduction

The relevance of the conditional scalar dissipation rate for turbulent premixed flames has been demonstrated in Chapters 3 and 4. In the mixing models studied in this dissertation, the conditional scalar dissipation rate has been used to reconstruct the Favre-averaged mixing frequency. However, in some mixing models, such as the Fokker-Planck model proposed by Fox [116], the conditional scalar dissipation rate itself must be specified as an input, which, as the author notes, is a challenging task [117]. In addition to its importance in the TPDF method, the conditional scalar dissipation rate also plays a pivotal role in flamelet [12-15] and Flame Surface Density [16-20] turbulent combustion modeling methods. In the Conditional Moment Closure (CMC) [23-25] approach, the conditional scalar dissipation rate is the key unclosed component to be modeled, and the primary source of difficulty in extending this method to premixed flames.

In Chapter 4, the conditional scalar dissipation rate is closed by reconstructing its distribution from a 1D, freely propagating laminar flame. This ad hoc closure does not account for turbulence in a rigorous manner, and ignores the physiochemical processes such as turbulence-chemistry interaction, dilatation, flame stretch, etc., that may alter the conditional scalar dissipation rate within a turbulent flame. Most modeling efforts to close the conditional scalar dissipation rate have focused on conserved scalars, such as the mixture fraction in non-premixed flames [60,118-121]. In the context of premixed flames, Kolla proposed a model relating the conditional scalar dissipation rate to the unconditional mean scalar dissipation rate as

$$\langle \chi | \zeta \rangle = \frac{\tilde{\chi}_c f(\zeta)}{\int_0^1 f(\zeta)\tilde{P}(\zeta)d\zeta} \qquad (5.1)$$

where $f(\zeta)$ is the inverse of the progress variable gradient in an unstrained laminar flame and $\tilde{P}(\zeta)$ is the progress variable Favre PDF [6,122]. This model has shown promising results; however it assumes

the flame brush is a collection of strained laminar flames and is limited by the accuracy of the model for the Favre-averaged scalar dissipation rate, which the previous chapters in this dissertation have shown to be a difficult task. Amzin proposed an alternative approach to modeling the conditional scalar dissipation rate by solving the inverse problem posed by

$$\tilde{\chi}_c = \int_0^1 \langle \chi | \zeta \rangle \tilde{P}(\zeta) d\zeta \tag{5.2}$$

using the Tikhonov regularization algorithm [123]. This approach was found to be very sensitive to the initial guess used in the solution algorithm, and thus not attractive as a modeling approach.

In this study, a transport equation for the conditional scalar dissipation rate is derived and analyzed with the aim of developing a new modeling methodology. An order of magnitude analysis is performed to identify the most important terms in the newly derived transport equation, and the transport budgets are analyzed using DNS data. Models for the leading order terms are proposed and evaluated using DNS. Finally, a modelled equation for the conditional scalar dissipation rate is found, and its solution is compared against existing approaches.

## 5.2. Conditional Scalar Dissipation Rate Transport Equation Derivation

The transport equation for the instantaneous scalar dissipation rate of the progress variable, $\chi = \Gamma \nabla c \cdot \nabla c$, has been derived by Swaminathan and Bray in Ref. [84] and can be written as

$$\rho \frac{\partial \chi}{\partial t} + \rho u_i \frac{\partial \chi}{\partial x_i} = \frac{\partial}{\partial x_j}\left(\rho \Gamma \frac{\partial \chi}{\partial x_j}\right) + 2\rho\chi \frac{\partial u_l}{\partial x_l} - 2\rho\Gamma \frac{\partial c}{\partial x_j} e_{jk} \frac{\partial c}{\partial x_k} + 2\Gamma \frac{\partial c}{\partial x_k}\frac{\partial \dot{\omega}}{\partial x_k} - 2\rho\Gamma^2 \frac{\partial^2 c}{\partial x_j \partial x_k}\frac{\partial^2 c}{\partial x_j \partial x_k} \tag{5.3}$$

where Γ is the progress variable diffusivity. This formulation assumes that the Lewis number of the mixture is close to unity and that the diffusivity has a weak dependence on temperature. Additionally, it is assumed that combustion occurs at low Mach number conditions.

The derivation of the corresponding conditionally averaged scalar dissipation rate transport equation follows the method of decomposition outlined by Klimenko and Bilger in their work on the Conditional Moment Closure method [23]. First, we define the conditional scalar dissipation rate as

$$Q(\zeta, \vec{\boldsymbol{x}}, t) = \langle \chi(\vec{\boldsymbol{x}}, t) | c = \zeta \rangle \tag{5.4}$$

where $\langle * \,| c = \zeta \rangle$ is the Favre conditional average of a given quantity and $\zeta$ is the sample space variable corresponding to the progress variable. Using this definition, the instantaneous scalar dissipation rate can be decomposed into a mean and fluctuating component,

$$\chi(\vec{\boldsymbol{x}}, t) = Q(c, \vec{\boldsymbol{x}}, t) + \chi"(\vec{\boldsymbol{x}}, t) \tag{5.5}$$

Additionally, the following notation is used in the derivation below for the various derivatives of Q

$$Q' = \frac{\partial Q}{\partial \zeta}, \qquad Q_x = \frac{\partial Q}{\partial x_i}, \qquad \dot{Q} = \frac{\partial Q}{\partial t}$$

According to the chain rule, the derivatives of the instantaneous scalar dissipation rate can be rewritten as

$$\frac{\partial \chi(\vec{\boldsymbol{x}}, t)}{\partial t} = \frac{\partial}{\partial t}(Q(c, \vec{\boldsymbol{x}}, t) + \chi"(\vec{\boldsymbol{x}}, t)) = \dot{Q} + Q' \frac{\partial c}{\partial t} + \frac{\partial \chi"}{\partial t} \tag{5.6}$$

$$\frac{\partial \chi(\vec{\boldsymbol{x}}, t)}{\partial x_i} = \frac{\partial}{\partial x_i}(Q(c, \vec{\boldsymbol{x}}, t) + \chi"(\vec{\boldsymbol{x}}, t)) = Q_x + Q' \frac{\partial c}{\partial x_i} + \frac{\partial \chi"}{\partial x_i} \tag{5.7}$$

$$\begin{aligned} \frac{\partial}{\partial x_j}\left(\rho\Gamma \frac{\partial \chi(\vec{\boldsymbol{x}}, t)}{\partial x_j}\right) &= \frac{\partial}{\partial x_j}\left(\rho\Gamma \frac{\partial}{\partial x_j}[Q(c, \vec{\boldsymbol{x}}, t) + \chi"(\vec{\boldsymbol{x}}, t)]\right) \\ &= \frac{\partial}{\partial x_j}(\rho\Gamma Q_x) + \frac{\partial}{\partial x_j}\left(\rho\Gamma \frac{\partial \chi"}{\partial x_j}\right) + Q' \frac{\partial}{\partial x_j}\left(\rho\Gamma \frac{\partial c}{\partial x_j}\right) \\ &\quad + \rho\chi Q'' + \rho\Gamma \frac{\partial c}{\partial x_j}\frac{\partial Q'}{\partial x_j}. \end{aligned} \tag{5.8}$$

Inserting Equations 5.6-5.8 into 5.3 and rearranging yields the following equation

$$\rho\dot{Q} + \rho u_i Q_x = -Q'\left[\rho\frac{\partial c}{\partial t} + \rho u_i\frac{\partial c}{\partial x_i} - \frac{\partial}{\partial x_j}\left(\rho\Gamma\frac{\partial c}{\partial x_j}\right)\right] + \frac{\partial}{\partial x_j}(\rho\Gamma Q_x) + \rho\chi Q''$$
$$+ \rho\Gamma\frac{\partial c}{\partial x_j}\frac{\partial Q'}{\partial x_j} + 2\rho\chi\frac{\partial u_l}{\partial x_l} - 2\rho\Gamma\frac{\partial c}{\partial x_j}e_{jk}\frac{\partial c}{\partial x_k} + 2\Gamma\frac{\partial c}{\partial x_k}\frac{\partial\dot{\omega}}{\partial x_k}$$
$$- 2\rho\Gamma^2\frac{\partial^2 c}{\partial x_j\partial x_k}\frac{\partial^2 c}{\partial x_j\partial x_k} - \left[\rho\frac{\partial\chi''}{\partial t} + \rho u_i\frac{\partial\chi''}{\partial x_i} - \frac{\partial}{\partial x_j}\left(\rho\Gamma\frac{\partial\chi''}{\partial x_j}\right)\right]. \quad (5.9)$$

Using $\rho\frac{\partial c}{\partial t} + \rho u_i\frac{\partial c}{\partial x_i} - \frac{\partial}{\partial x_j}\left(\rho\Gamma\frac{\partial c}{\partial x_j}\right) = \dot{\omega}$, Equation 5.9 can be simplified to

$$\rho\dot{Q} + \rho u_i Q_x = \frac{\partial}{\partial x_j}(\rho\Gamma Q_x) - Q'\dot{\omega} + \rho\chi Q'' + 2\rho\chi\frac{\partial u_l}{\partial x_l} - 2\rho\Gamma\frac{\partial c}{\partial x_j}e_{jk}\frac{\partial c}{\partial x_k}$$
$$+ 2\Gamma\frac{\partial c}{\partial x_k}\frac{\partial\dot{\omega}}{\partial x_k} - 2\rho\Gamma^2\frac{\partial^2 c}{\partial x_j\partial x_k}\frac{\partial^2 c}{\partial x_j\partial x_k} + e_Q + e_{\chi''} \quad (5.10)$$

where

$$e_Q = \rho\Gamma\frac{\partial c}{\partial x_j}\frac{\partial Q'}{\partial x_j} \quad (5.11)$$

$$e_{\chi''} = -\left[\rho\frac{\partial\chi''}{\partial t} + \rho u_i\frac{\partial\chi''}{\partial x_i} - \frac{\partial}{\partial x_j}\left(\rho\Gamma\frac{\partial\chi''}{\partial x_j}\right)\right]. \quad (5.12)$$

Finally, taking the conditional average of Equation 5.10, and noting that $\langle Q|c=\zeta\rangle = Q$, the conditional scalar dissipation rate transport equation is

$$\rho_\zeta\dot{Q} + \rho_\zeta u_{i,\zeta} Q_x$$
$$= \left\langle\frac{\partial}{\partial x_j}(\rho\Gamma Q_x)\middle|\zeta\right\rangle + \rho_\zeta QQ'' - \underbrace{\langle\dot{\omega}|\zeta\rangle Q'}_{R1} + \underbrace{\left\langle 2\rho\chi\frac{\partial u_l}{\partial x_l}\middle|\zeta\right\rangle}_{T2}$$
$$- \underbrace{\left\langle 2\rho\Gamma\frac{\partial c}{\partial x_j}e_{jk}\frac{\partial c}{\partial x_k}\middle|\zeta\right\rangle}_{T3} + \underbrace{\left\langle 2\Gamma\frac{\partial c}{\partial x_k}\frac{\partial\dot{\omega}}{\partial x_k}\middle|\zeta\right\rangle}_{T4}$$
$$- \underbrace{\left\langle 2\rho\Gamma^2\frac{\partial^2 c}{\partial x_j\partial x_k}\frac{\partial^2 c}{\partial x_j\partial x_k}\middle|\zeta\right\rangle}_{D2} + \langle e_{\chi''}|\zeta\rangle + \langle e_Q|\zeta\rangle \quad (5.13)$$

where the subscript $\zeta$ represents a conditionally averaged quantity.

The physical meaning of the terms in Equation 5.13 are as follows: The left-hand side represents the temporal and convective change in Q. The first term on the right-hand side is the molecular diffusion of Q in physical space. The second term is the turbulent diffusion of Q in composition space. The third term represents the influence of reaction on Q in composition space. The fourth and fifth terms are the effect of dilatation and turbulence-scalar interaction, respectively. The sixth term is the effect of reaction gradients in physical space. The seventh term is the molecular dissipation, and the final two terms are the influence of the fluctuations on the evolution of Q and the molecular diffusion, respectively.

## 5.3. Order of Magnitude Analysis

In the asymptotic description of the structure of steady premixed flames it is recognized that different physical processes are of importance in different regions of the flame. For instance, convection and diffusion are expected to balance in the preheat zone while reactions are considered negligible. Conversely, reaction and diffusion are expected to balance in the reaction zone, while convection is considered to be negligible. Along the lines of the asymptotic description of premixed flames, the order of magnitude analysis performed here segments the flame into a preheat zone and a reaction zone, each of which is governed by its own set of scaling rules. Additionally, the scaling rules are constructed under the assumption that the premixed flame exists in the thin reaction zones regime. Common parameters used throughout the order of magnitude analysis are:

$$\rho \sim \rho_u \qquad \Gamma \sim \delta_L S_L \qquad Re = \frac{u'\Lambda}{\delta_L S_L} \qquad Da = \frac{S_L \Lambda}{u' \delta_L} \qquad Ka = \frac{{\delta_L}^2}{\eta^2} = \frac{{u_\eta}^2}{{S_L}^2} \qquad \frac{u_\eta}{u'} \sim Re^{-1/4}$$

where $\rho_u$ is the density in the unburned reactants, $\delta_L$ and $S_L$ are the thermal thickness and laminar flame speed, respectively, from an unstretched laminar flame. The integral length scale and RMS velocity fluctuation are denoted by $\Lambda$ and u' while the Kolmogorov turbulence scales use the standard notation. In the preheat zone, the scaling rules follow the arguments made by Peters in his development of the

G-equation for the thin reaction zones regime [21]. According to Peters, the Taylor scale, defined as $\lambda = u' t_\eta$, is the appropriate length scale for mixing in the preheat zone. This length scale represents the distance over which an integral eddy will transport a Kolmogorov eddy during time $t_\eta$. During this time, $Y_i$ and T will fully diffuse across $\eta$, making the Taylor scale representative of the distance necessary for mixing. With the chosen length and timescales, the scaling in the preheat zone follows as

$$\frac{\partial}{\partial x} \sim \frac{1}{u' t_\eta} \qquad \frac{\partial}{\partial t} \sim \frac{1}{t_\eta} \qquad Q \sim \chi \sim \frac{\delta_L S_L}{u'^2 {t_\eta}^2}$$

In the reaction zone, it is anticipated that chemical time scales will dominate the spatial and temporal gradients. Along the lines of the underlying arguments of asymptotic flame structure, we assume that the reaction zone is an order of magnitude thinner than the preheat zone. This leads to the expression: $\delta_{RZ} \sim \epsilon \delta_L$ where $\epsilon \sim O(0.1)$. The scaling in the reaction zone follows as:

$$\frac{\partial}{\partial x} \sim \frac{1}{\epsilon \delta_L} \qquad \frac{\partial}{\partial t} \sim \frac{S_L}{\epsilon \delta_L} \qquad Q \sim \chi \sim \frac{S_L}{\epsilon^2 \delta_L}$$

It should also be noted that the fluctuations in scalar dissipation rate are expected to be the same order of magnitude as both the conditional mean and the instantaneous values of the SDR for a flame in the thin reactions zone regime based on the study in Chapter 3.

Finally, in addition to the difference in scaling rules based on flame zone, the scaling rules also differ when considering derivatives inside of the conditional average compared to derivatives of conditional quantities themselves. Derivatives appearing inside of the conditional averages follow the rules outlined above for each flame zone, while the derivatives of the conditional quantities themselves are scaled by the relevant turbulence quantities. In the context of RANs averaging, the derivatives of the conditional quantities scale as follows:

$$\frac{\partial}{\partial x} \sim \frac{1}{\Lambda} \qquad \frac{\partial}{\partial t} \sim \frac{u'}{\Lambda}$$

Applying the scaling rules outlined above to Equation 5.13 yields the order of magnitude for each term in each flame zone shown in Table 5-1.

Table 5-1: Order of Magnitude Analysis of the Conditional Scalar Dissipation Rate Transport Equation

| Term | Preheat Zone Scaling | Reaction Zone Scaling |
|---|---|---|
| $\rho_\zeta \dot{Q}$ | $O\left(\rho_u \left(\frac{S_L}{\delta_L}\right)^2 \frac{1}{Da^2}; 1\right)$ | $O\left(\rho_u \left(\frac{S_L}{\delta_L}\right)^2 \frac{1}{\epsilon^2}; \frac{1}{Da}\right)$ |
| $\rho_\zeta u_{i,\zeta} Q_x$ | $O\left(\rho_u \left(\frac{S_L}{\delta_L}\right)^2 \frac{1}{Da^2}; \frac{U_{ref}}{u'}\right)$ | $O\left(\rho_u \left(\frac{S_L}{\delta_L}\right)^2 \frac{1}{\epsilon^2}; \frac{U_{ref}}{u'Da}\right)$ |
| $\left\langle \frac{\partial}{\partial x_j}(\rho \Gamma Q_x) \middle\vert \zeta \right\rangle$ | $O\left(\rho_u \left(\frac{S_L}{\delta_L}\right)^2 \frac{1}{Da^2}; \frac{1}{\sqrt{Re}}\right)$ | $O\left(\rho_u \left(\frac{S_L}{\delta_L}\right)^2 \frac{1}{\epsilon^2}; \frac{1}{\sqrt{ReDa}}\right)$ |
| $\rho_\zeta Q Q''$ | $O\left(\rho_u \left(\frac{S_L}{\delta_L}\right)^2 \frac{1}{Da^2}; 1\right)$ | $O\left(\rho_u \left(\frac{S_L}{\delta_L}\right)^2 \frac{1}{\epsilon^2}; \frac{1}{\epsilon^2}\right)$ |
| $\langle \dot{\omega} \vert \zeta \rangle Q'$ | 0 | $O\left(\rho_u \left(\frac{S_L}{\delta_L}\right)^2 \frac{1}{\epsilon^2}; \frac{1}{\epsilon}\right)$ |
| $\left\langle 2\rho\chi \frac{\partial u_l}{\partial x_l} \middle\vert \zeta \right\rangle$ | $O\left(\rho_u \left(\frac{S_L}{\delta_L}\right)^2 \frac{1}{Da^2}; \frac{U_{ref}\sqrt{Da}}{S_L}\right)$ | $O\left(\rho_u \left(\frac{S_L}{\delta_L}\right)^2 \frac{1}{\epsilon^2}; \frac{1}{\epsilon}\right)$ |
| $\left\langle 2\rho\Gamma \frac{\partial c}{\partial x_j} e_{jk} \frac{\partial c}{\partial x_k} \middle\vert \zeta \right\rangle$ | $O\left(\rho_u \left(\frac{S_L}{\delta_L}\right)^2 \frac{1}{Da^2}; \frac{U_{ref}\sqrt{Da}}{S_L}\right)$ | $O\left(\rho_u \left(\frac{S_L}{\delta_L}\right)^2 \frac{1}{\epsilon^2}; \frac{1}{\epsilon}\right)$ |
| $\left\langle 2\Gamma \frac{\partial c}{\partial x_k} \frac{\partial \dot{\omega}}{\partial x_k} \middle\vert \zeta \right\rangle$ | 0 | $O\left(\rho_u \left(\frac{S_L}{\delta_L}\right)^2 \frac{1}{\epsilon^2}; \frac{1}{\epsilon}\right)$ |
| $\left\langle 2\rho\Gamma^2 \frac{\partial^2 c}{\partial x_j \partial x_k} \frac{\partial^2 c}{\partial x_j \partial x_k} \middle\vert \zeta \right\rangle$ | $O\left(\rho_u \left(\frac{S_L}{\delta_L}\right)^2 \frac{1}{Da^2}; 1\right)$ | $O\left(\rho_u \left(\frac{S_L}{\delta_L}\right)^2 \frac{1}{\epsilon^2}; \frac{1}{\epsilon^2}\right)$ |
| $\langle e_{\chi''} \vert \zeta \rangle$ | $O\left(\rho_u \left(\frac{S_L}{\delta_L}\right)^2 \frac{1}{Da^2}; \frac{U_{ref}\sqrt{Da}}{S_L}\right)$ | $O\left(\rho_u \left(\frac{S_L}{\delta_L}\right)^2 \frac{1}{\epsilon^2}; \frac{1}{\epsilon^2}\right)$ |
| $\langle e_Q \vert \zeta \rangle$ | $O\left(\rho_u \left(\frac{S_L}{\delta_L}\right)^2 \frac{1}{Da^2}; \frac{1}{\sqrt{Re}}\right)$ | $O\left(\rho_u \left(\frac{S_L}{\delta_L}\right)^2 \frac{1}{\epsilon^2}; \frac{1}{\sqrt{ReDa}}\right)$ |

The order of magnitude analysis indicates that, in the preheat zone and in the limit of large Re and Da, the convection, dilatation, turbulence-scalar interaction, and fluctuating term should balance to leading order:

$$\rho_\zeta u_{i,\zeta} Q_x \approx \left\langle 2\rho\chi \frac{\partial u_l}{\partial x_l} \middle| \zeta \right\rangle - \left\langle 2\rho\Gamma \frac{\partial c}{\partial x_j} e_{jk} \frac{\partial c}{\partial x_k} \middle| \zeta \right\rangle + \langle e_{\chi''} | \zeta \rangle \quad (5.14)$$

This result is expected as it implies that convection balances the effects of turbulent mixing in the preheat zone.

In the reaction zone, the order of magnitude analysis indicates that the leading order terms are the turbulent diffusion in composition space, the molecular dissipation, and the fluctuating term in the limit of large Re and Da. Depending on the value of $\epsilon$, the two reaction terms, the turbulence-scalar interaction, and the dilatation may be important as well. Consistent with asymptotic flame theory, the convective term is expected to be negligible in the reaction zone. This leads to a balance equation in the reaction zone of:

$$\rho_\zeta Q Q'' - \langle \dot{\omega} | \zeta \rangle Q' + \left\langle 2\rho\chi \frac{\partial u_l}{\partial x_l} \middle| \zeta \right\rangle - \left\langle 2\rho\Gamma \frac{\partial c}{\partial x_j} e_{jk} \frac{\partial c}{\partial x_k} \middle| \zeta \right\rangle + \left\langle 2\Gamma \frac{\partial c}{\partial x_k} \frac{\partial \dot{\omega}}{\partial x_k} \middle| \zeta \right\rangle$$
$$- \left\langle 2\rho\Gamma^2 \frac{\partial^2 c}{\partial x_j \partial x_k} \frac{\partial^2 c}{\partial x_j \partial x_k} \middle| \zeta \right\rangle + \langle e_{\chi''} | \zeta \rangle \approx 0 \quad (5.15)$$

It is interesting to note that the order of magnitude analysis indicates that the direct influence of the reaction terms plays only a secondary role in the anticipated balance equation. Also of note is that the fluctuating term is expected to be of leading order across the flame. This is to be expected as the fluctuations in the scalar dissipation rate can be of the same order of magnitude as the instantaneous scalar dissipation rate.

## 5.4. Transport Budget Analysis using DNS

In this section, we utilize direct numerical simulation data to evaluate each term in the conditional scalar dissipation rate transport equation to confirm the findings of the order of magnitude analysis. Two flame configurations, and three cases in total are analyzed. A description of the DNS databases is provided in the following subsections.

### *5.4.1. Description of DNS Databases*

#### 5.4.1.1. Lean Methane-Air Bunsen Flame

The first flame database studied here is the premixed lean methane-air Bunsen flame described in [124,125]. The full details of the flame configuration can be found in [124,125] and are briefly summarized here for completeness. The flame is in a 3D spatially developing slot burner configuration, and is simulated using the DNS code S3D [95]. A detailed chemical kinetics mechanism with 13 species and 73 reactions is used for the chemical reactions and constant species Lewis numbers are assumed for the transport properties. A preheated lean methane-air mixture with equivalence ratio of $\phi = 0.7$ and temperature of 800 K flows through the Bunsen flames inlet slot. The main jet is surrounded by a hot coflow comprised of equilibrium product composition and temperature. The domain is configured such that the streamwise, crosswise, and spanwise directions are x, y, and z, respectively. The flame configuration and structure is shown in Figure 5-1.

Three cases are simulated in [124,125] from which we analyze the two extreme conditions, Case A and Case C, in this work. Both cases lie in the thin reaction zones regime. The relevant flame parameters are summarized in Table 5-2. In the analysis that follows the reaction progress variable is defined based on the mass fraction of $O_2$. Although the progress variable is typically defined based on the deficient reactant, it was found in [124,125] that a progress variable defined on the mass fraction of $CH_4$ omits a significant portion of the oxidation layer.

The flow studied here is statistically homogeneous in the spanwise (z) direction and stationary in time, meaning that average quantities may be accumulated in both z and time. In practice, averages are accumulated over a finite length in the streamwise direction equal to approximately one turbulence integral length scale to increase the statistical sample size. It is found that 50 bins in c-space provides optimal resolution of the conditional statistics.

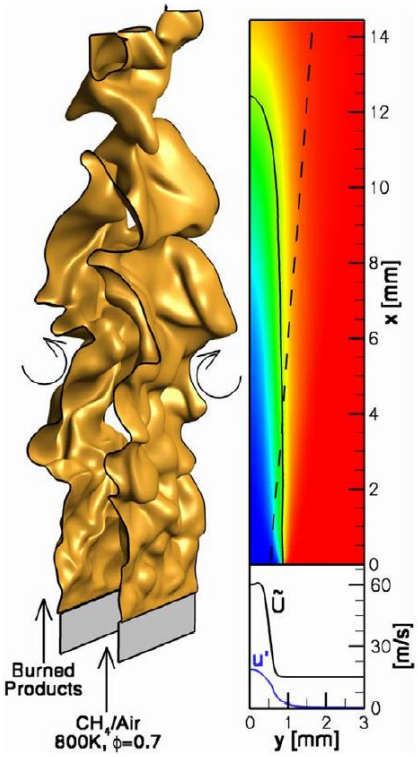


Figure 5-1: Left: Instantaneous iso-contour of c = 0.65. Right: contour plot of mean progress variable. Also shown on the contour plot is the isocontour of $\tilde{c} = 0.65$ (solid line) and the location of the shear layer (dashed line). The bottom right shows the mean and fluctuating velocity profiles at the inlet. Image reproduced from [124].

Table 5-2: Bunsen Flame DNS Parameters. Turbulence Quantities Computed at x/L = ¼.

| **Quantity** | **Case A** | **Case C** |
|---|---|---|
| Slot Width (h) | 1.2 mm | 1.8 mm |
| Domain Size, $L_x$ x $L_y$ x $L_z$ | 12h x 12h x 3h | 12h x 12h x 3h |
| Turbulent Jet Velocity, U | 60 m/s | 100 m/s |
| Laminar Coflow Velocity | 15 m/s | 20 m/s |
| Turbulence Intensity, $u'/S_L$ | 3 | 10 |
| Jet Reynolds Number, $Re_{jet} = Uh/\nu$ | 840 | 2100 |
| Turbulence Reynolds Number, $Re_t = u'l_{33}/\nu$ | 40 | 250 |
| Karlovitz Number, $Ka = \delta_L/\eta$ | 100 | 400 |
| Damköhler Number, $Da = S_L l_{33}/u'\delta_L$ | 0.7 | 0.4 |

The conditional scalar dissipation rate distribution through the flame brush at x/L = ½ for both cases, as well as the values computed from an unstrained laminar flame, are shown in Figure 5-2. This location is chosen for the remainder of this analysis as it is where the authors in Ref. [124,125] consider the turbulence to be free of effects from the inlet while providing the largest span of mean progress variable across the flame brush.

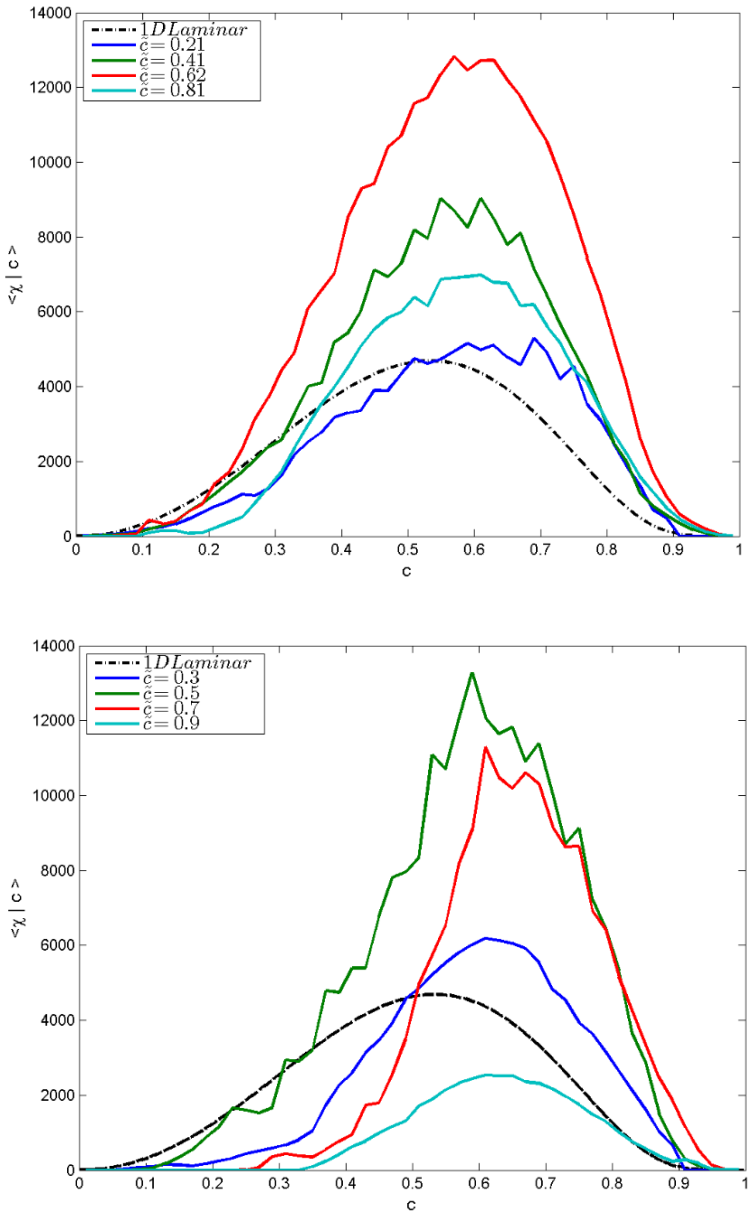


Figure 5-2: Variation of the conditional scalar dissipation rate through the flame brush for Case A (top) and Case C (bottom) at x/L = ½. Dashed black line extracted from a 1D, freely propagating premixed flame.

#### 5.4.1.2. Statistically Planar Flame

The second flame database chosen for this study is the statistically stationary, planar premixed lean methane-air flame from Ref. [126]. The full details of the DNS can be found in [126] and are briefly summarized here for completeness. The flame is configured as shown in Figure 5-3, where a turbulent stream of unburnt reactants flows in the positive x direction, and stabilizes the flame in the center of the 3D domain. The flame is simulated using the DNS code S3D [95]. A chemical kinetics mechanism with 6 species and 2 reactions is used for the chemical reactions [127] and unity species Lewis numbers are assumed for the transport properties. The unburnt, lean methane-air mixture has an equivalence ratio of $\phi = 0.7$, temperature of 300 K, and atmospheric pressure. The mean inflow velocity is initialized with the unstrained laminar flame speed, and modulated as the simulation progresses to maintain the flame location within the center of the domain as the flame accelerates due to wrinkling.

The simulation domain is 1 cm long in each direction, which is approximately 5 integral length scales under the flow conditions studied. The simulation used a time step of 10 ns and the domain is discretized with a uniform grid size of 20 μm. The transverse (y) and spanwise (z) boundaries are periodic, and characteristic inflow and outflow boundary conditions are imposed in the streamwise (x) direction. In the analysis that follows for this flame, the reaction progress variable is defined based on the mass fraction of $CH_4$. The relevant flame parameters are summarized in Table 5-3.

The flow studied here is statistically homogeneous in the transverse and spanwise directions, and stationary in time, meaning that average quantities may be accumulated in y, z, and time. Similar to the conditional averaging performed in the Bunsen flame, averages are collected across a finite length in the streamwise direction equal to approximately 10% of one turbulence integral length scale to increase the statistical sample size. It is found that 50 bins in c-space provides sufficient resolution of

the conditional statistics. The conditional scalar dissipation rate distribution through the flame brush as well as the values computed from an unstrained laminar flame, are shown in Figure 5-4.

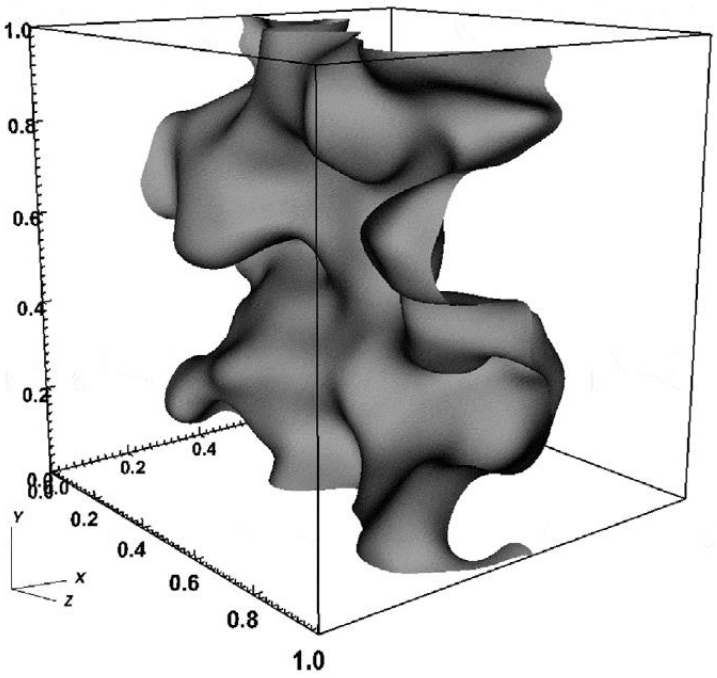


Figure 5-3: Iso-surface of T = 1,200K in the statistically planar methane-air flame. The mean flow direction is in the positive x-direction. Figure reproduced from [126].

Table 5-3: Statistically Stationary Planar Flame DNS Parameters.

| **Quantity** | **Stat. Planar** |
|---|---|
| Domain Size, $L_x$ x $L_y$ x $L_z$ | 1 cm x 1 cm x 1 cm |
| Turbulence Intensity, $u'/S_L$ | 8 |
| Turbulence Reynolds Number, $Re_t = u'l_{33}/\nu$ | 200 |
| Karlovitz Number, $Ka = \delta_L/\eta$ | 4.6 |
| Damköhler Number, $Da = S_L l_{33}/u'\delta_L$ | 3.1 |

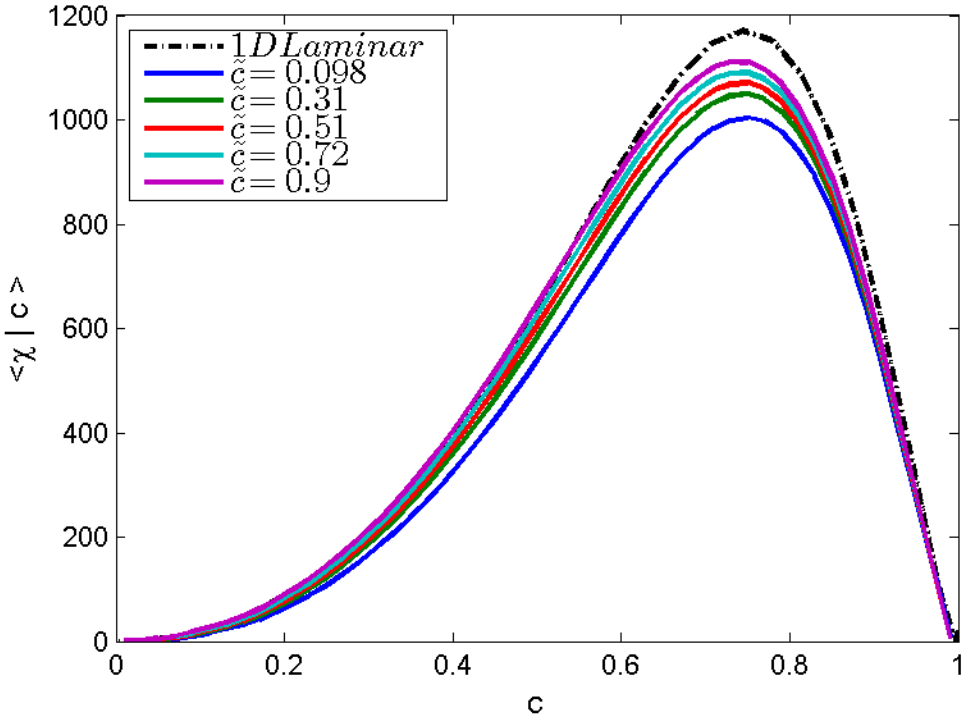


Figure 5-4: Variation of the conditional scalar dissipation rate through the flame brush for the statistically planar flame. Dashed black line extracted from a 1D, freely propagating premixed flame.

### *5.4.2. DNS Budgets*

The budget of terms in Equation 5.13 are shown in Figure 5-7 and Figure 5-6 for the Bunsen flames and Figure 5-7 for the statistically planar flame at three locations in the flame brush. In general, the transport budgets show good agreement with the order of magnitude analysis for both flames, confirming the physical importance of the leading order terms. In the preheat zone, the leading order terms in the DNS budget are the fluctuating term, the molecular dissipation, and the turbulence-scalar interaction. The convective term is not of leading order in the preheat zone despite the reasoning made in the order of magnitude analysis. However, it is found that the molecular dissipation term is of leading order even in the preheat zone in the Bunsen flames. The importance of the molecular dissipation term in the preheat zone in the Bunsen flames may be attributed to the elevated inlet temperature, which nullifies the assumption that the preheat zone is inert and therefore induces this region to scale more like the reaction zone.

In the reaction zone, the three largest terms for all cases are the turbulent diffusion, molecular dissipation, and the fluctuating term, which is consistent with the expectations from the order of magnitude analysis. Of the second order terms, the dilatation term is significant in the planar flame but small in the Bunsen flames, which is due to the elevated preheat temperature at the jet inlet. The turbulence-scalar interaction term is non-negligible in all three cases. The reaction terms are of expected order of magnitude based on the scaling analysis in the Bunsen flames, and are of leading order in the planar flame and thus must be carefully modelled. As expected for a turbulent flame, the contributions of the molecular diffusion are negligible across the flame.

The contributions of the fluctuating term are of leading order across the flame. This behavior is to be expected in the thin reaction zones regime as turbulent eddies are able to disrupt the structure of the preheat zone. The effect of this disruption will naturally propagate through the flame structure, leading to fluctuations in the dissipation rate across the entire progress variable space.

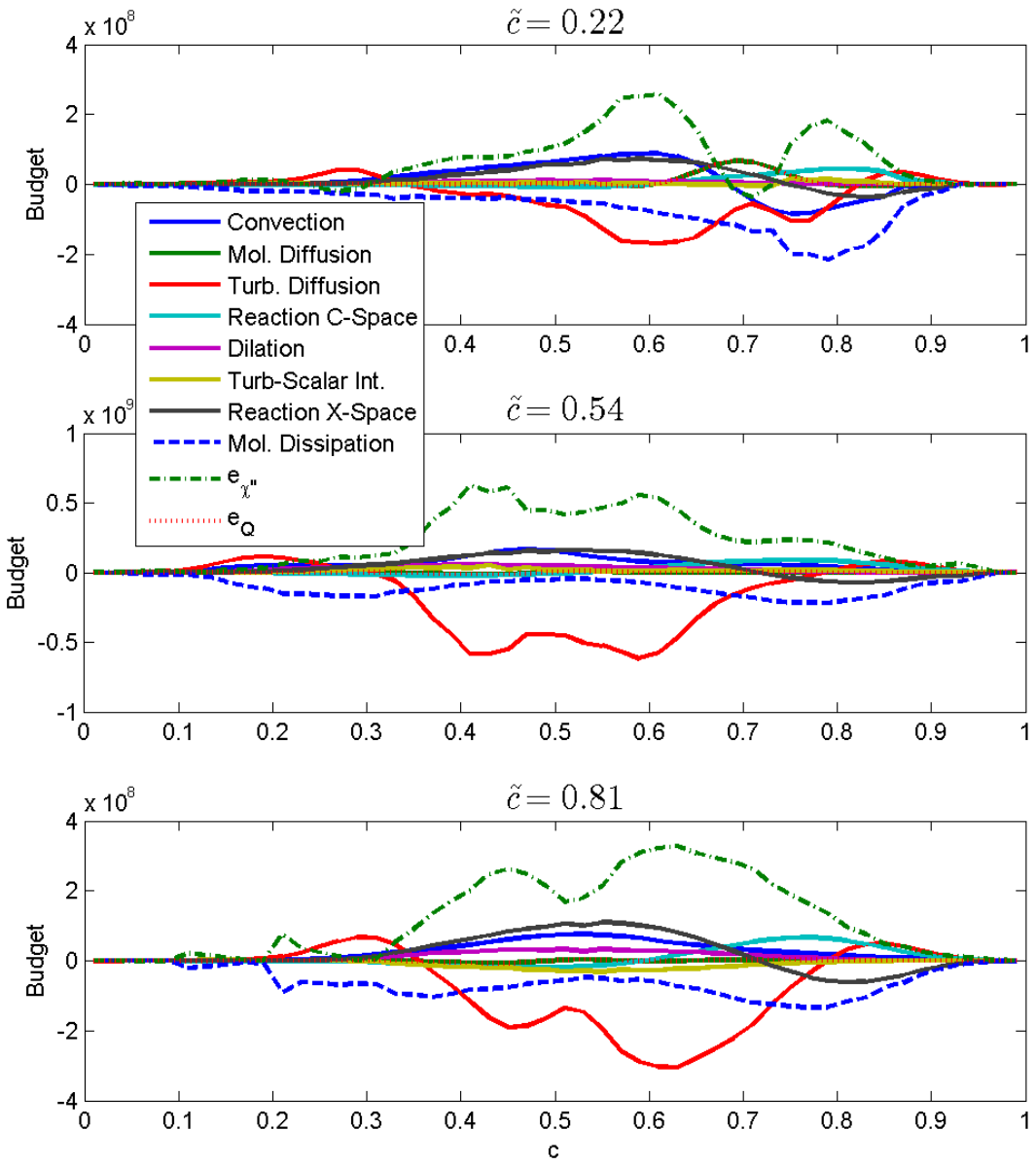


Figure 5-5: Budget of terms in Equation 5.13 at 3 locations in the flame brush for the Bunsen flame, Case A at x/L = ½.

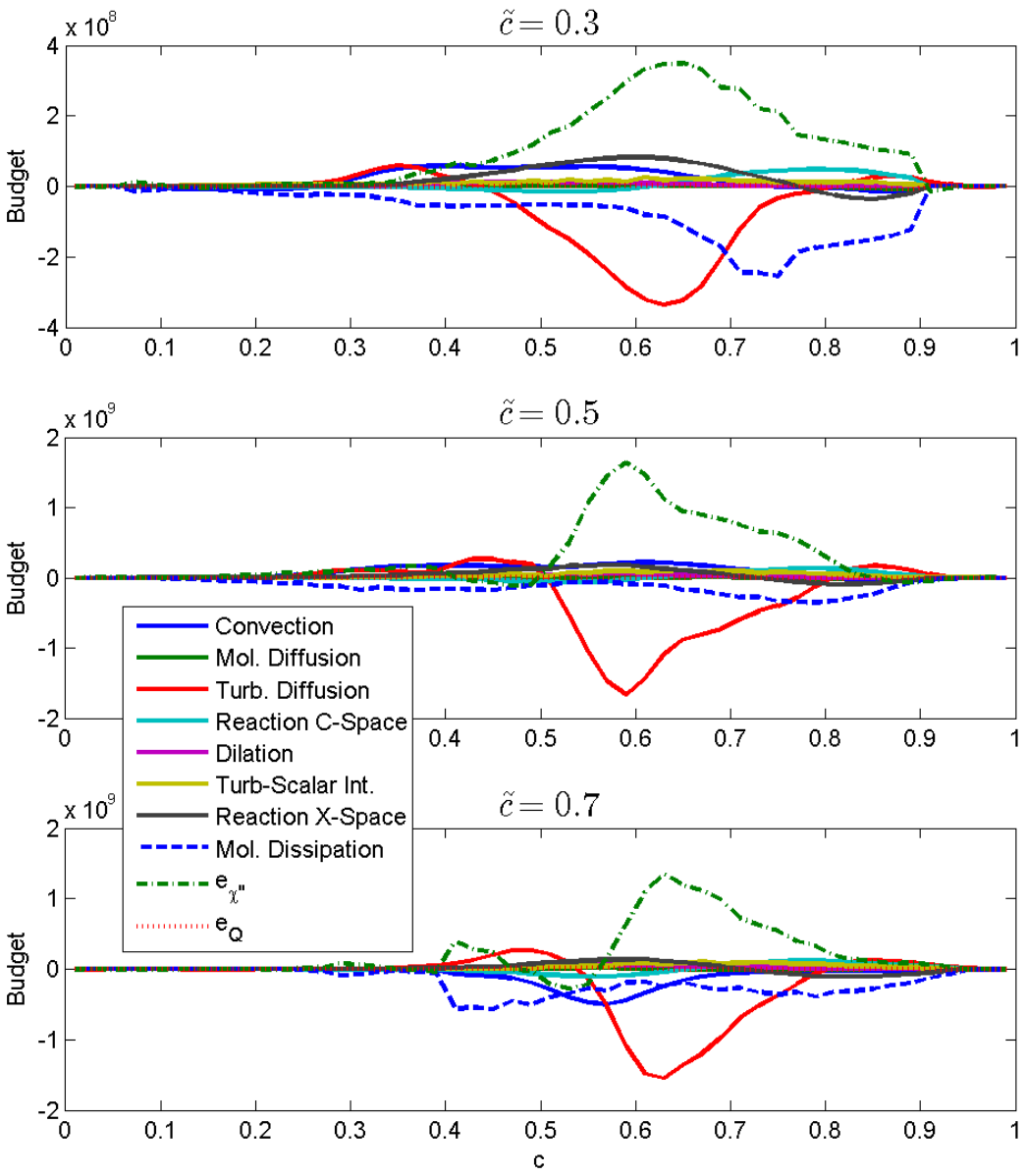


Figure 5-6: Budget of terms in Equation 5.13 at 3 locations in the flame brush for the Bunsen flame, Case C at x/L = ½.

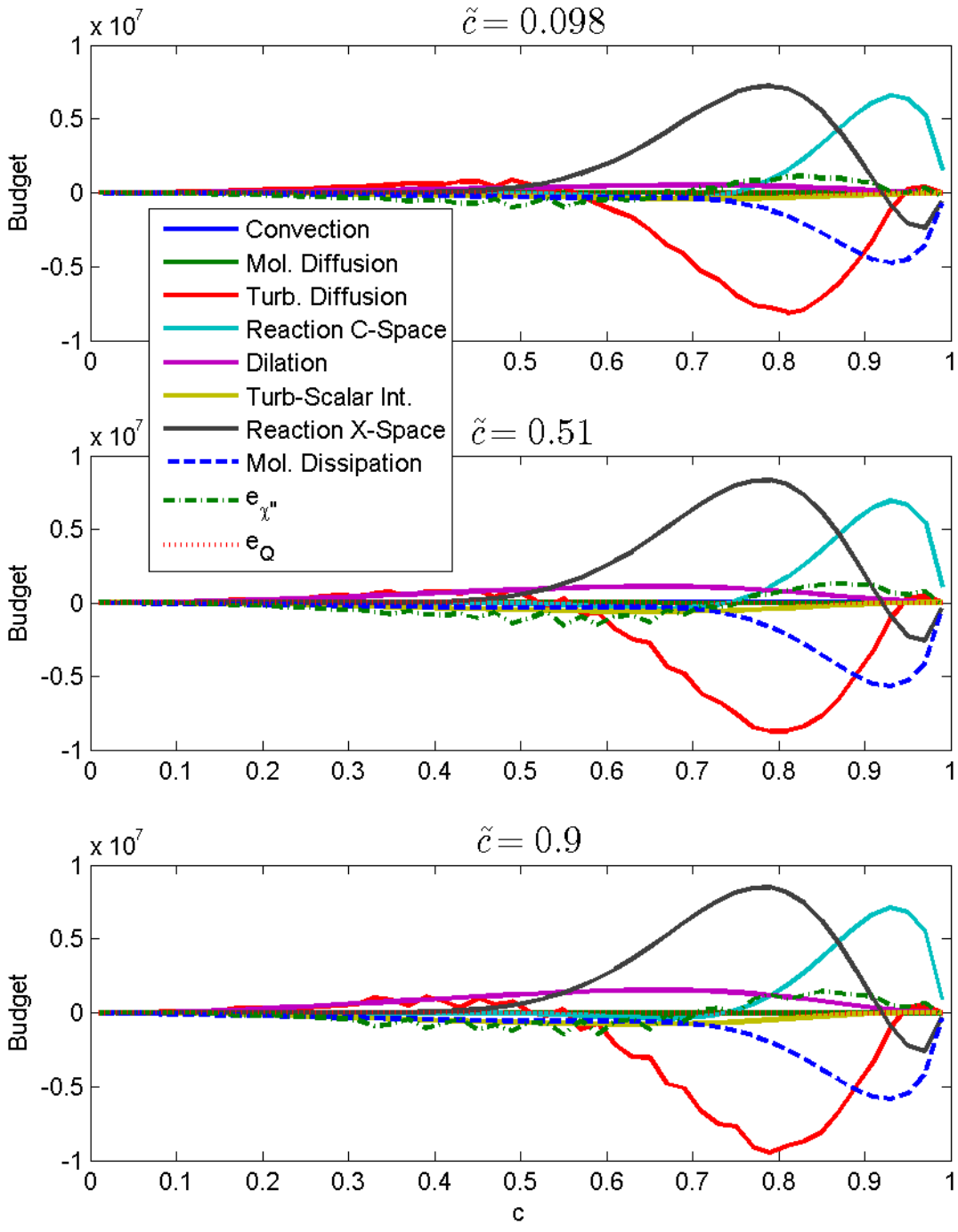


Figure 5-7: Budget of terms in Equation 5.13 at 3 locations in the flame brush of the statistically planar flame.

## 5.5. Modelling of Leading Order Terms

The DNS budget analysis confirms the importance of the leading order terms identified in the order of magnitude analysis, and leads to the reduced equation

$$\rho_\zeta Q Q'' - \underbrace{\langle \dot{\omega} | \zeta \rangle Q'}_{R1} + \underbrace{\left\langle 2\rho\chi \frac{\partial u_l}{\partial x_l} \middle| \zeta \right\rangle}_{T2} - \underbrace{\left\langle 2\rho\Gamma \frac{\partial c}{\partial x_j} e_{jk} \frac{\partial c}{\partial x_k} \middle| \zeta \right\rangle}_{T3} + \underbrace{\left\langle 2\Gamma \frac{\partial c}{\partial x_k} \frac{\partial \dot{\omega}}{\partial x_k} \middle| \zeta \right\rangle}_{T4}$$

$$- \underbrace{\left\langle 2\rho\Gamma^2 \frac{\partial^2 c}{\partial x_j \partial x_k} \frac{\partial^2 c}{\partial x_j \partial x_k} \middle| \zeta \right\rangle}_{D2} + \langle e_{\chi''} | \zeta \rangle \approx 0. \qquad (5.16)$$

To check the ability of the leading order equation above to reproduce the conditional scalar dissipation rate from the DNS, Equation 5.16 is integrated at several locations through the flame brush for both flames and plotted against the DNS in Figure 5-8 through Figure 5-10. The agreement between the DNS and Equation 5.16 is excellent for the statistically planar flame, and qualitatively correct for the Bunsen flames. Due to the statistical noise in the Bunsen flame data, smoothing of the DNS data is performed prior to performing the integration of Equation 5.16. In general, the integration of Equation 5.16 demonstrates that the leading order equation is able to capture the effects of the physical mechanisms that govern the conditional scalar dissipation rate behavior in a turbulent premixed flame.

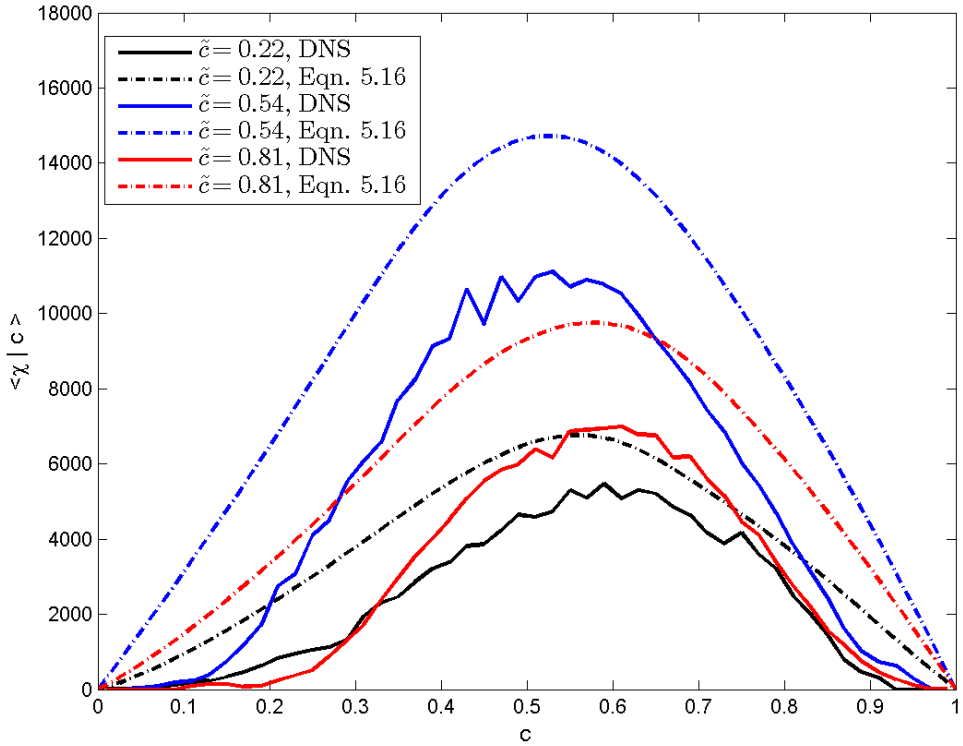


Figure 5-8: Comparison of the conditional scalar dissipation rate predicted by the leading order Equation 5.16 to the DNS through the flame brush for the Bunsen flame, Case A at x/L = ½.

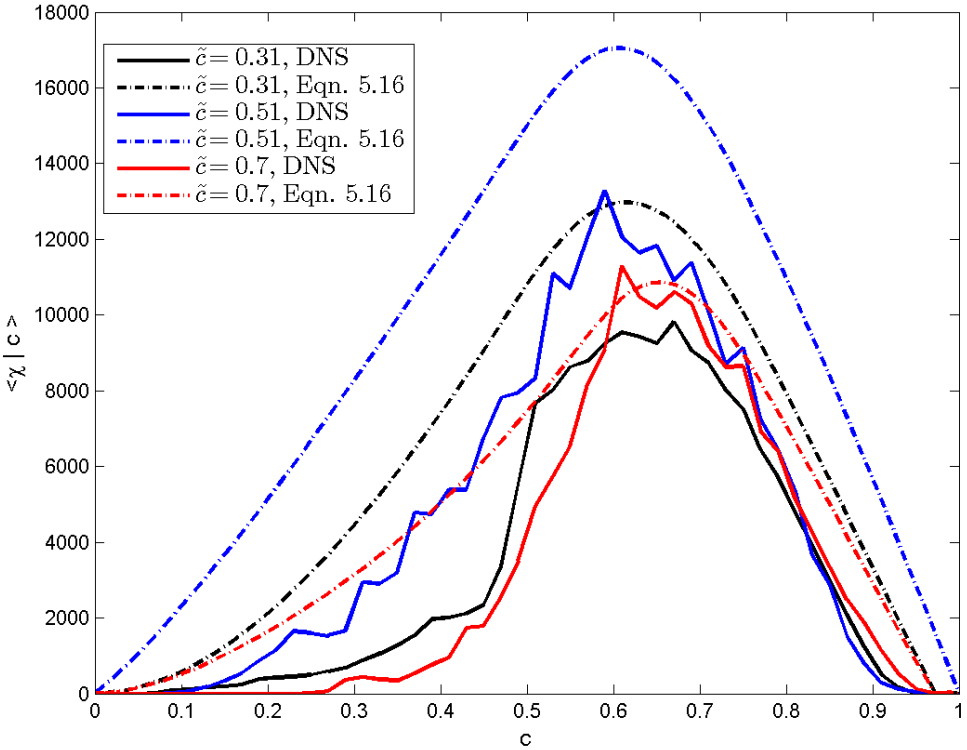


Figure 5-9: Comparison of the conditional scalar dissipation rate predicted by the leading order Equation 5.16 to the DNS through the flame brush for the Bunsen flame, Case C at x/L = ½.

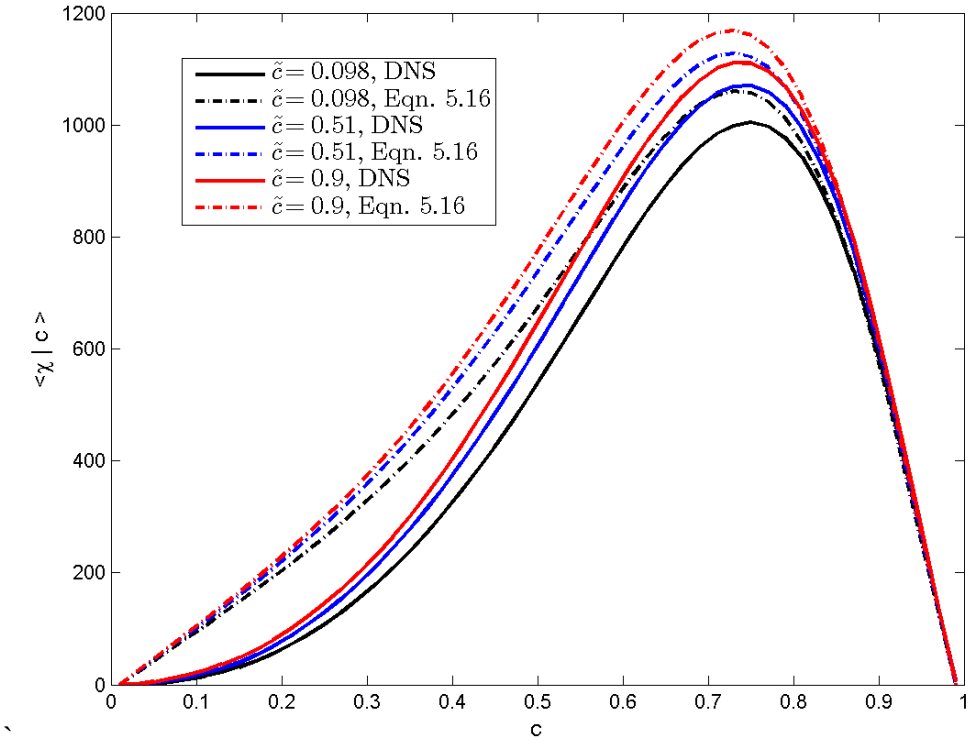


Figure 5-10: Comparison of the conditional scalar dissipation rate predicted by the leading order Equation 5.16 to the DNS through the flame brush for the statistically planar flame.

In practice, all terms in Equation 5.16, aside from the turbulent diffusion of Q in composition space, must be modeled. We adopt a similar nomenclature as in Ref. [83] to concisely refer to each term that requires modeling. In the sections that follow, modelling approaches for each of these terms are proposed and evaluated using the DNS databases.

### *5.5.1. Reaction in Composition Space, R1*

In the TPDF method, the conditional reaction rate appearing in R1 is closed, and thus R1 as a whole does not require modeling. However, in other modeling approaches that require closure of the conditional scalar dissipation rate, such as CMC, this term requires modeling. To close the reaction rate, the conditional fluctuations in the scalar fields are ignored, and the reaction rate is computed using the first order closure shown in Equation 5.17 that is commonly used in CMC [23].

$$\langle \dot{\omega}(T, \boldsymbol{Y}, P)|\zeta\rangle \approx \dot{\omega}(\langle T|\zeta\rangle, \langle \boldsymbol{Y}|\zeta\rangle, \langle P|\zeta\rangle) \qquad (5.17)$$

This leads to a model for R1 of

$$\langle \dot{\omega}(T, \boldsymbol{Y}, P)|\zeta\rangle Q' \approx \dot{\omega}(\langle T|\zeta\rangle, \langle \boldsymbol{Y}|\zeta\rangle, \langle P|\zeta\rangle) Q'. \quad (5.18)$$

The model in Equation 5.18 is computed using the conditionally averaged DNS data and compared to the exact term extracted from the DNS in Figure 5-11 through Figure 5-13. The closure model shows excellent agreement with the DNS throughout the entire flame brush for all three flames.

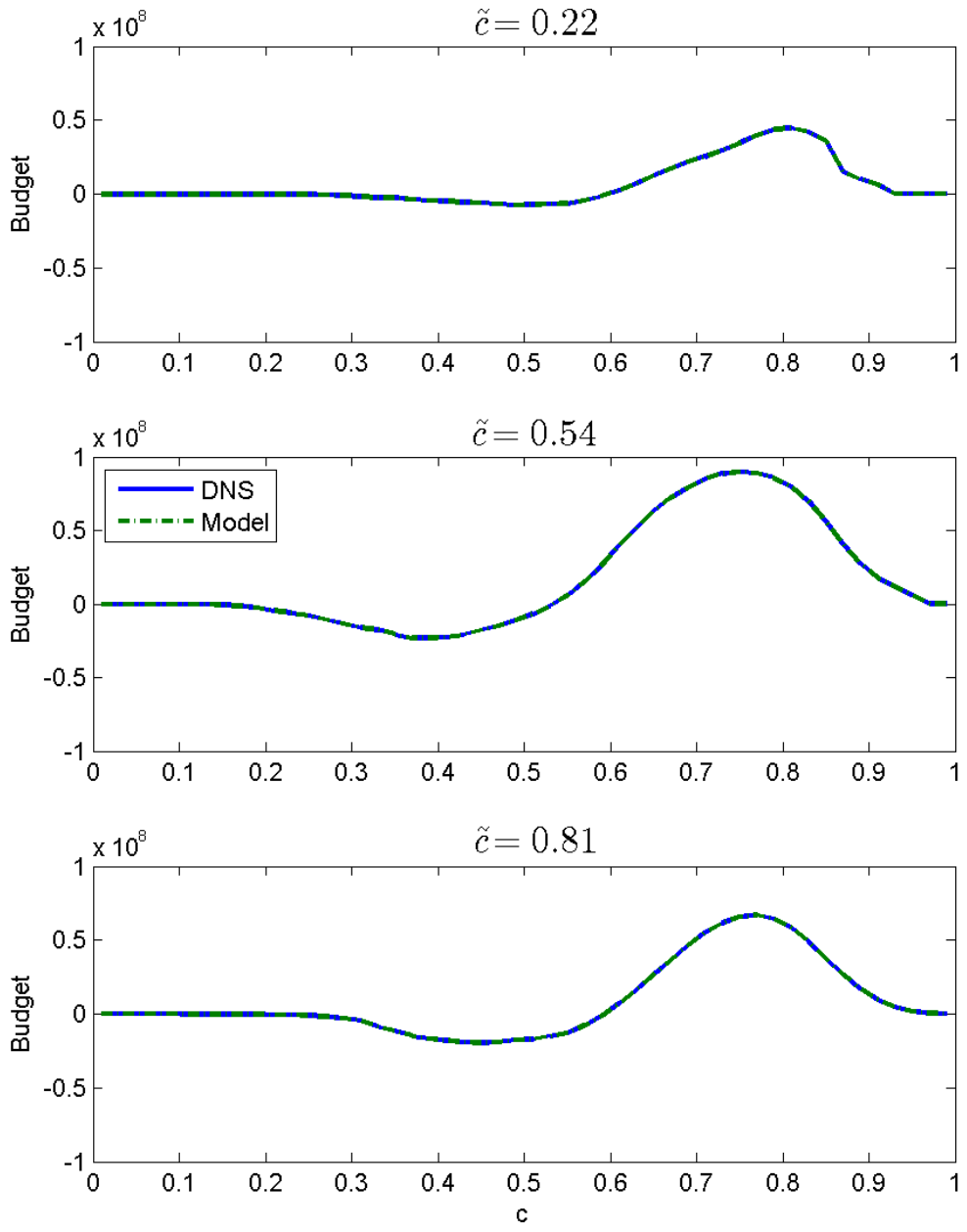


Figure 5-11: Performance of the closure for the reaction in composition space term in Equation 5.18 at 3 locations in the flame brush for the Bunsen flame Case A at x/L = ½.

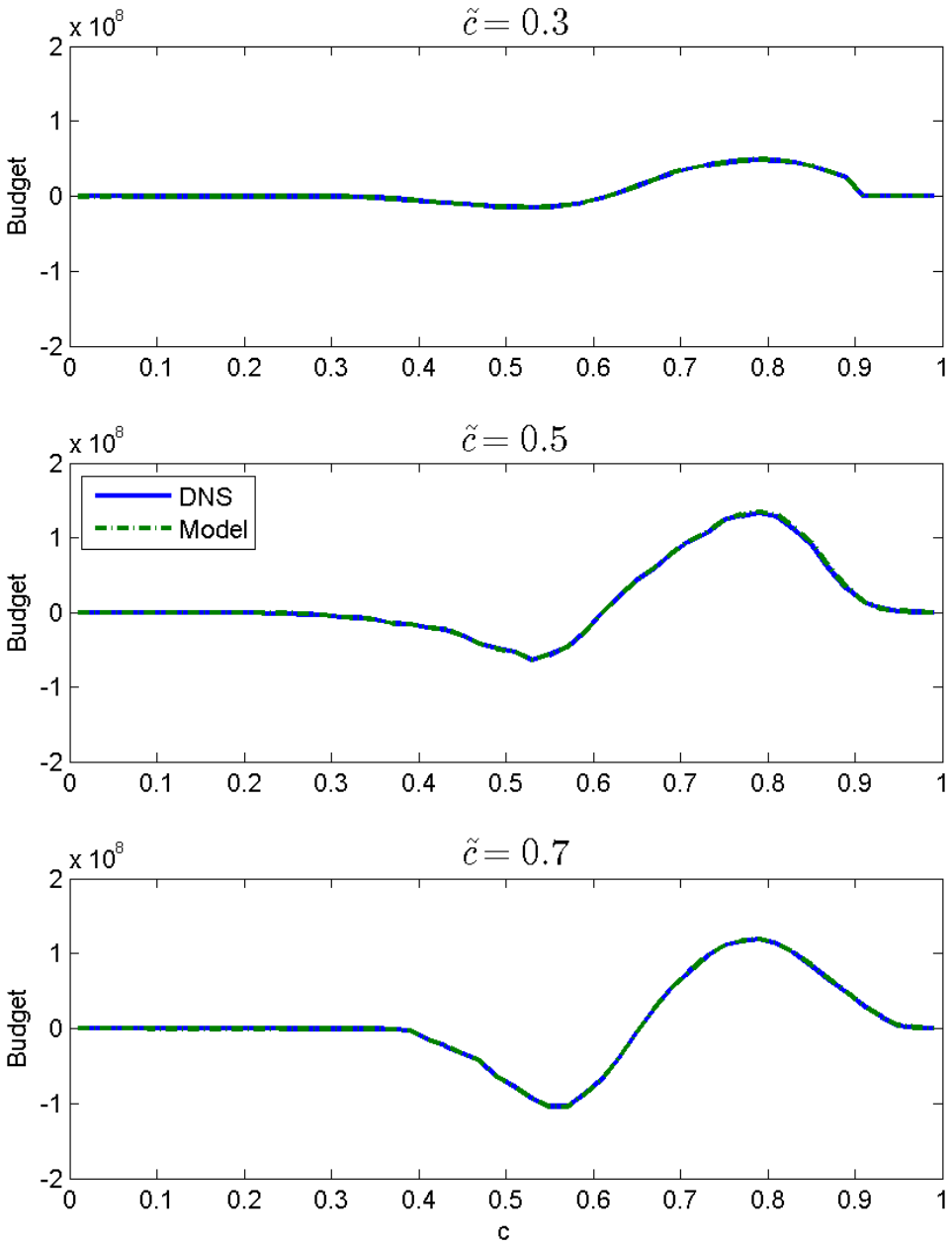


Figure 5-12: Performance of the closure for the reaction in composition space term in Equation 5.18 at 3 locations in the flame brush for the Bunsen flame Case C at x/L = ½.

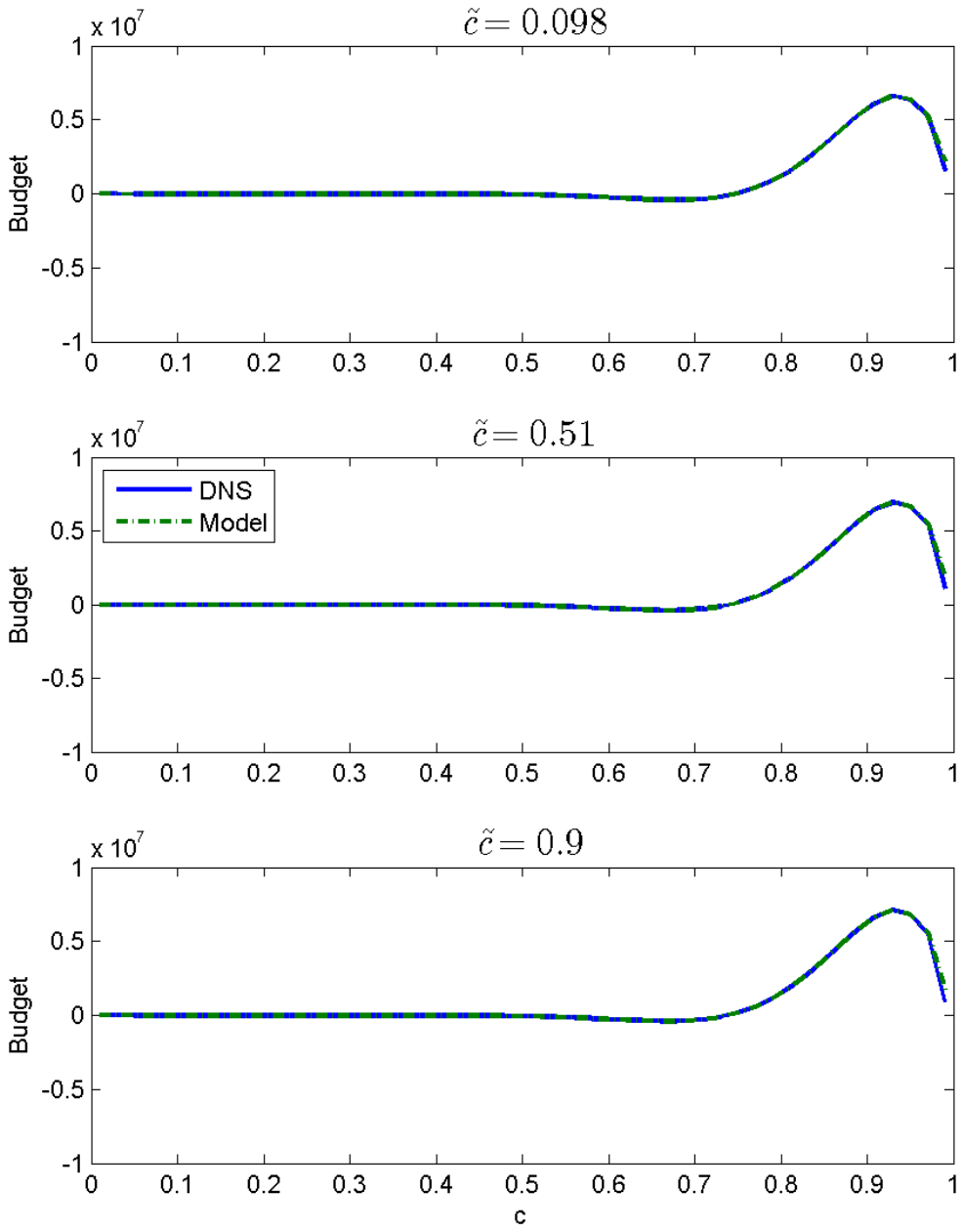


Figure 5-13: Performance of the closure for the reaction in composition space term in Equation 5.18 at 3 locations in the flame brush for the statistically planar flame.

### *5.5.2. Dilatation, T2, and Turbulence-Scalar Interaction, T3*

The dilatation term, T2, represents the correlation between dissipation rate and dilatation rates within the flame. A similar term appears in the transport equation for the Favre-averaged scalar dissipation, and Kolla et al. [90] extended the model of Swaminathan and Bray [83], which assumes

the internal flame structure is largely undisturbed by the turbulence. With this assumption, they construct a model for T2 as

$$T2 = 2\left(\frac{S_L}{\delta_L}\right) K_c^* \bar{\rho}\tilde{\chi}_c \quad (5.19)$$

where

$$K_c^* = \left(\frac{\delta_L}{S_L}\right) \frac{\int\{\rho\chi(\nabla\cdot u)\}_L f(\zeta)d\zeta}{\int\{\rho\chi\}_L f(\zeta)d\zeta}, \quad (5.20)$$

which is evaluated using a 1D, freely propagating premixed flame. In the Favre-averaged context, this model has shown good agreement with DNS [107,128], and thus a similar approach is proposed by adapting Equation 5.19 using conditional quantities as

$$\langle T2|\zeta\rangle = 2\left(\frac{S_L}{\delta_L}\right) K_c^* \langle\rho|\zeta\rangle Q \quad (5.21)$$

A number of modeling approaches have been proposed for the T3 term that appears in the transport equation for the Favre-averaged scalar dissipation rate in both inert and reacting flows. The classic approach is to consider T3 to be linearly proportional to the turbulence time scale [81]. Kolla et al. [107] extended the reactive scalar models of Mantel and Borghi [81] and Swaminathan and Bray [83] to account for the effect of heat release on the fluid dynamic strain rates. Their model for T3 can be written as

$$T3 = (C_3 - \tau C_4 Da_L)\left(\frac{\tilde{\varepsilon}}{\tilde{k}}\right)\bar{\rho}\tilde{\chi}_c \quad (5.22)$$

where

$$Da_L = \frac{S_L/\delta_L}{\tilde{\varepsilon}/\tilde{k}}, \quad (5.23)$$

$\tau$ is the heat release parameter, $\tau = (T_{ad} - T_u)/T_u$. The definition of the model parameters by their original authors are retained here such that $C_3 = 1.5$ and $C_4 = (1 + Ka)^{-0.4}$ where Ka is the global Karlovitz number. This model can be adapted to model the T3 term in the conditional scalar dissipation rate transport equation by substituting conditional quantities into Equation 5.22,

$$\langle T3|\zeta\rangle = (C_3 - \tau C_4 Da_L)\left(\frac{\tilde{\varepsilon}}{\tilde{k}}\right)\langle\rho|\zeta\rangle Q. \quad (5.24)$$

An alternative modeling approach to those outlined above can be constructed by recognizing that dilatation does not contribute to the overall generation or destruction of scalar dissipation rate as the influence of dilatation on T3 is balanced by T2 [129]. Thus, the terms T2 and T3 can be combined and expressed as

$$\underbrace{\left\langle 2\rho\chi \frac{\partial u_l}{\partial x_l} \middle| \zeta \right\rangle}_{T2} - \underbrace{\left\langle 2\rho\Gamma \frac{\partial c}{\partial x_j} e_{jk} \frac{\partial c}{\partial x_k} \middle| \zeta \right\rangle}_{T3} = \langle 2\rho\chi a_t | \zeta \rangle \tag{5.25}$$

where $a_t$ is the tangential strain rate exerted on a flame surface. In the proposed modeling approach, the tangential strain rate is modeled as being proportional to the turbulence strain rate, based on the findings of scalar gradient alignment within a premixed flame brush in Ref. [129]. The new model for T2-T3 is proposed as

$$\langle T2|\zeta\rangle - \langle T3|\zeta\rangle = \langle 2\rho\chi a_t|\zeta\rangle \approx C_{23}\left(\frac{\tilde{\varepsilon}}{\tilde{k}}\right)\langle\rho|\zeta\rangle Q \tag{5.26}$$

where the model constant $C_{23} = 0.15\sqrt{Re_t}$ as in Ref. [81].

The model in Equation 5.26 is computed and compared to the DNS, as well as the combination of Equation 5.19 and 5.24, in Figure 5-14 through Figure 5-16. In Case A, the model proposed in Equation 5.26 shows better qualitative agreement with the DNS than the combination of Equations 5.19 and 5.24 through most of the flame brush. In the more strongly turbulent Case C, both models are similar as the correction for heat release in Equation 5.24 is negligible. In the statistically planar flame, where dilatation is strongest among the cases studied, the model in Equation 5.26 shows the most accurate behavior, while the combination of the other models is qualitatively incorrect, making the model in Equation 5.26 the better choice.

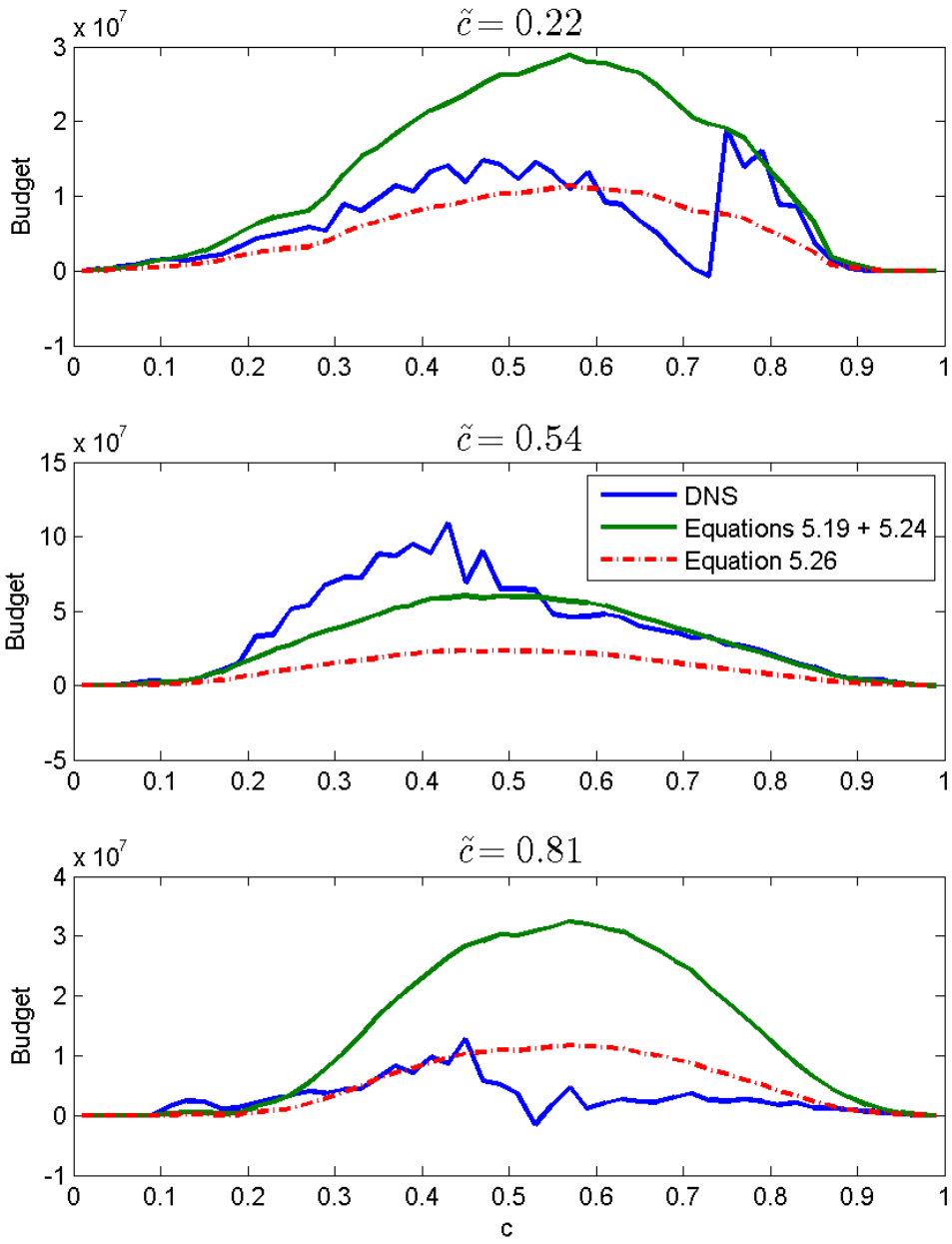


Figure 5-14: Performance of the closure for the terms T2 and T3 in Equation 5.18 at 3 locations in the flame brush for the Bunsen flame Case A at x/L = ½.

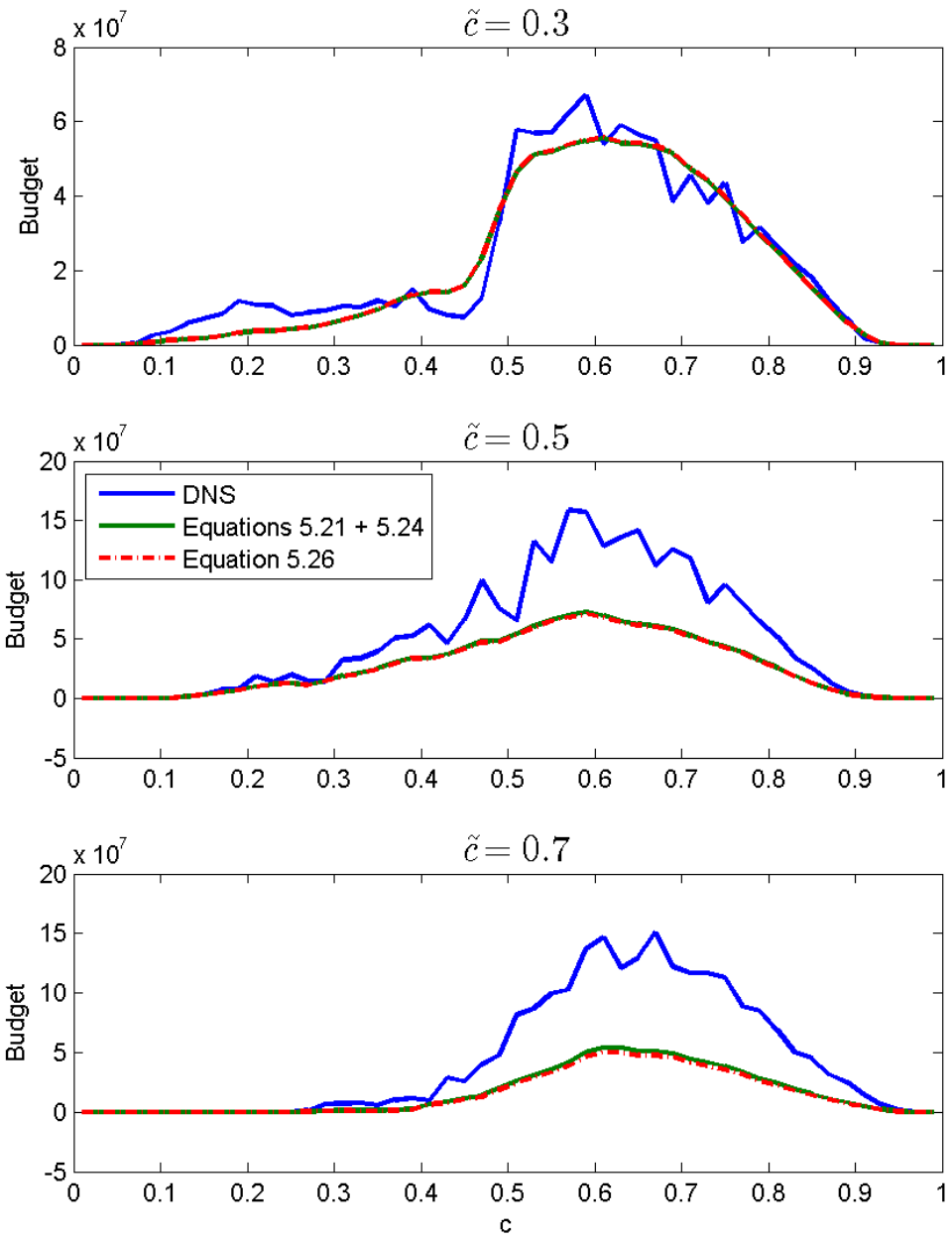


Figure 5-15: Performance of the closure for the terms T2 and T3 in Equation 5.18 at 3 locations in the flame brush for the Bunsen flame Case C at x/L = ½.

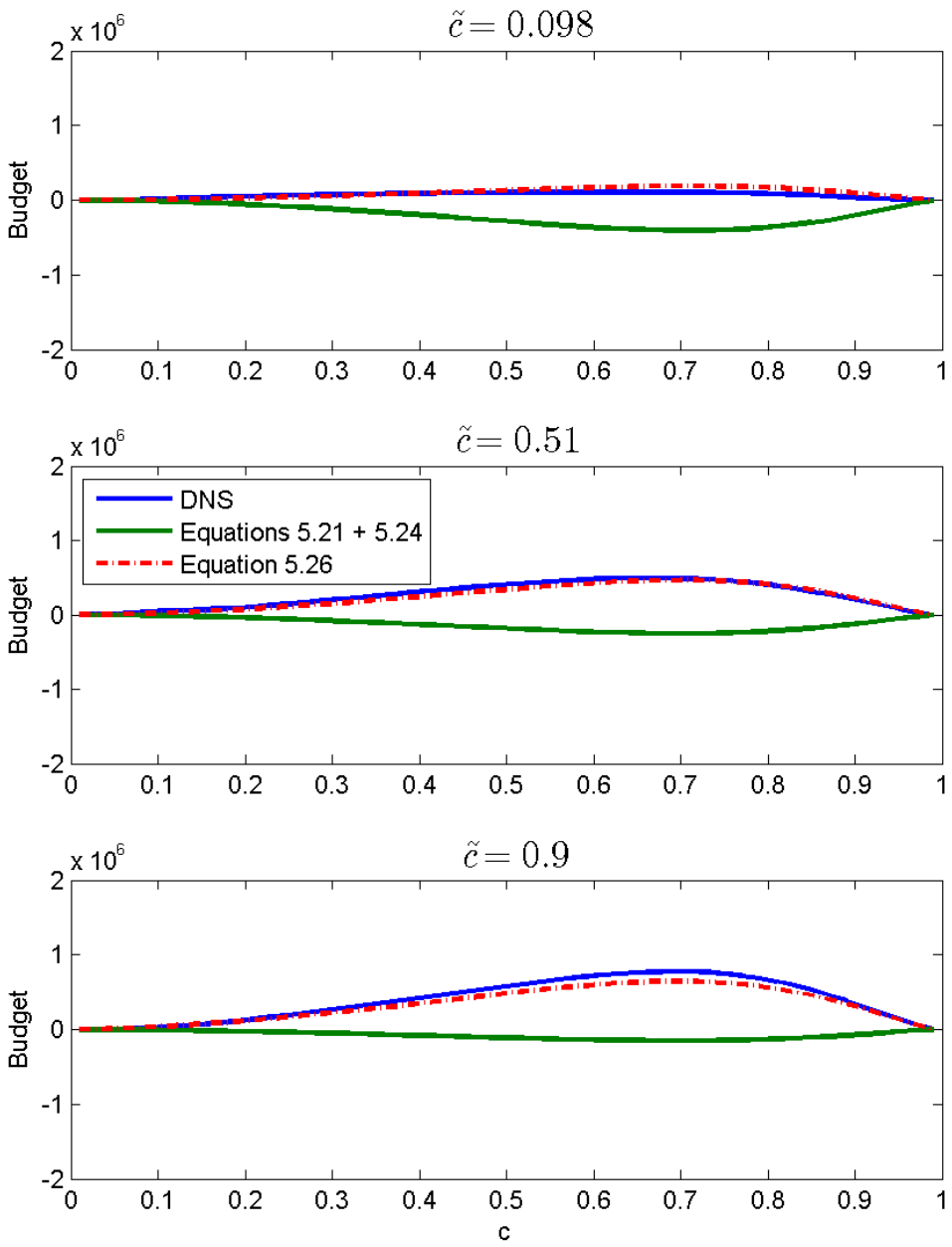


Figure 5-16: Performance of the closure for the terms T2 and T3 in Equation 5.18 at 3 locations in the flame brush for the statistically planar flame.

### *5.5.3. Reaction-Dissipation, T4-D2*

The reaction term, T4, and the dissipation term, D2, represent the correlation between scalar gradients and reaction within the flame brush and the flamelet curvature, respectively. In the context of the Favre-averaged scalar dissipation rate, several authors have modelled these two terms together

by assuming that locally, steady, 1D laminar flamelets are present within the flame brush [81,82]. With this assumption, the local progress variable can be expressed in a coordinate system attached to the flame normal, n, as

$$\rho_u S_L \frac{\partial c}{\partial n} = \rho\Gamma \frac{\partial^2 c}{\partial n^2} + \dot{\omega} \tag{5.27}$$

Differentiating Equation 5.27 with respect to n and multiplying by $2\Gamma\frac{\partial c}{\partial n}$ yields after manipulation

$$2\Gamma \frac{\partial c}{\partial x_k}\frac{\partial \dot{\omega}}{\partial x_k} = 2\Gamma \frac{\partial c}{\partial n}\frac{\partial \dot{\omega}}{\partial n} = \rho_u S_L \frac{\partial \chi}{\partial n} + 2\rho\Gamma^2 \frac{\partial^2 c}{\partial n^2}\frac{\partial^2 c}{\partial n^2} - \rho\Gamma \frac{\partial^2 \chi}{\partial n^2} \tag{5.28}$$

Similarly, the dissipation term can be written in a flame attached coordinate system, where isotropy in the tangential directions, τ, is assumed

$$2\rho\Gamma^2 \frac{\partial^2 c}{\partial x_j \partial x_k}\frac{\partial^2 c}{\partial x_j \partial x_k} = 2\rho\Gamma^2 \frac{\partial^2 c}{\partial n^2}\frac{\partial^2 c}{\partial n^2} + 8\rho\Gamma^2 \frac{\partial^2 c}{\partial \tau \partial n}\frac{\partial^2 c}{\partial \tau \partial n} + 2\rho\Gamma^2 \frac{\partial^2 c}{\partial \tau^2}\frac{\partial^2 c}{\partial \tau^2} \tag{5.29}$$

The expressions for T4 and D2 above can be combined, and conditionally averaged to form

$$\begin{aligned}\left\langle 2\Gamma \frac{\partial c}{\partial x_k}\frac{\partial \dot{\omega}}{\partial x_k}\middle|\zeta\right\rangle - \left\langle 2\rho\Gamma^2 \frac{\partial^2 c}{\partial x_j \partial x_k}\frac{\partial^2 c}{\partial x_j \partial x_k}\middle|\zeta\right\rangle \\ = \left\langle \rho_u S_L \frac{\partial \chi}{\partial n}\middle|\zeta\right\rangle - \left\langle \rho\Gamma \frac{\partial^2 \chi}{\partial n^2}\middle|\zeta\right\rangle - \left\langle 8\rho\Gamma^2 \frac{\partial^2 c}{\partial \tau \partial n}\frac{\partial^2 c}{\partial \tau \partial n}\middle|\zeta\right\rangle \\ - \left\langle 8\rho\Gamma^2 \frac{\partial^2 c}{\partial \tau^2}\frac{\partial^2 c}{\partial \tau^2}\middle|\zeta\right\rangle\end{aligned} \tag{5.30}$$

In the Favre averaged scalar dissipation rate modeling approach in [81,82], all but the final two terms on the right-hand side of Equation 5.30 can be neglected based on an order of magnitude analysis. However, for the conditional scalar dissipation rate, all terms in Equation 5.30 retain leading order and must be accounted for.

To model the first two terms on the right-hand side of Equation 5.30, which represent the propagation and diffusion, respectively, it is again assumed that locally, steady, 1D laminar flamelets are present within the flame brush. Using the chain rule, the first term can be written as

$$\left\langle \rho_u S_L \frac{\partial \chi}{\partial n} \middle| \zeta \right\rangle = \left\langle \rho_u S_L \frac{\partial c}{\partial n} \frac{\partial \chi}{\partial c} \middle| \zeta \right\rangle = \left\langle \rho_u S_L \sqrt{\frac{\chi}{\Gamma}} \frac{\partial \chi}{\partial c} \middle| \zeta \right\rangle \approx \rho_u S_L \sqrt{\frac{Q}{\Gamma}} Q' \quad (5.31)$$

The second term on the right-hand side of Equation 5.30 can be split into two components using the chain rule, as in Equation 5.32.

$$\left\langle \rho \Gamma \frac{\partial^2 \chi}{\partial n^2} \middle| \zeta \right\rangle = \left\langle \rho \chi \frac{\partial^2 \chi}{\partial c^2} \middle| \zeta \right\rangle + \left\langle \rho \Gamma \frac{\partial \chi}{\partial c} \frac{\partial^2 c}{\partial n^2} \middle| \zeta \right\rangle \quad (5.32)$$

To model the first component, conditional fluctuations are ignored and it is assumed that $\left\langle \rho \chi \frac{\partial^2 \chi}{\partial c^2} \middle| \zeta \right\rangle \approx \rho_\zeta Q Q"$. To model the second component, it is assumed that the gradient of the scalar dissipation rate in progress variable space is statistically independent from the diffusion of the progress variable normal to the flame front, and thus this term can be decomposed as $\left\langle \rho \Gamma \frac{\partial \chi}{\partial c} \frac{\partial^2 c}{\partial n^2} \middle| \zeta \right\rangle \approx \left\langle \rho \frac{\partial \chi}{\partial c} \middle| \zeta \right\rangle \left\langle \Gamma \frac{\partial^2 c}{\partial n^2} \middle| \zeta \right\rangle$. Then, using the conditional diffusion-dissipation relationship in Equation 3.1, this term can be written as

$$\left\langle \rho \Gamma \frac{\partial \chi}{\partial c} \frac{\partial^2 c}{\partial n^2} \middle| \zeta \right\rangle \approx \left\langle \rho \frac{\partial \chi}{\partial c} \middle| \zeta \right\rangle \left\langle \Gamma \frac{\partial^2 c}{\partial n^2} \middle| \zeta \right\rangle \approx \left\langle \rho \frac{\partial \chi}{\partial c} \middle| \zeta \right\rangle \left\langle \frac{1}{2} \frac{\partial Q}{\partial c} - \Gamma \frac{\partial^2 \widetilde{P_c}}{\partial n^2} \middle| \zeta \right\rangle \approx \frac{1}{2} \rho_\zeta Q' Q',$$

again ignoring conditional fluctuations as well as gradients of the progress variable PDF. This leads to a model of the second term on the right-hand side of Equation 5.30 of

$$\left\langle \rho \Gamma \frac{\partial^2 \chi}{\partial n^2} \middle| \zeta \right\rangle = \left\langle \rho \chi \frac{\partial^2 \chi}{\partial c^2} \middle| \zeta \right\rangle + \left\langle \rho \Gamma \frac{\partial \chi}{\partial c} \frac{\partial^2 c}{\partial n^2} \middle| \zeta \right\rangle \approx \rho_\zeta Q Q" + \frac{1}{2} \rho_\zeta Q' Q' \quad (5.33)$$

Finally, the final two terms on the right-hand side of Equation 5.30 are modeled in a similar manner to their counterparts in the Favre averaged scalar dissipation rate equation of [82].

$$-\left\langle 8 \rho \Gamma^2 \frac{\partial^2 c}{\partial \tau \partial n} \frac{\partial^2 c}{\partial \tau \partial n} \middle| \zeta \right\rangle - \left\langle 8 \rho \Gamma^2 \frac{\partial^2 c}{\partial \tau^2} \frac{\partial^2 c}{\partial \tau^2} \middle| \zeta \right\rangle$$

$$\approx -\left(\frac{2}{3}\right) C_{23} \langle \rho | \zeta \rangle Q \left(\frac{\tilde{\varepsilon}}{\tilde{k}}\right) \left[1.5 - C_f \frac{S_L}{\sqrt{\tilde{k}}}\right] \quad (5.34)$$

This formulation is intended to account for curvature due to both turbulence and flame scales, with the model constant $C_f = 1.0$. The full model for the reaction and dissipation terms can now be written as

$$\left\langle 2\Gamma \frac{\partial c}{\partial x_k}\frac{\partial \dot{\omega}}{\partial x_k}\middle|\zeta\right\rangle - \left\langle 2\rho\Gamma^2 \frac{\partial^2 c}{\partial x_j \partial x_k}\frac{\partial^2 c}{\partial x_j \partial x_k}\middle|\zeta\right\rangle$$

$$= \rho_u S_L \sqrt{\frac{Q}{\Gamma}} Q' - \rho_\zeta Q Q'' - \frac{1}{2}\rho_\zeta Q' Q'$$

$$- \left(\frac{2}{3}\right) C_{23} \langle \rho|\zeta\rangle Q \left(\frac{\tilde{\varepsilon}}{\tilde{k}}\right)\left[1.5 - C_f \frac{S_L}{\sqrt{\tilde{k}}}\right] \qquad (5.35)$$

The model in Equation 5.35 is computed and compared to the DNS in Figure 5-17 through Figure 5-19. In the Bunsen flame, the DNS data is noisy and so only qualitative conclusions can be drawn from the comparison. In general, the model proposed in Equation 5.35 shows good qualitative agreement with the DNS through most of the flame brush. The model captures the correct distribution, but is not precise in magnitude. However, this can be attributed in part to the noise in the DNS data. In the statistically planar flame, the model in Equation 5.35 is accurate across the flame brush, closely following the DNS across progress variable space.

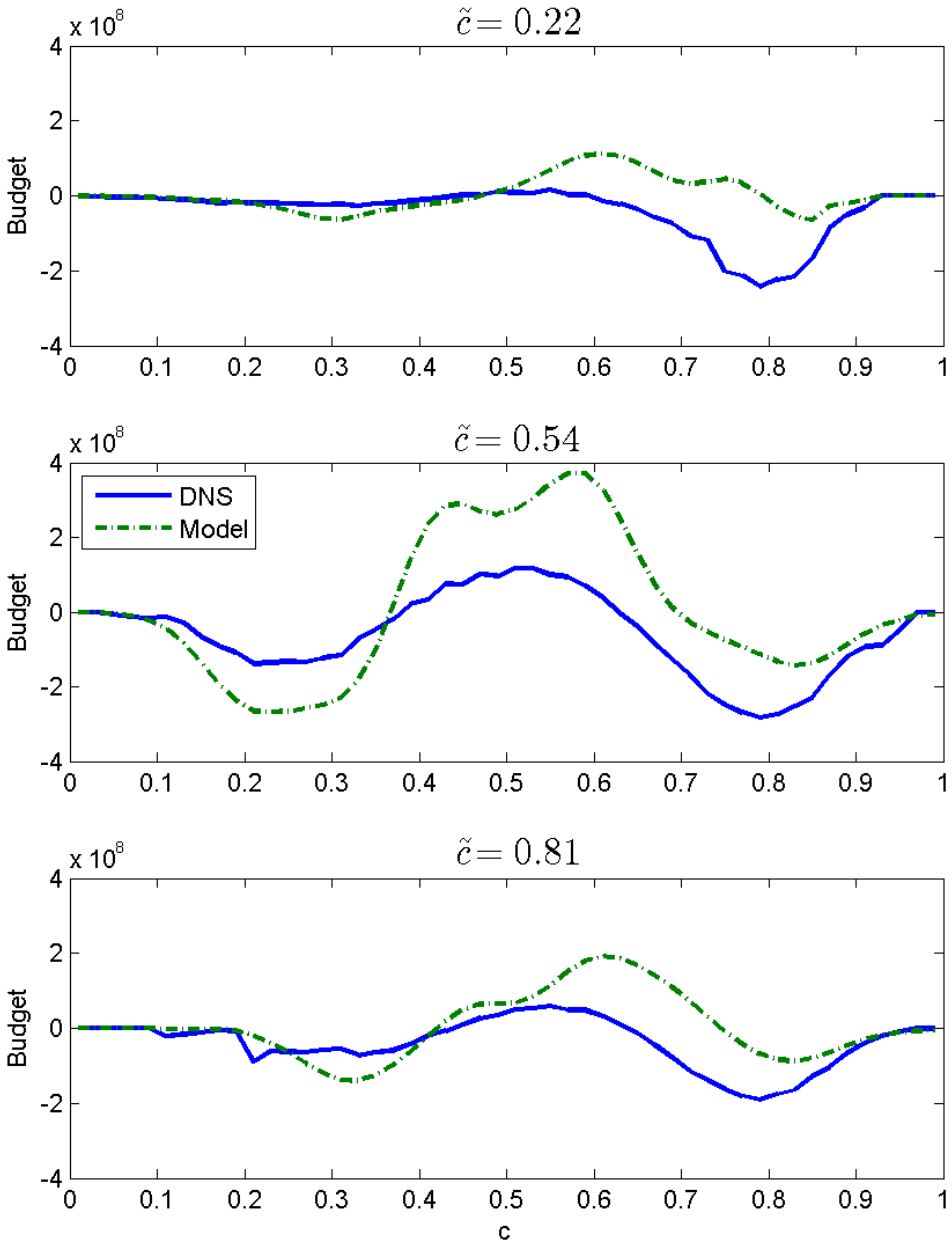


Figure 5-17: Performance of the closure for the terms T4 and D2 in Equation 5.35 at 3 locations in the flame brush for the Bunsen flame Case A at x/L = ½.

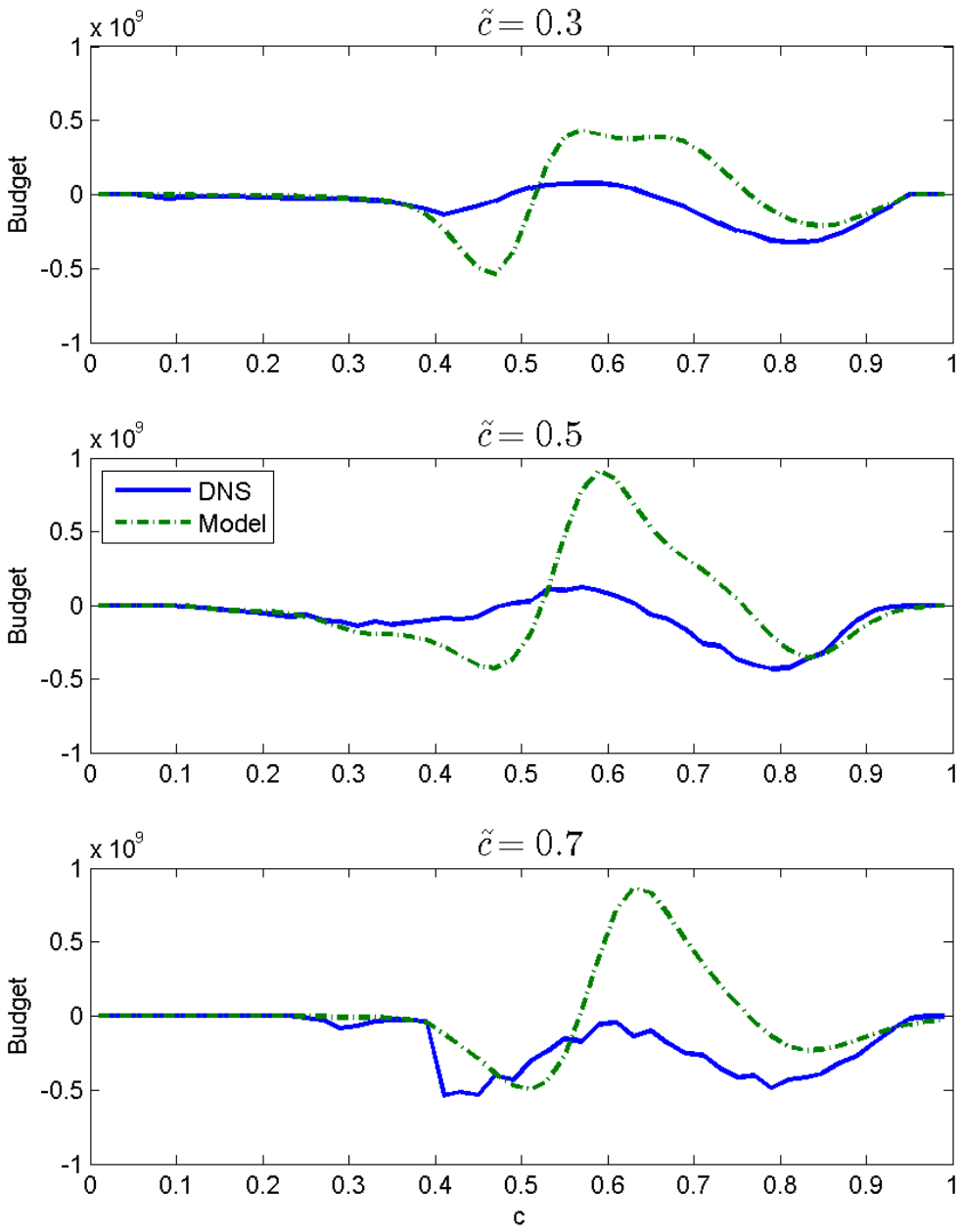


Figure 5-18: Performance of the closure for the terms T4 and D2 in Equation 5.35 at 3 locations in the flame brush for the Bunsen flame Case C at x/L = ½.

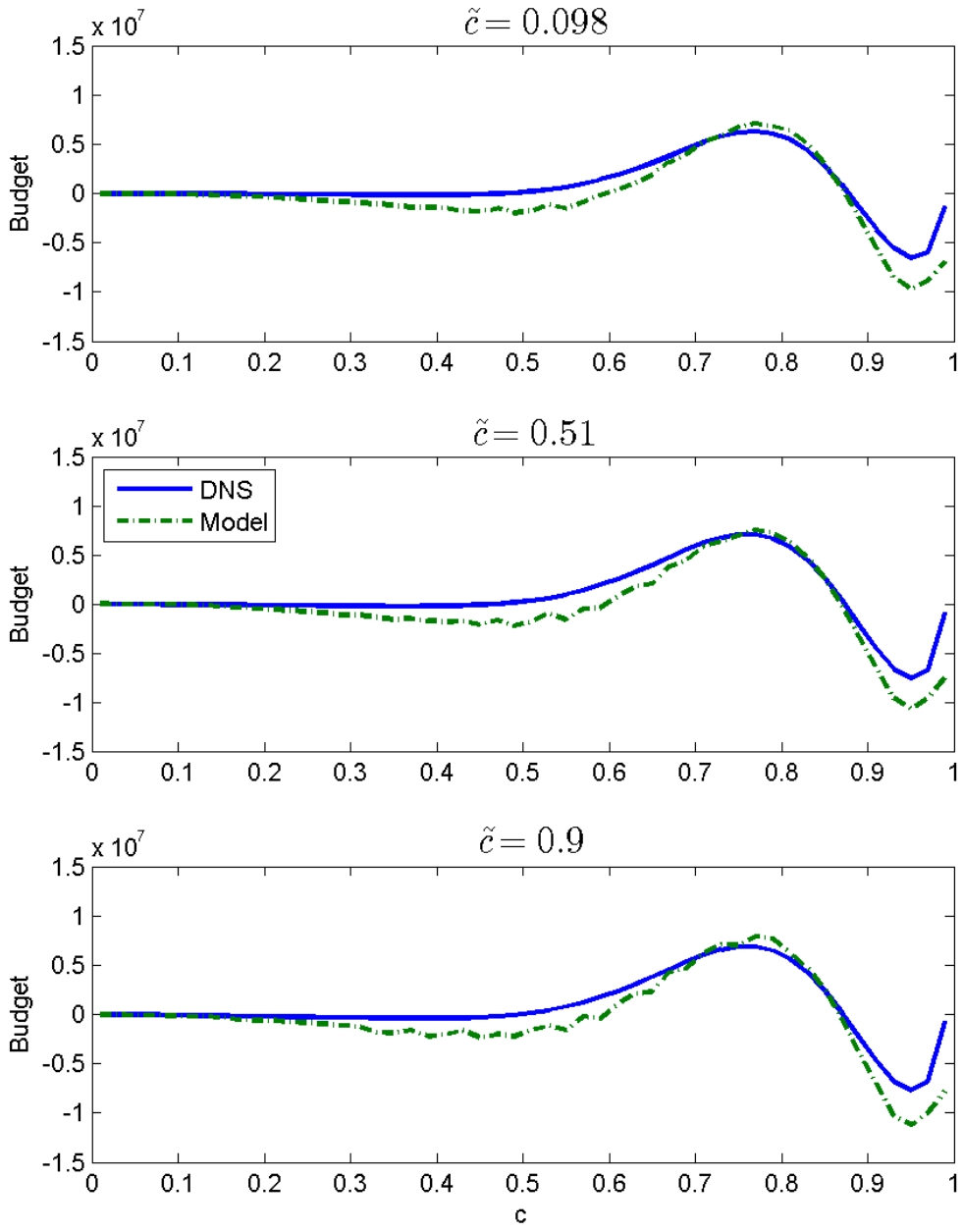


Figure 5-19: Performance of the closure for the terms T4 and D2 in Equation 5.35 at 3 locations in the flame brush for the statistically planar flame.

### *5.5.4. Fluctuating Term*

The fluctuating term, $\langle e_{\chi''} | \zeta \rangle$, plays a leading order role in throughout the flame brush as demonstrated in section 5.4.2 and thus its modeling is important to the prediction of the conditional scalar dissipation rate. In the development of the CMC method, Klimenko and Bilger propose a model

for the fluctuating term that they refer to as the primary closure hypothesis [23]. Recognizing that the integration of $\langle \nabla \chi'' | \zeta \rangle \tilde{P}(\zeta)$ and $\langle \partial \chi'' / \partial t \, | \zeta \rangle \tilde{P}(\zeta)$ across progress variable space are zero by definition, the unconditional average of the fluctuating term can be written, after some manipulation, as

$$\int \langle e_{\chi''} | \zeta \rangle \tilde{P}(\zeta) d\zeta = -\int \left\langle \rho \frac{\partial \chi''}{\partial t} + \rho u_i \frac{\partial \chi''}{\partial x_i} - \frac{\partial}{\partial x_j}\left(\rho \Gamma \frac{\partial \chi''}{\partial x_j}\right) \middle| \zeta \right\rangle \tilde{P}(\zeta) d\zeta$$

$$= -\nabla \cdot \left( \int \langle \rho | \zeta \rangle \langle u'' \chi'' | \zeta \rangle \tilde{P}(\zeta) d\zeta \right). \quad (5.36)$$

It is noted that the gradient and time derivative of the fluctuating scalar dissipation rate are not exactly zero across progress variable space after conditional averaging, however their integral contribution to the unconditional average is in fact zero. Thus, a model for the conditionally averaged fluctuating term according to the primary closure hypothesis can be constructed as in Equation 5.37, similar to what is found in Ref. [23].

$$\langle e_{\chi''} | \zeta \rangle = -\frac{\nabla \cdot \left( \langle \rho | \zeta \rangle \langle u'' \chi'' | \zeta \rangle \tilde{P}(\zeta) \right)}{\tilde{P}(\zeta)}. \quad (5.37)$$

In neglecting the contributions of the temporal and diffusive terms of $e_{\chi''}$, the local value in progress variable space of the conditionally averaged fluctuating term is determined by the magnitude of the convective term in $\langle e_{\chi''} | \zeta \rangle$.

To assess the viability of this modeling assumption, the contributions of each component in $\langle e_{\chi''} | \zeta \rangle$ are plotted in Figure 5-20 through Figure 5-22. It is clear through the budget of fluctuating term components that the temporal term plays the dominant role in the behavior of $\langle e_{\chi''} | \zeta \rangle$ and that the convective term is negligible. Therefore, the primary closure hypothesis is not a viable modeling approach to ensure that the distribution of $\langle e_{\chi''} | \zeta \rangle$ is accurately captured across progress variable space and an alternative model must be sought out.

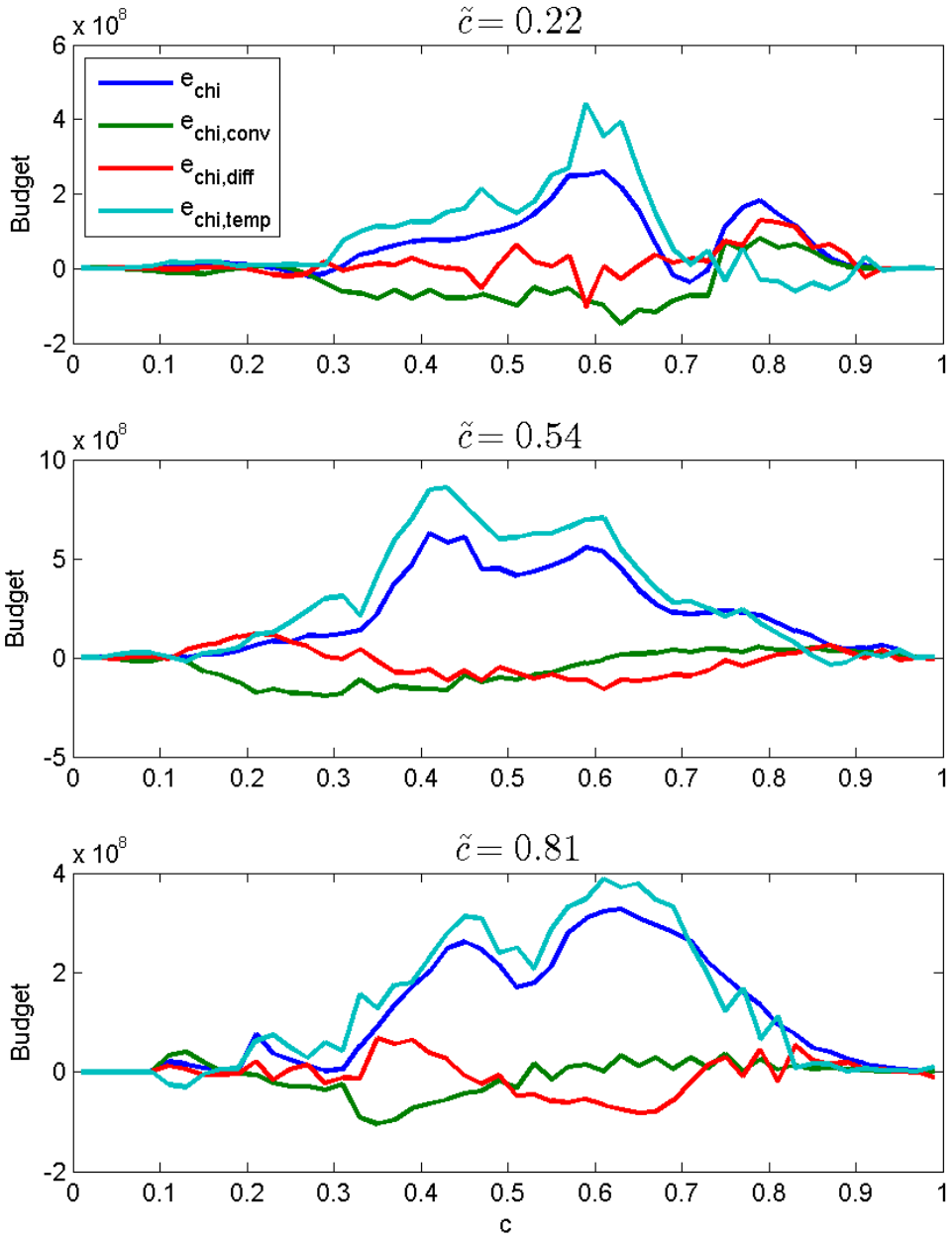


Figure 5-20: Budget of components in the $e_{\chi''}$ term at 3 locations through the flame brush for the Bunsen flame Case A at x/L = ½.

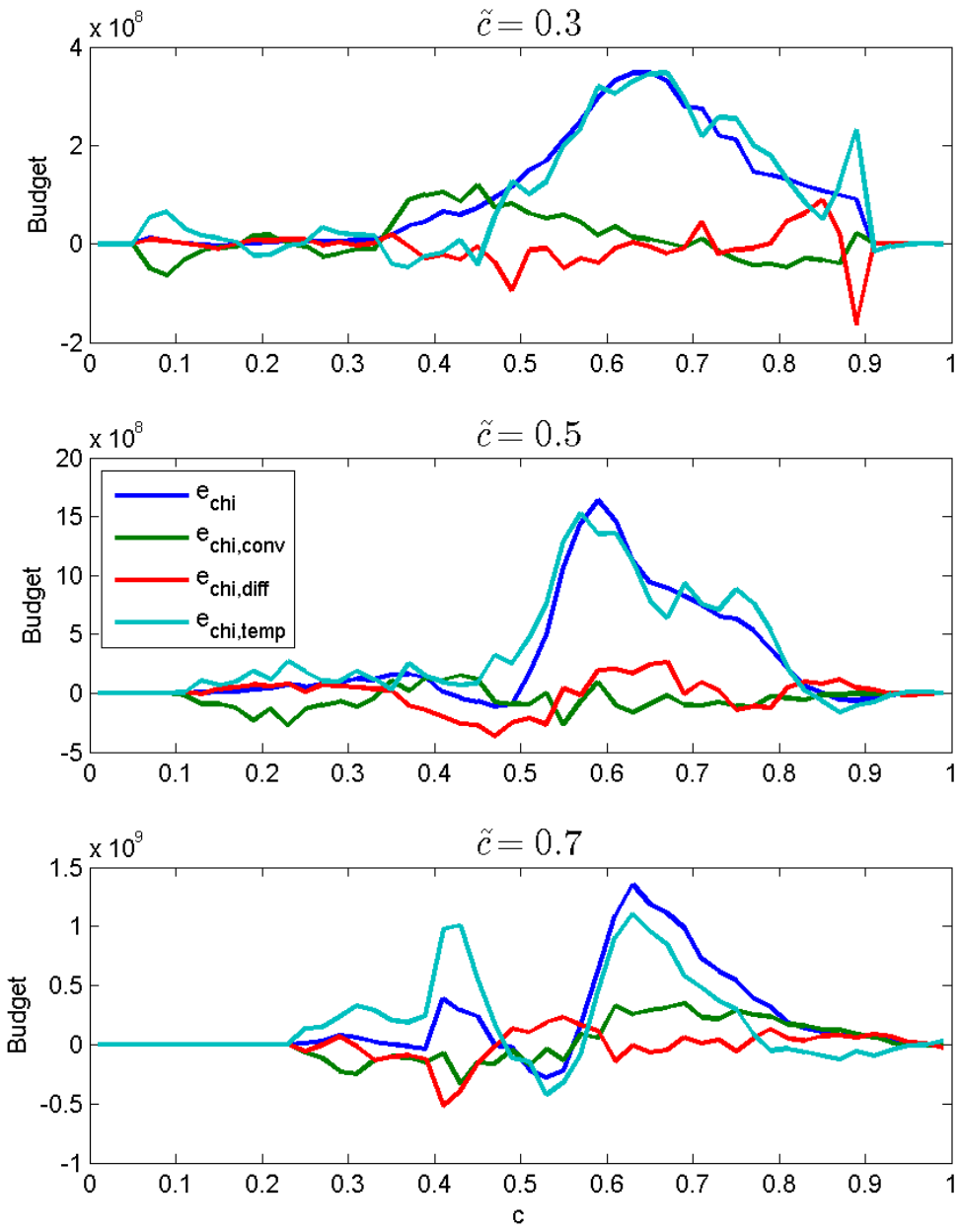


Figure 5-21: Budget of components in the $e_{\chi''}$ term at 3 locations through the flame brush for the Bunsen flame Case C at x/L = ½.

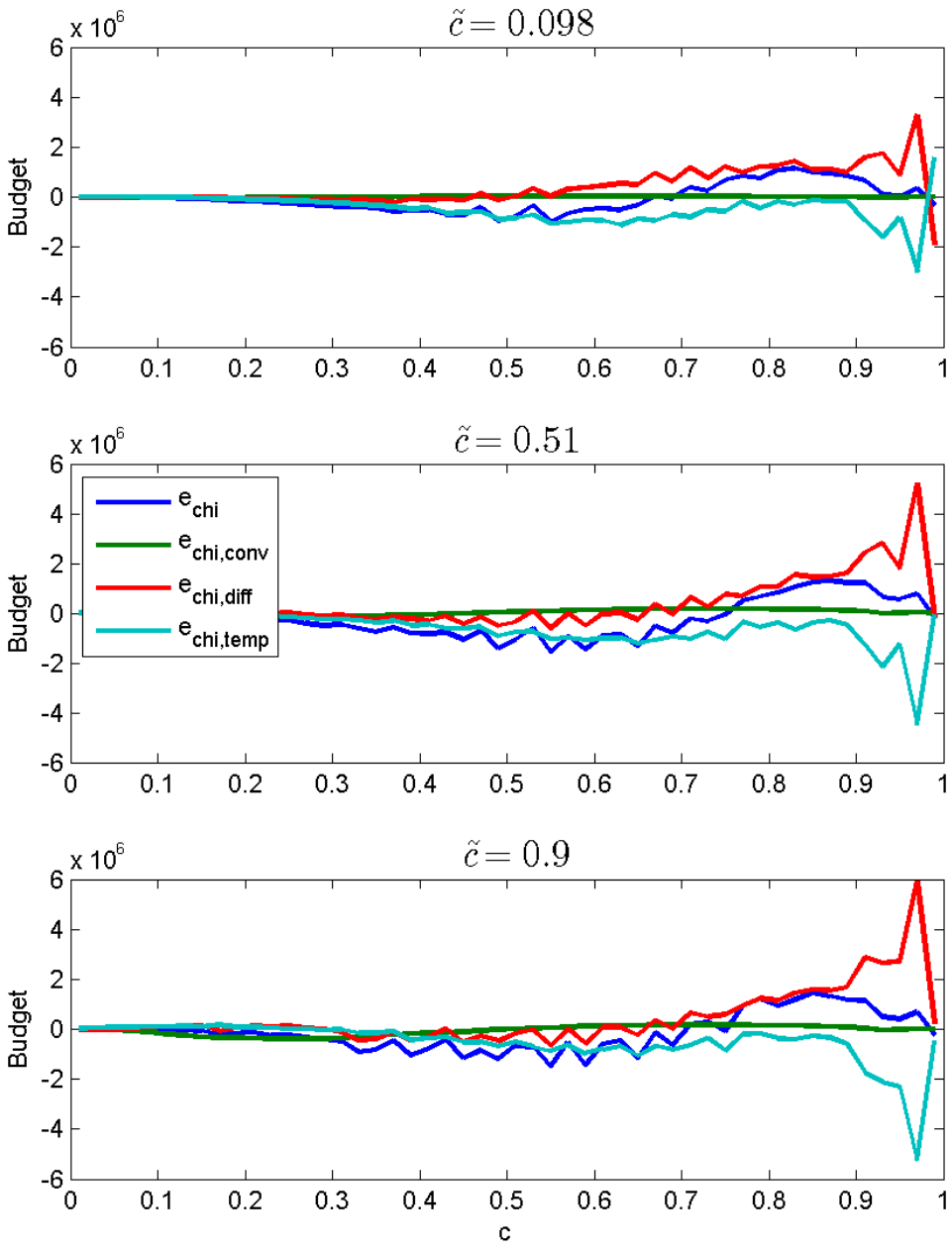


Figure 5-22: Budget of components in the $e_{\chi''}$ term at 3 locations through the flame brush for the statistically planar flame.

As an alternative modeling approach to the primary closure hypothesis, a linear relaxation model for the conditional scalar dissipation rate fluctuations is proposed. To characterize the magnitude of the conditional scalar dissipation rate fluctuations, the flame structure of a 1D, freely propagating

premixed flame is utilized, and it is assumed that the mean fluctuation relaxes to the 1D profile in a time proportional to the turbulence timescale. This leads to a model in the form of

$$\langle e_{\chi''}|\zeta\rangle = \alpha\left(\frac{\tilde{\varepsilon}}{\tilde{k}}\right)\sqrt{(Q-\chi_{1D})^2} \qquad (5.38)$$

where $\alpha$ is a model constant. To determine the appropriate value of the model constant, the order of magnitude of Equation 5.38 in the reaction zone is compared to the expected order of magnitude based on the results of section 5.3

$$\langle e_{\chi''}|\zeta\rangle \sim O\left(\rho_u\left(\frac{S_L}{\delta_L}\right)^2\frac{1}{\epsilon^2};\frac{1}{\epsilon^2}\right)$$

$$\alpha\left(\frac{\tilde{\varepsilon}}{\tilde{k}}\right)\sqrt{(Q-\chi_{1D})^2}\langle e_{\chi''}|\zeta\rangle \sim O\left(\rho_u\left(\frac{S_L}{\delta_L}\right)^2\frac{1}{\epsilon^2};\frac{\alpha}{Da}\right)$$

Therefore, the model constant $\alpha$ must be equivalent to $C_{\chi''}Da/\epsilon^2$ in order to maintain the expected order of magnitude, where $C_{\chi''}$ is a constant chosen to be 0.7, and $\epsilon$ is estimated as the ratio of the Z'eldovich thickness to the thermal thickness, $\epsilon = \delta_L/\delta_{th}$. The completed model for the fluctuating term is now expressed as

$$\langle e_{\chi''}|\zeta\rangle = C_{\chi''}\left(\frac{Da}{\epsilon^2}\right)\left(\frac{\tilde{\varepsilon}}{\tilde{k}}\right)\sqrt{(Q-\chi_{1D})^2} \qquad (5.39)$$

The model in Equation 5.39 is computed and compared to the DNS in Figure 5-23 through Figure 5-25. In the Bunsen flame, the model proposed in Equation 5.39 shows good qualitative agreement with the DNS. In general, the model captures the gross distribution of the DNS, but is inexact in terms of the local variations in progress variable space. The model agreement is acceptable in light of the statistical noise in the DNS data. In the statistically planar flame, the proposed closure for the fluctuating term again accurately captures the behavior of the DNS, particular in the reaction zone where its magnitude is greatest.

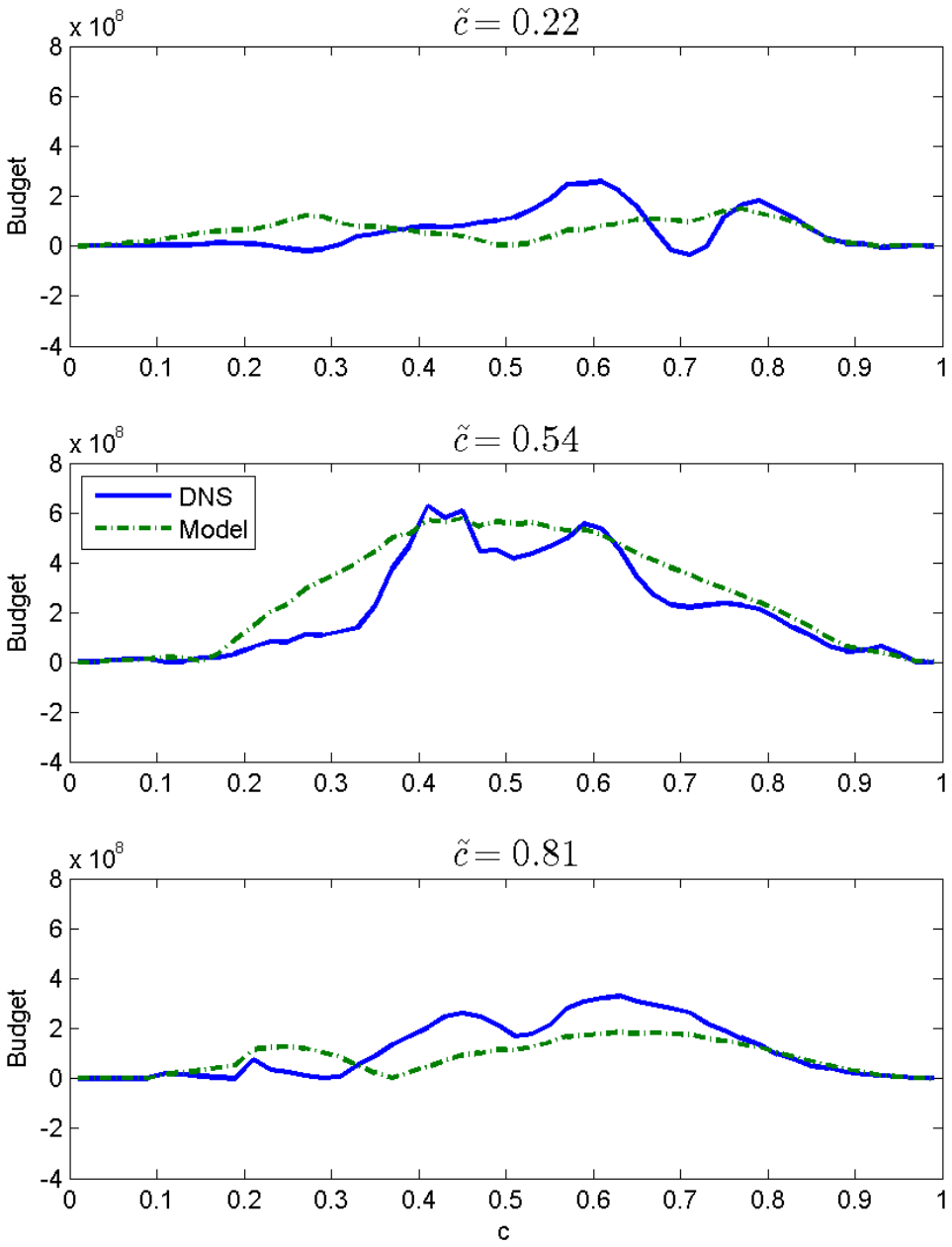


Figure 5-23: Performance of the closure for the $e_{\chi''}$ term in Equation 5.18 at 3 locations in the flame brush for the Bunsen flame Case A at x/L = ½.

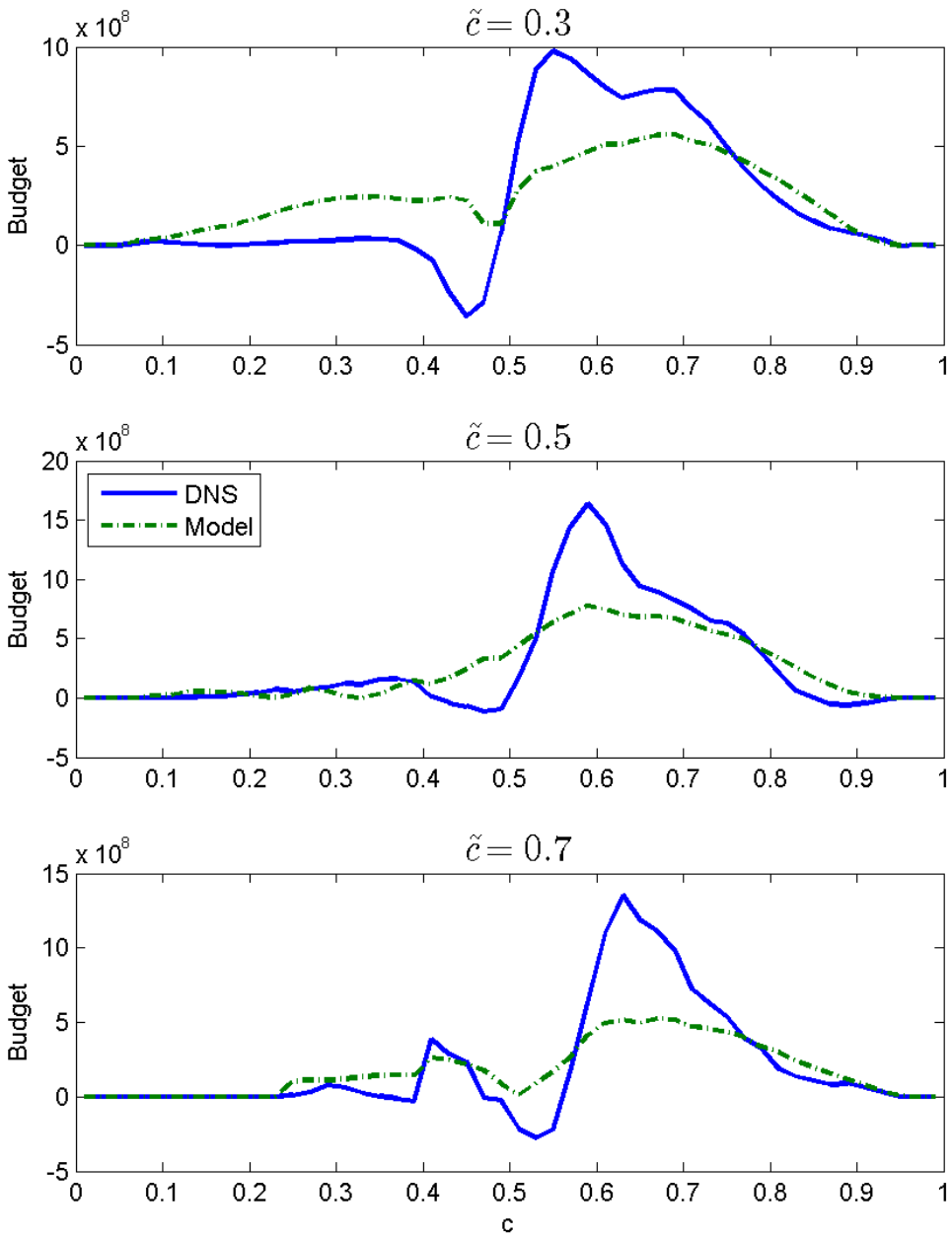


Figure 5-24: Performance of the closure for the $e_{\chi''}$ term in Equation 5.18 at 3 locations in the flame brush for the Bunsen flame Case C at x/L = ½.

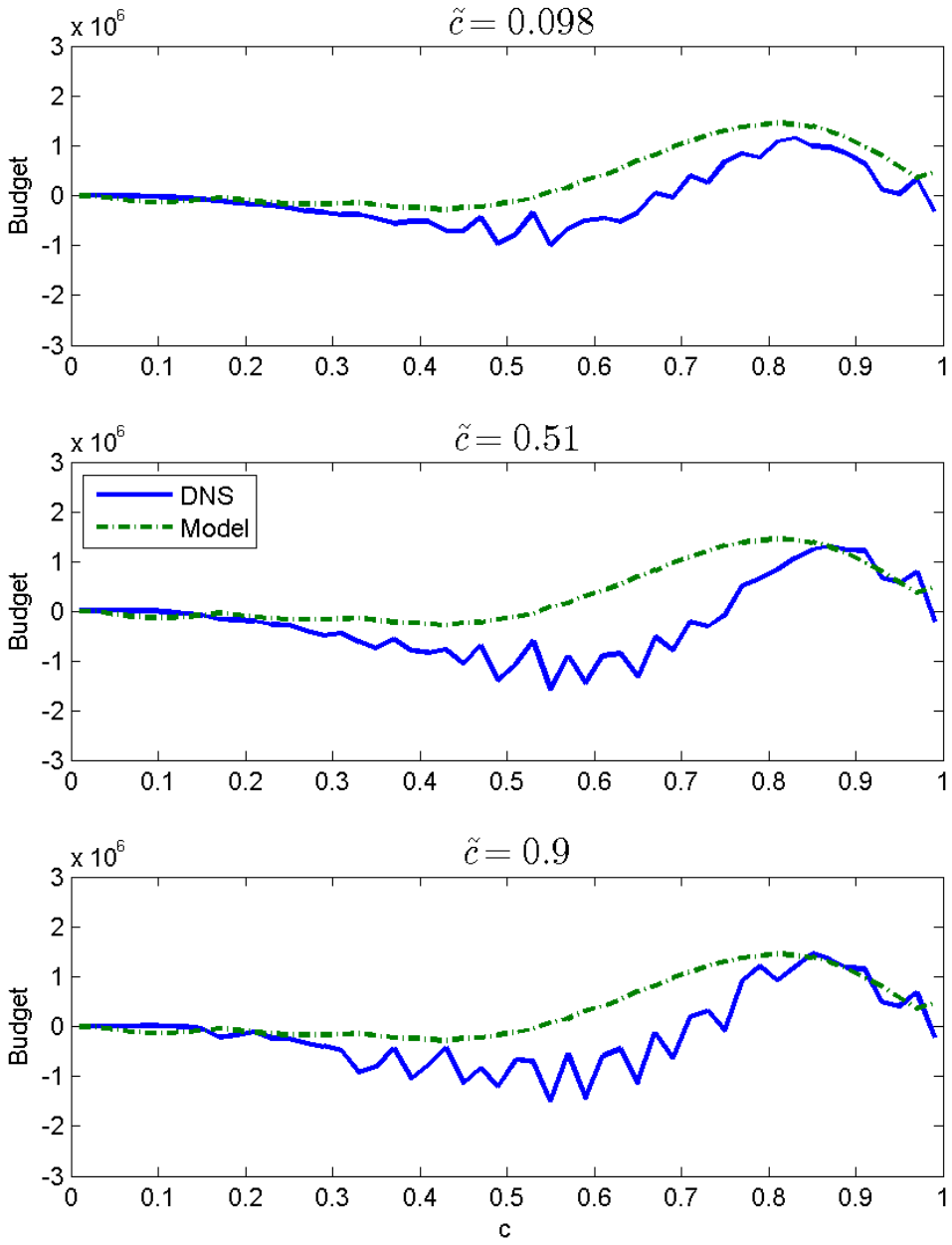


Figure 5-25: Performance of the closure for the $e_{\chi''}$ term in Equation 5.18 at 3 locations in the flame brush for the statistically planar flame.

5.6. Evaluation of Modelled Equation Performance

Modeling closures for the individual terms in Equation 5.16 have been proposed in the previous subsections. Substituting the models in Equation 5.26, 5.35, and 5.39 into Equation 5.16 yields the following modelled equation for the conditional scalar dissipation rate

$$-\langle\dot{\omega}|\zeta\rangle Q' - \frac{1}{2}Q'Q' + \frac{2}{3}C_{23}\langle\rho|\zeta\rangle Q\left(\frac{\tilde{\varepsilon}}{\tilde{k}}\right)\left(C_f\frac{S_L}{\sqrt{\tilde{k}}}\right) + C_{\chi''}\left(\frac{Da}{\epsilon^2}\right)\left(\frac{\tilde{\varepsilon}}{\tilde{k}}\right)\sqrt{(Q-\chi_{1D})^2} \approx 0 \quad (5.40)$$

The resulting modelled equation accounts for the effects of both chemical reaction and turbulence on the conditional scalar dissipation rate.

To evaluate the performance of Equation 40, the modelled equation is integrated and compared to both the model of Kolla et al. in Equation 5.1 [6,122] as well as the DNS in Figure 5-26 through Figure 5-28. The model of Equation 5.1 requires closure of both the Favre averaged scalar dissipation rate, $\tilde{\chi}_c$, and the Favre PDF of the progress variable, $\tilde{P}(\zeta)$. The Favre averaged scalar dissipation rate is closed using the model of Kolla from Equation 4.2, while the model for the Favre PDF proposed in [6], which is reproduced in Equations 5.41 and 5.42, is adopted to complete the model.

$$\tilde{P}(\zeta) = \frac{\Gamma(a+b)}{\Gamma(a)\Gamma(b)}\zeta^{a-1}(1-\zeta)^{b-1} \quad (5.41)$$

$$a = \tilde{c}\left(\frac{\tilde{c}(1-\tilde{c})}{\widetilde{c''^2}} - 1\right), \text{ and } b = a\left(\frac{1}{\tilde{c}} - 1\right) \quad (5.42)$$

As with the individual modelled terms, the conditional scalar dissipation rate predicted by Equation 5.40 in the Bunsen flames is qualitatively correct, but not precise in magnitude. In general, the predicted conditional scalar dissipation rate is larger than the actual DNS value. Conversely, the conditional scalar dissipation rate predicted by Kolla's model is significantly smaller than the DN throughout the flame brush. The new model of Equation 5.40 does capture the qualitative variation through the flame brush in that the predicted conditional scalar dissipation rate is larger in the middle of the flame brush than in either the preheat zone or post-flame zone, as in the DNS. The model is able to capture the correct relative magnitude of conditional scalar dissipation rate at the evaluated locations in the flame brush.

In the statistically planar flame, the solution of Equation 5.40 yields an accurate prediction of the conditional scalar dissipation rate for the evaluated locations in the flame brush, while the model of Kolla again under-predicts the dissipation rate magnitude. The new model provides a greatly improved prediction of the conditional scalar dissipation rate as the error in the peak dissipation rate in progress variable space is only 10%. The improved agreement between the modelled equation and the DNS for this flame can be attributed in part to the smoother statistical data available in the planar flame. Overall, the conditional scalar dissipation rate predicted by the solution of Equation 5.40 is a good approximation to the DNS data.

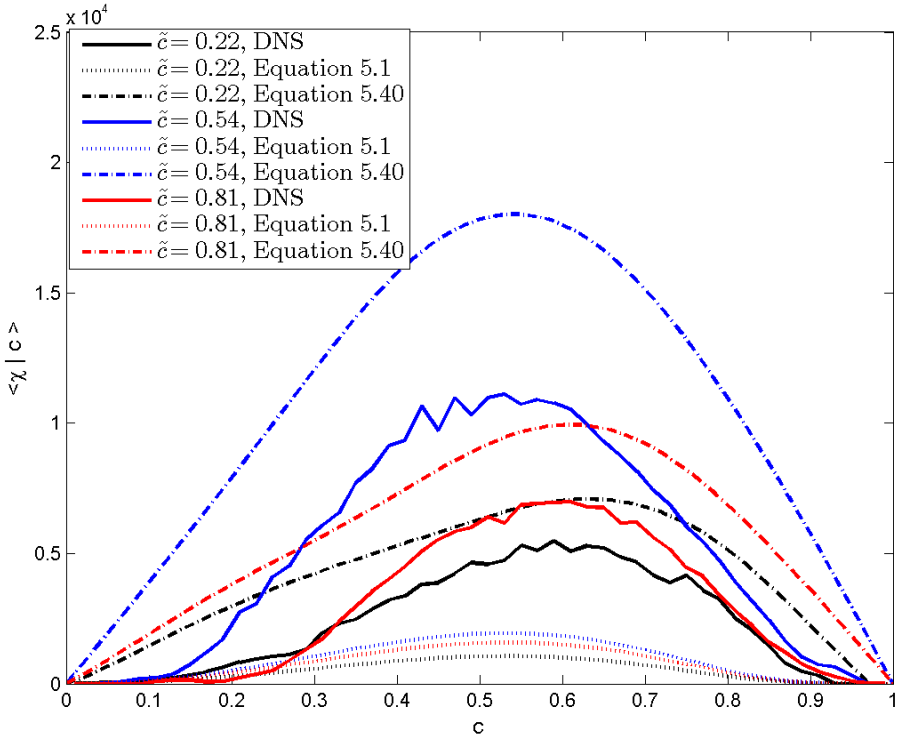


Figure 5-26: Comparison of the conditional scalar dissipation rate predicted by the models in Equation 5.1 and Equation 5.40 to the DNS through the flame brush for the Bunsen flame Case A at x/L = ½.

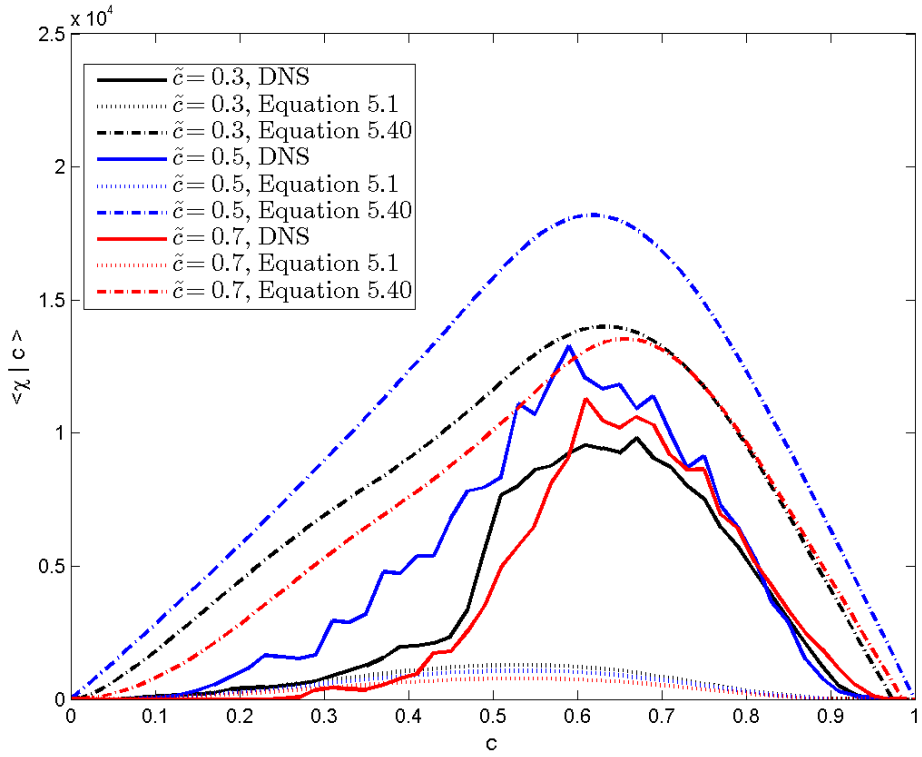


Figure 5-27: Comparison of the conditional scalar dissipation rate predicted by the models in Equation 5.1 and Equation 5.40 to the DNS through the flame brush for the Bunsen flame Case C at x/L = ½.

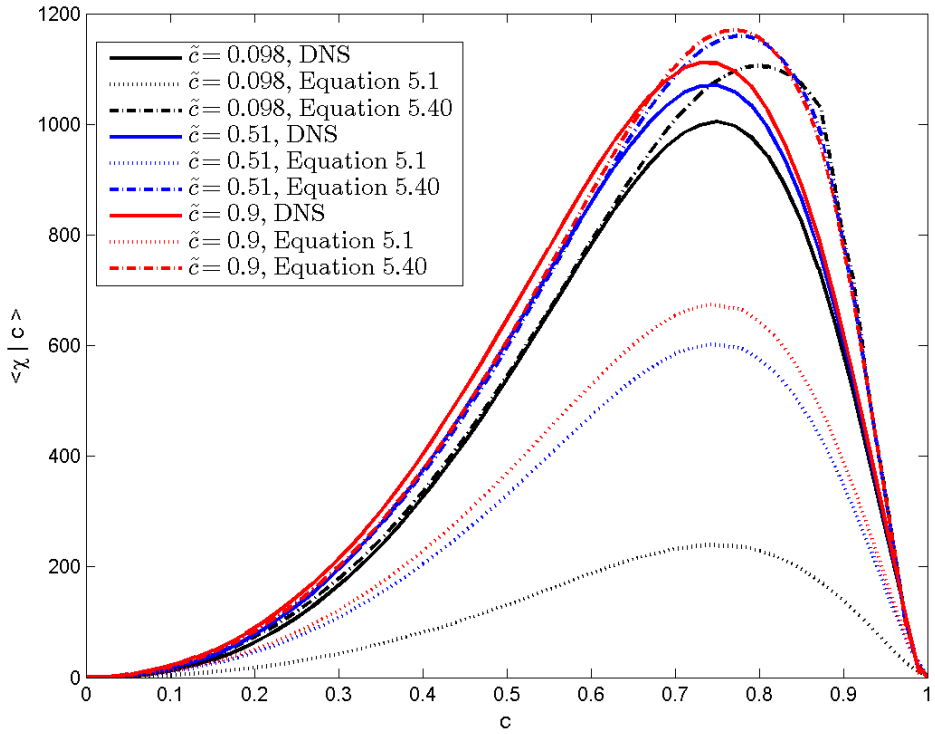


Figure 5-28: Comparison of the conditional scalar dissipation rate predicted by the models in Equation 5.1 and Equation 5.40 to the DNS through the flame brush for the statistically planar flame.

## 5.7. Conclusions

In this chapter, a transport equation for the conditional scalar dissipation rate is derived and analyzed. To the author's knowledge, this work represents the first time that the transport equation for the conditional scalar dissipation rate of a reactive scalar has been derived. An order of magnitude analysis is performed, and the leading order terms are identified as turbulent diffusion in composition space, dilatation, turbulence-scalar interaction, reaction in composition space, reaction in physical space, molecular dissipation, and the fluctuating term in the limit of large Re and Da.

The individual terms in the governing transport equation are then evaluated using three DNS data sets. The first flame database studied here is the premixed lean methane-air Bunsen flame described in [124,125], from which the two extreme conditions, Case A and Case C, are used for this analysis. The second flame database chosen for this study is the statistically stationary, planar premixed lean methane-air flame from Ref. [126]. The budget of terms in the conditional scalar dissipation rate transport equation is extracted from the DNS, and confirms the results of the scaling analysis. Based on the results of the DNS budget analysis, a leading order equation for the conditional scalar dissipation rate is identified, which requires the modeling of five terms.

The terms in the leading order equation that require modeling are the dilatation, turbulence-scalar interaction, reaction in physical space, molecular dissipation, and the fluctuating term. Parallels are drawn between the modeling efforts for the conditional scalar dissipation rate and the Favre-averaged scalar dissipation rate, a topic which has received much more attention in the literature. Models for each term requiring closure are proposed and compared to the DNS. Excellent agreement between the proposed models and the DNS is found for the statistically planar flame, while good qualitative agreement is found for the Bunsen flames in light of the statistical noise incurred by the averaging.

Using the models developed for each individual term in the leading order equation, a modelled equation is identified for the conditional scalar dissipation rate. The predictions of the modelled

equation are compared to the DNS as well as an existing algebraic model, and are generally found to provide an improved approximation of the conditional scalar dissipation rate through the flame brush.

## Chapter 6: Summary and Perspectives on Future Work

The findings presented within this dissertation are aimed at extending and enhancing the applicability of the Transported Probability Density Function methods to turbulent premixed flames. The nonlinear chemical source term appears in closed form in the TPDF methods, while micro-mixing requires modeling. The primary advantage of the TPDF method is its ability to treat turbulence-chemistry interaction without aggressive assumptions, however the accurate modeling of molecular mixing has proved challenging. A rigorous assessment of the two components of existing micro-mixing models, namely the mixing model format and the mixing timescale, has been performed and models for the Favre-averaged and conditionally averaged scalar dissipation rate have been proposed.

In Chapter 2, DNS of a temporally evolving premixed Hydrogen-Air slot jet [94] is used as a numerical test bed to evaluate the IEM, MC and EMST mixing models in the context of turbulent premixed flames. The aim of this study is to rigorously benchmark the performance of the three mixing models using DNS data to assess their suitability for turbulent premixed flames. The DNS database is used to supply the initial conditions and all time varying inputs to the governing equations in the composition TPDF method, including the mean velocity, turbulent diffusion coefficient, and mixing rate, thus allowing an exclusive focus on the mixing model. Comparison of the TPDF predictions of the mean and RMS scalar values with those from the DNS using the mixing rate based on the mass fraction of H2 reveals that the EMST mixing model provides the most accurate solutions for the flame studied. Additionally, it is found that the EMST model can accurately capture the conditional mean diffusion rates, which is the primary aim of the mixing model. Ultimately, it is found that the TPDF approach using with the EMST mixing model is capable of simulating turbulent premixed flames assuming that an accurate model for the mixing timescale can be provided. A further study on the effect of the commonly used constant mechanical-to-scalar timescale ratio on the TPDF solution indicates that there is no single value of the mechanical-to-scalar timescale ratio that is optimal for all cases.

The results found in Chapter 2 underscore the need for a deeper understanding of the scalar dissipation rate behavior of reactive scalars and more sophisticated mixing rate modeling approaches. In Chapter 3, chemical explosive mode analysis (CEMA) and DNS data with realistic chemistry are used to identify physiochemical processes that govern the conditional scalar dissipation rate behavior and evaluate mixing timescales. A local Damköhler number is defined based on the CEMA results and four flame zones are identified. It is found that large fluctuations in the instantaneous scalar dissipation rate occur in the explosive zone, where the local Damköhler number is much larger than unity. Two mechanisms have been identified that account for the large degree of scatter in the explosive zone: flame-flame interactions and flame-assisted ignition. One-dimensional laminar flames have been simulated with ANSYS Fluent to mimic the behavior of the conditional scalar dissipation rate in these two scenarios. The results of the 1-D analyses demonstrate that the conditional scalar dissipation rate is not single valued for a given value of the progress variable where flame-flame interaction or autoignition occur. This behavior leads to the large variance of the scalar dissipation rate which cannot be explained by turbulent intermittency alone. The consequence for the modelling of the conditional scalar dissipation rate in the context of LES is that the quasi-steady and equilibrium modelling approaches widely used in RANS applications may not be applicable in the presence of highly transient flame behavior. The effects of such transient flame behavior on the variance of the scalar dissipation rate likely will need to be captured in the modelling, which is a topic that merits further study.

As shown by the analysis of the scalar dissipation rate in Chapter 3, reactive scalar mixing rates in turbulent premixed flames depend on the local state of both the flow turbulence and the chemical reactions. For low global Damköhler number, the scalar mixing rate can be expected to be controlled by the small scale turbulent motions, which in turn are driven by large-scale motions, as is found to be a reasonable approximation in studies of passive scalar mixing. Conversely, in the limit of large global Damköhler number, i.e., in the limit of laminar flamelets embedded in a turbulent flow field, the mixing rate is expected to be dependent on the laminar flame structure. A new hybrid timescale model is

constructed to take advantage of the statistical data naturally available in a TPDF simulation and to properly describe the mixing rate in both the strongly turbulent and flamelet limits. An a priori assessment of the new model is performed using the same DNS data as the mixing model evaluation in Chapter 2. The hybrid model accurately captures the spatial and temporal variation of the scalar dissipation rate in the flame considered. An *a posteriori* TPDF study is then performed using the same methodology as in Chapter 2. The new mixing timescale model is compared with the constant mechanical-to-scalar mixing timescale ratio coupled with the EMST mixing model, as well as a laminar flamelet closure by Pope and Anand. It is found that the EMST model coupled with the new mixing timescale model provides the best prediction of the flame structure and flame propagation among the models tested, as the dynamics of reactive scalar mixing across different flame regimes are appropriately accounted for.

The hybrid model developed in Chapter 4 relies on a closure for the conditional scalar dissipation rate assumes the flame structure resembles that of a steady 1D, laminar premixed flame. In Chapter 5, a more rigorous model for the conditional scalar dissipation rate is sought by deriving its transport equation. An order of magnitude analysis is then performed, and the leading order terms requiring modeling are identified. The individual terms in the governing transport equation are evaluated using DNS and the budget of terms is extracted, confirming the results of the scaling analysis. Based on the results of the DNS budget analysis and the order of magnitude analysis, a leading order equation for the conditional scalar dissipation rate is identified. Models for the unclosed terms in the leading order equation are proposed by drawing parallels between the modeling efforts for the conditional scalar dissipation rate and the Favre-averaged scalar dissipation rate where appropriate. The models for each term requiring closure are then compared to the DNS and excellent agreement is found for the flames studied. Finally, using the models developed for each individual term in the leading order equation, a modelled equation for the conditional scalar dissipation rate is proposed. The modelled equation is

integrated for the flames studied, and good overall agreement is found between the predicted conditional scalar dissipation rate and the DNS.

While substantial progress has been made in this dissertation in applying the TPDF method to turbulent premixed flames, further work remains. In practical engines, combustion typically occurs in partially-premixed conditions due to safety concerns, and thus a study similar to the one performed in Chapter 2 for a partially premixed flame would be useful. Also, validation of newer mixing models, such as the shadow position mixing model, is a worthwhile topic of investigation. The modeling of the scalar dissipation rate in this dissertation has been performed in the RANs context, however the results of Chapter 3 demonstrate that mixing timescales can have strong transient effects. It would be useful to consider timescale models that include transient effects, especially in the context of LES. The models developed in Chapter 4 and Chapter 5 have shown promising results, however further validation under a wider array of conditions would be helpful to better understand the limitations of the models. Extensions to LES and partially premixed mixtures would be beneficial for the generality of the proposed models, and are topics that merit further research.

## References


[1] International Energy Agency, World Energy Outlook, (2015).

[2] IPCC (2014), Climate Change 2014: Synthesis Report. Intergovernmental Panel on Climate Change, Geneva, Switzerland.

[3] N. Swaminathan, K.N.C. Bray, Turbulent Premixed Flames. Cambridge University Press, Cambridge, UK, 2011.

[4] M. Matalon, Proc. Comb. Inst. 32 (2009) 57-82.

[5] S.B. Pope, Turbulent Flows, Cambridge University Press, Cambridge, UK, 2000.

[6] H. Kolla, "Scalar Dissipation Rate based Flamelet Modelling of Turbulent Premixed Flames", Ph.D. Dissertation, 2009.

[7] D. Veynante, L. Vervisch, Prog. Energy Comb. Sci. 28 (2002) 193-266.

[8] S.B. Pope, Proc. Combust. Inst. 34 (2013) 1-31.

[9] K.N.C. Bray, J.B. Moss, Acta Astronaut. 4 (1977) 291-319.

[10] K.N.C. Bray, P.A. Libby, Phys. Fluids. 19 (1976) 1687-1701.

[11] K.N.C. Bray, Turbulent flows with premixed reactants, in: P.A. Libby, F.A. Williams (Eds.), Turbulent Reacting Flows, Springer Berlin Heidelberg, Berlin, Heidelberg, 1980, pp. 115-183.

[12] D. Bradley, P.H. Gaskell, X.J. Gu, Combust. Flame. 96 (1994) 221-248.

[13] T. Poinsot, D. Veynante, Theoretical and Numerical Combustion, Edwards, Philadelphia, 2001.

[14] J.A.V. Oijen, L.P.H.D. Goey, Combustion Sci. Technol. 161 (2000) 113-137.

[15] O. Gicquel, N. Darabiha, D. Thévenin, Proc. Combust. Inst. 28 (2000) 1901-1908.

[16] F.E. Marble, J.E. Broadwell, The Coherent Flame Model for Turbulent Chemical Reactions, Tech. Rep. TRW-9-PU (1977).

[17] S.B. Pope, Int. J. Eng. Sci. 26 (1988) 445-469.

[18] S.M. Candel, T.J. Poinsot, Combust. Sci. Technol. 70 (1990) 1-15.

[19] A. Trouvé, T. Poinsot, J. Fluid Mech. 278 (1994) 1-31.

[20] K.N.C. Bray, R.S. Cant, Proc. Royal Society of London A: Mathematical, Physical and Engineering Sciences. 434 (1991) 217-240.

[21] N. Peters, J. Fluid Mech. 384 (1999) 107-132.

[22] N. Peters, Turbulent Combustion, Cambridge University Press, Cambridge, UK, 2000.

[23] A.Y. Klimenko, R.W. Bilger, Prog. Energy Combust. Sci. 25 (1999) 595-687.

[24] R.W. Bilger, Phys. Fluids A: Fluid Dynamics. 5 (1993) 436-436.

[25] A.Y. Klimenko, Fluid Dyn. 25 (1990) 327-334.

[26] A.R. Kerstein, Combust. Sci. Technol. 60 (1988) 391-421.

[27] S. Menon, A.R. Kerstein, The Linear-Eddy Model, in: T. Echekki, E. Mastorakos (Eds.), Turbulent Combustion Modeling: Advances, New Trends and Perspectives, Springer Netherlands, Dordrecht, 2011, pp. 221-247.

[28] A.R. Kerstein, J. Fluid Mech. 392 (1999) 277-334.

[29] T. Echekki, A.R. Kerstein, J.C. Sutherland, The One-Dimensional-Turbulence Model, in: T. Echekki, E. Mastorakos (Eds.), Turbulent Combustion Modeling: Advances, New Trends and Perspectives, Springer Netherlands, Dordrecht, 2011, pp. 249-276.

[30] A.Y. Klimenko, S.B. Pope, Phys. Fluids. 15 (2003) 1907-1925.

[31] M.J. Cleary, A.Y. Klimenko, Multiple Mapping Conditioning: A New Modelling Framework for Turbulent Combustion, in: T. Echekki, E. Mastorakos (Eds.), Turbulent Combustion Modeling: Advances, New Trends and Perspectives, Springer Netherlands, Dordrecht, 2011, pp. 143-173.

[32] R.C. Flagan, J.P. Appleton, Combust. Flame. 23 (1974) 249-267.

[33] E.E. O'Brien, The probability density function (pdf) approach to reacting turbulent flows, in: P.A. Libby, F.A. Williams (Eds.), Turbulent Reacting Flows, Springer Berlin Heidelberg, Berlin, Heidelberg, 1980, pp. 185-218.

[34] S.B. Pope, Prog. Energy Combust. Sci. 11 (1985) 119-192.

[35] Libby, Paul A., Williams,F.A., Turbulent Reacting Flows, Academic Press, London; New York, 1994.

[36] L. Valiño, Flow, Turb. Combust. 60 (1998) 157-172.

[37] D.C. Haworth, Prog. Energy Combust. Sci. 36 (2010) 168-259.

[38] S. Mitarai, J.J. Riley, G. Kosály, Phys. Fluids. 17 (2005) 047101.

[39] D.H. Rowinski, S.B. Pope, Combust. Theory Model. 15 (2011) 245-266.

[40] D.H. Rowinski, S.B. Pope, Combust. Theory Model. 17 (2013) 610-656.

[41] A. Krisman, J.C.K. Tang, E.R. Hawkes, D.O. Lignell, J.H. Chen, Combust. Flame. (2014) 1-22.

[42] S.B. Pope, D.C. Haworth, The mixing layer between turbulent fields of different scales, in: F. Durst, B.E. Launder, J.L. Lumley, F.W. Schmidt (Eds.), Turbulent Shear Flows, 5th ed., Springer-Verlag, Berlin, 1987, pp. 44-53.

[43] S.B. Pope, Y.L. Chen, Phys. Fluids A. 2 (1990) 1437-1449.

[44] S.B. Pope, Phys Fluids A. 3 (1991) 1947-1957.

[45] A.T. Norris, S.B. Pope, Combust. Flame. 100 (1995) 211-220.

[46] R.E. Meyers, E.E. O'Brien, Combust. Sci. Technol. 26 (1981) 123-134.

[47] R.R. Cao, S.B. Pope, Combust. Flame. 143 (2005) 450-470.

[48] A.T. Norris, S.B. Pope, Combust. Flame. 83 (1991) 27-42.

[49] R.O. Fox, C.M. Cha, P. Trouillet, Lagrangian PDF mixing models for reacting flows, Proc. Summer Prog., Center for Turb. Research, 2002.

[50] R.O. Fox, Computational Models for Turbulent Reacting Flows. Cambridge University Press, Cambridge, UK, 2003.

[51] S. Subramaniam, S.B. Pope, Combust. Flame. 115 (1998) 487-514.

[52] J.C.D. J. Villermaux, Proc. 2nd Int. Symp. on Chem. Reaction Eng. (1972) 1-13.

[53] C. Dopazo, E.E. O'Brien, Acta Astronaut. 1 (1974) 1239-1266.

[54] R.L. Curl, AIChE J. 9 (1963) 175-181.

[55] J. Janicka, W. Kolbe, W. Kollmann, J. Non Equilib. Thermodyn. 4 (1979) 47-66.

[56] C. Dopazo, Phys. Fluids. 22 (1979) 20-30.

[57] Z. Ren, S.B. Pope, Combust. Flame. 136 (2004) 208-216.

[58] Z. Ren, S. Subramaniam, S.B. Pope, Implementation of the EMST mixing model, (2002).

[59] L. Valiño, C. Dopazo, Phys. Fluids A. 3 (1991) 3034-3037.

[60] H. Chen, S. Chen, R.H. Kraichnan, Phys. Rev. Lett. 63 (1989) 2657-2660.

[61] S.B. Pope, Theor. Comput. Fluid Dyn. 2 (1991) 255-270.

[62] S. Subramaniam, S.B. Pope, Combust. Flame. 117 (1999) 732-754.

[63] S.B. Pope, Phys. Fluids. 25 (2013) 110803.

[64] J.C.K. Tang, A. Kong, E.R. Hawkes, S.B. Pope, J.H. Chen, Proc. 19th Australasian Fluid Mechanics Conference.

[65] X. Zhao, A. Bhagatwala, J.H. Chen, D.C. Haworth, S.B. Pope, Combust. Flame. 165 (2016) 223-245.

[66] S.B. Pope, M.S. Anand, Proc. Combust. Inst. 20 (1984) 403-410.

[67] A. Mura, F. Galzin, R. Borghi, Combust. Sci. Tech. 175 (2003) 1573-1609.

[68] Y. Chen, N. Peters, G.A. Schneemann, N. Wruck, U. Renz, M.S. Mansour, Combust. Flame. 107 (1996).

[69] S.M. Correa, Combust. Flame. 103 (1995) 194-206.

[70] F. Bisetti, J.-. Chen, E.R. Hawkes, J.H. Chen, Combust. Flame. 155 (2008) 571-584.

[71] E.R. Hawkes, R. Sankaran, P.P. Pébay, J.H. Chen, Combust. Flame. 145 (2006) 145-159.

[72] T. Hůlek, R.P. Lindstedt, Combust. Flame. 104 (1996) 481-504.

[73] S.M. Cannon, B.S. Brewster, L.D. Smoot, Combust. Flame. 119 (1999) 233-252.

[74] R. Lindstedt, E. Vaos, Modeling of mixing processes in non-isothermal and combusting flows, in: C. Dopazo (Ed.), Advances in Turbulence, Vol. 8 (2000) 493-496.

[75] R.P. Lindstedt, E.M. Vaos, Combust. Flame. 145 (2006) 495-511.

[76] T.S. Kuan, R.P. Lindstedt, E.M. Vaos, in: G. Roy (Ed.), Advances in Confined Detonations and Pulse Detonation Engines, Torus Press, Moscow, 2003, pp. 17-40.

[77] M. Stöllinger, S. Heinz, Combust. Flame. 157 (2010) 1671-1685.

[78] M.J. Dunn, A.R. Masri, R.W. Bilger, Combust. Flame. 151 (2007) 46-60.

[79] K. Bray, M. Champion, P.A. Libby, N. Swaminathan, Combust. Flame. 158 (2011) 2017-2022.

[80] R. Borghi, Combust. Flame. 80 (1990) 304-312.

[81] T. Mantel, R. Borghi, Combust. Flame. 96 (1994) 443-457.

[82] A. Mura, R. Borghi, Combust. Flame. 133 (2003) 193-196.

[83] N. Swaminathan, K.N.C. Bray, Combust. Flame. 143 (2005) 549-565.

[84] N. Swaminathan, K. Bray, Combust. Flame. 143 (2005) 549-565.

[85] N. Swaminathan, R.W. Grout, Phys. Fluids. 18 (2006) 045102.

[86] N. Chakraborty, N. Swaminathan, Phys. Fluids. 19 (2007) 045103.

[87] N. Chakraborty, N. Swaminathan, Phys. Fluids. 19 (2007) 045104.

[88] N. Chakraborty, J.W. Rogerson, N. Swaminathan, Phys. Fluids. 20 (2008) 045106-045106.

[89] G. Hartung, J. Hult, C.F. Kaminski, J.W. Rogerson, N. Swaminathan, Phys. Fluids. 20 (2008) 035110.

[90] H. Kolla, J.W. Rogerson, N. Chakraborty, N. Swaminathan, Combust. Sci. Technol. 181 (2009) 518-535.

[91] N. Chakraborty, N. Swaminathan, Combust. Sci. Technol. 185 (2013) 676-709.

[92] D.H. Rowinski, S.B. Pope, Phys. Fluids. 25 (2013) 105105-105105.

[93] R.P. Lindstedt, E.M. Vaos, Combust. Flame. 145 (2006) 495-511.

[94] E.R. Hawkes, O. Chatakonda, H. Kolla, A.R. Kerstein, J.H. Chen, Combust. Flame. 159 (2012) 2690-2703.

[95] J.H. Chen, A. Choudhary, B. de Supinski, M. DeVries, E.R. Hawkes, S. Klasky, W.K. Liao, K.L. Ma, J. Mellor-Crummey, N. Podhorszki, R. Sankaran, S. Shende, C.S. Yoo, Comp. Sci. Disc. 2 (2009) 015001-015001.

[96] J. Li, Z. Zhao, A. Kazakov, F.L. Dryer, Int J Chem Kinet. 36 (2004) 566-575.

[97] S.B. Pope, Proc. Combust. Inst. 34 (2013) 1-31.

[98] S. Viswanathan, H. Wang, S.B. Pope, J. Comp. Phys. 230 (2011) 6916-6957.

[99] N. Swaminathan, K.N.C. Bray, Turbulent Premixed Flames. Cambridge University Press, Cambridge, UK, 2011.

[100] M. Stöllinger, S. Heinz, Combust. Flame. 157 (2010) 1671-1685.

[101] T. Sponfeldner, I. Boxx, F. Beyrau, Y. Hardalupas, W. Meier, A.M.K.P. Taylor, Proc. Combust. Inst. 35 (2015) 1269-1276.

[102] N. Chakraborty, N. Swaminathan, Flow, Turb., Combust. 87 (2011) 261-292.

[103] N. Swaminathan, R.W. Bilger, Combust. Theory Model. 5 (2001) 429-446.

[104] T.F. Lu, C.S. Yoo, J.H. Chen, C.K. Law, J. Fluid Mech. 652 (2010) 45-64.

[105] Z. Luo, C.S. Yoo, E.S. Richardson, J.H. Chen, C.K. Law, T. Lu, Combust. Flame. 159 (2012) 265-274.

[106] M. Kuron, Z. Ren, E. Hawkes, H. Zhou, J. Tang, J.H. Chen, T. Lu, Proc. Combust. Inst. (2016) In press.

[107] H. Kolla, "Scalar Dissipation Rate based Flamelet Modelling of Turbulent Premixed Flames", Ph.D. Dissertation, 2009.

[108] Z. Zhou, S. Li, H. Wang, Z. Ren, 68th Annual Meeting of the APS Division of Fluid Dynamics. (2015).

[109] C. Béguier, I. Dekeyser, B.E. Launder, Phys. Fluids. 21 (1978) 307-310.

[110] E.R. Hawkes, R. Sankaran, J.C. Sutherland, J.H. Chen, Proc. Combust. Inst. 31 (2007) 1633-1640.

[111] O. Chatakonda, E.R. Hawkes, A.J. Aspden, A.R. Kerstein, H. Kolla, J.H. Chen, Combust. Flame. 160 (2013) 2422-2433.

[112] N. Punati, H. Wang, E.R. Hawkes, J.C. Sutherland, Flow, Turb. Combust. (2016).

[113] P. Trisjono, K. Kleinheinz, E.R. Hawkes, H. Pitsch, Combust. Flame. Submitted (2015).

[114] M. Kuron, Z. Ren, H. Kolla, E.R. Hawkes, J.H. Chen, T. Lu, 9th U. S. National Combustion Meeting.

[115] C.A. Kennedy, M.H. Carpenter, R.M. Lewis, Appl. Numer. Math. 35 (2000) 177-219.

[116] R.O. Fox, Phys. Fluids. 11 (1999) 1550-1571.

[117] R.O. Fox, Computational Models for Turbulent Reacting Flows, Cambridge University Press, Cambridge, 2003.

[118] S.S. Girimaji, Phys. Fluids A. 4 (1992) 2529-2537.

[119] A. Kronenburg, R.W. Bilger, J.H. Kent, Flow, Turb. Combust. 64 (2000) 145-159.

[120] C.B. Devaud, R.W. Bilger, T. Liu, Phys. Fluids. 16 (2004) 2004-2011.

[121] R.W. Bilger, Some Aspects of Scalar Dissipation, Flow, Turb. Combust. 72 (2004) 93-114.

[122] H. Kolla, N. Swaminathan, Combust. Flame. 157 (2010) 943-954.

[123] S. Amzin, N. Swaminathan, Combust. Theory Model. 17 (2013) 1125-1153.

[124] R. Sankaran, E.R. Hawkes, J.H. Chen, T. Lu, C.K. Law, Proc. Combust Inst. 31 (2007) 1291-1298.

[125] R. Sankaran, E.R. Hawkes, C.S. Yoo, J.H. Chen, Combust. Flame. 162 (2015) 3294-3306.

[126] H. Kolla, X. Zhao, J.H. Chen, N. Swaminathan, Combust. Sci. Technol. (2016).

[127] B. Franzelli, E. Riber, L.Y.M. Gicquel, T. Poinsot, Combust. Flame. 159 (2012) 621-637.

[128] J.W. Rogerson, N. Swaminathan, M. Tanahashi, N. Shiwaku, 3rd European Combustion Meeting, (2007).

[129] A.M. Steinberg, J.F. Driscoll, N. Swaminathan, Combust. Flame. 159 (2012) 2576-2588.